MASTER OF PHILOSOPHY

Development of Property Prediction Methods for Sodium-ion Battery Electrolytes

Zhang, Jiaxin

Award date:
2017

Awarding institution:
Queen's University Belfast

Queen's University of Belfast

Development of Property Prediction Methods for Sodium-ion Battery Electrolytes

Zhang Jiaxin, BEng

This thesis is submitted for the degree of

Master of Philosophy

to the

School of Chemistry and Chemical Engineering

October 2017

Abstract

In this project, we model the interaction between the sodium ion and the organic solvents, which are widely used in sodium ion batteries (SIBs). The research mainly focuses on how a sodium cation coordinates with the solvent molecules and how its coordination affects the resulting complex structures and infrared vibrations. Three carbonates were used as solvent molecules for this study - propylene carbonate (PC), dimethyl carbonate (DMC) and ethylene carbonate (EC). A larger B3LYP/6-311++G** basis set was used to optimize the geometry and compute the vibrational spectrum of a single molecule EC and its complex including the sodium cation as a benchmark. Both the efficiency and accuracy of ab initio calculations were taken into account for these systems. The coordination of one Na^+ with 1–5 solvent molecules were studied using the density functional theory (DFT) method with a smaller basis set B3LYP/6-31G* in the gas phase. The stability of these complexes was then assessed through the determination of their thermodynamic properties. The data obtained confirmed that the four-coordinated complex is the most stable solvation shell structure, which gives a tetrahedral shape. However, results using the larger and more accurate basis set def2-svp suggests that $Na^+(DMC)_3$ can be the most stable structure. The accuracy of formed complexes was then assessed by comparing the data obtained from computed infrared spectroscopy with experimental measurements, which clearly demonstrates similar trends by increasing the molar ratio of sodium salts in solution. Finally, the structures generated from the simulation were then also confirmed using NMR measurements including ^{1}H, ^{13}C, and ^{23}Na NMR spectra.

List of symbols and abbreviations

E	Total energy
G	Gibbs free energy
H	Total enthalpy
O_c	Carbonyl oxygen
S	Total entropy
T	Temperature
V	Volume
X	Mole fraction
ZC	Represents EC, PC, and DMC
v	Vibration mode
w	Weight fraction
M_w	Molar mass

Greek letters

ε	Dielectric constant
η	Viscosity
σ	Conductivity
Δ	Change of a given quantity
$\tilde{\nu}$	Wavenumber
ν	Frequency

Super / subscripts

+/-	Cation / Anion
B	Binary
T	Ternary
b	Boiling point
c	Carbonyl

corr	Correction of enthalpy
exp	Experimental
f	Flash point
m	Melting point
n	Number of molecules
vdW	Van der Waals energy

Abbreviations

EV	Electric vehicle
DFT	Density functional theory
HEV	Hybrid electric vehicles
IR	Infrared
PHEV	Plug-in hybrid electric vehicle
SHE	Standard hydrogen electrode
asym	Asymmetric
sym	Symmetric
e.g.	Exempli gratia
Sym	Symmetric
vs.	Versus
IL	Ionic liquid
LIBs	Lithium-ion batteries
SIBs	Sodium ion batteries
DSC	Differential scanning calorimetry

Chemical formula Name/solvent abbreviations

CH4	Methane
CO2	Carbon dioxide
DMC	Dimethyl carbonate

DME	1, 2-dimethoxyethane
EC	Ethylene carbonate
PC	Propylene carbonate
EMC	Ethyl methyl carbonate
BMImTFSI	1-Butyl-3-methylimidazolium bis(trifluoromethylsulfonyl)imide
EMImTFSI	1-Ethyl-3-methylimidazolium bis(trifluoromethylsulfonyl)imide
Pyr13TFSI	N-Propyl-N-methylpyrrolidinium bis(trifluoromethylsulfonyl)imide
HF	Hydrogen fluoride
TiS_2	Titanium(IV) sulfide
$LiPF_6$	Lithium hexafluorophosphate
LiTFSI	Lithium bis(trifluoromethanesulfonyl)amide
$LiClO_4$	Lithium perchlorate
LiFSI	Lithium bis(fluorosulfonyl)imide
NaFSI	Sodium bis(fluorosulfonyl)imide
NaPF6	Sodium hexafluorophosphate
NaBF4	Sodium tetrafluoroborate
NaTFSI	bis(trifluoromethylsulfonyl)imide
$NaClO_4$	Sodium perchlorate
Na_3Sb	Trisodium antimony
$CF_3SO_3^-$	Trifluoromethanesulfonate

Acknowledgement

I would like to express my special thanks to my second supervisor Dr. Stella who trained me to learn the Linux system and Density functional theory calculations as well as my principal supervisor Dr. Jacquemin who gave me the golden opportunity to do this wonderful project on the topic ‘Development of Property Prediction Methods for Sodium-ion Battery Electrolytes’. Their patience and detailed guidance helped me overcome difficulties one after another.

Then I would like to thank Peter Goodrich, Alex Neale and Sinead Murphy who helped me in the experiment part and share their opinions without reservation as well as Conrad Johnston who gave me suggestions on the simulation part.

Finally, I want to express my gratitude to my parents and all the friends who provided me continuous encouragement and support throughout my years of study in Queens University Belfast and through the process of researching and writing this thesis.

Content

Chapter 1
Introduction

1. Introduction

1.1 Background

Energy is the substantial foundation that supports the progress of human civilization. Since the first industrial revolution, human society's dependence on energy is exponentially increasing. At present, fossil fuels like coal, oil provide the main energy source. Facing the challenges of global warming and the exhaustion of fossil resources, energy sustainability has become one of the most important issues of human societies. [1]

Currently, the utilization of renewable and clean energies, such as the wind, solar, tidal and geothermal energies, is developed rapidly to generate greener sources of electricity. However, the generated electric energy is generally random and intermittent. In this situation, the development of efficient and safer energy storage technology has become an important research focus. [1]

At present, energy storage systems are classified into different categories driven by the way selected to store the energy which could be done using mechanical, electrochemical, electromagnetic and phase change energy storage systems. [2] In comparison with other systems, electrochemical energy storage system is the most promising technology, to date, mainly due to its high efficiency, low-cost investment, safety, and flexibility of its implementation and application. However, this is not a novel path to store the energy, as electrochemical energy storage was firstly studied as early as the late 1700’s to early 1800’s, and it is already more than 200 years old. [3] Sodium-sulfur, redox-flow, nickel-metal hydride and especially lithium-ion type batteries are four examples of relatively developed and more mature energy storage technologies used to date. [1]

Nowadays, metal-ion batteries (like LIBs) are widely used in portable electronic applications and play a key role in the development of electric vehicles (EV), plug-in hybrid electric vehicles (PHEVs), as well as large-scale energy storage systems. However, with the increasing demand for lithium, the limited lithium resources will face shortages as shown in Fig.1-1. Taking into account a relationship between demand/resource/cost for metal lithium, it is also necessary to develop other complementary energy storage technologies. A promising option is to introduce the sodium instead of lithium to the new generation of batteries. [4] Despite the fact that the sodium is 3.3 times heavier than lithium, the atomic weight of the Na-ion intercalation material $NaCoO_2$ (114 $g \cdot mol^{-1}$) is only 16.32% heavier than that of a convention Li-ion cathode material $LiCoO_2$ (98 $g \cdot mol^{-1}$). This leads to a smaller difference in the total gravimetric capacities of the full battery. [5] Gravimetric capacity in $mAh \cdot g^{-1}$ is the total charge capacity stored by the battery, per gram of the battery's weight.

The lithium salts are generally dissolved in organic solvents to formulate electrolytes in most commercial LIBs, which exhibit good ionic conductivities. However, this comes with the drawback of the high flammability and volatility of the formulated electrolytes. [4] The flash point of organic solvents is low and in the event of device malfunction/failure, exothermic reactions can lead to thermal runaway of cells and the pressure can build up rapidly inside the batteries, leading to explosions and burning. Sodium salts have generally a higher melting point and a larger thermal stability than lithium salts, which could be used as an advantage in terms of safety of their electrolytes in batteries. [6] Furthermore, Wei Luo et al. [7] suggest that "SIBs share a similar operation mechanism with LIBs, which potentially provides high reversibility and long cycling life", leading to a promising future for such technology.

Table 1 Physicochemical properties for Sodium and Lithium [8, 9]

Category	Sodium	Lithium
Relative atomic mass(g/mol^{-1})	22.99	6.94
Ionic radius (Å)	1.02	0.6
Eo *vs*. SHE (V)	-2.71	-3.04
First ionization energy (kJ mol^{-1})	495.8	520.2
Melting point (^{o}C)	97.70	180.50
Abundance in the earth crust (mg·kg^{-1})	23.6·10^{3}	20
Distribution	Global	70% in South America
Cost of carbonate ($/ton)	150	5000
Theoretical capacity ($MCoO_2$; mAh·g^{-1})	235	274

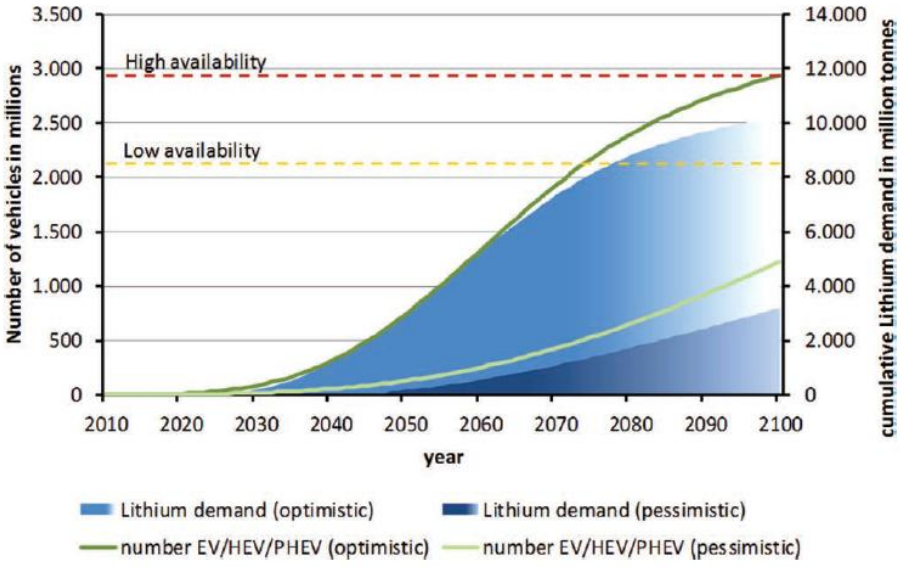

Fig1-1. Lithium demand and availability and some EVs, HEVs, and PHEVs over the time. In low availability of lithium/optimistic EV/HEV/PHEV production scenarios, lithium could run out in the near future. [9]

1.2 Sodium ion batteries

Historically, the first reversible sodium ion insertion into TiS_2 as a cathode was demonstrated at room temperature in 1980. [10] Branconnier et al. [11] published the electrochemical properties of sodium-containing layered oxides, at the same time. The studies on lithium insertion materials were at the beginning and most of the studies were focused on the development of LIBs in the late 1980's. Furthermore, the research conditions and devices such as electrolyte solutions, the binder, the separator and the glove box, were not sufficient for the treatment of the sodium metal. It was very difficult to sufficiently observe the potential as the electrode performance of the battery. In this situation, very few studies on sodium ion batteries and materials were conducted. One can see in the Figure1-2(b) that the number of scientific papers and patents on SIBs increased dramatically especially after the year 2010.

As sodium is the second-lightest (22.99 $g \cdot mol^{-1}$) [1] and second-smallest alkali metal, the sacrifice in energy density is expected to be compensated if electrochemical Na insertion/de-insertion is as efficient as that in lithium systems. For sodium metal, the electrochemical potential is −2.71 V *vs*. SHE (standard hydrogen electrode) and a theoretical specific capacity is 1116 $mAh \cdot g^{-1}$. [1] Figure 1-2(a) illustrates the basic principle of how a sodium ion battery works during charge/discharge cycles. The components and electrochemical storage mechanisms of SIBs are similar as LIBs except for the ion carriers. SIBs consist of two electrodes of sodium insertion materials for positive and negative electrodes and they are ionically connected by a sandwiched electrolyte which is generally a sodium salt (*e.g.* $NaPF_6$) dissolved in organic solvents (*e.g.* EC, PC or DMC).

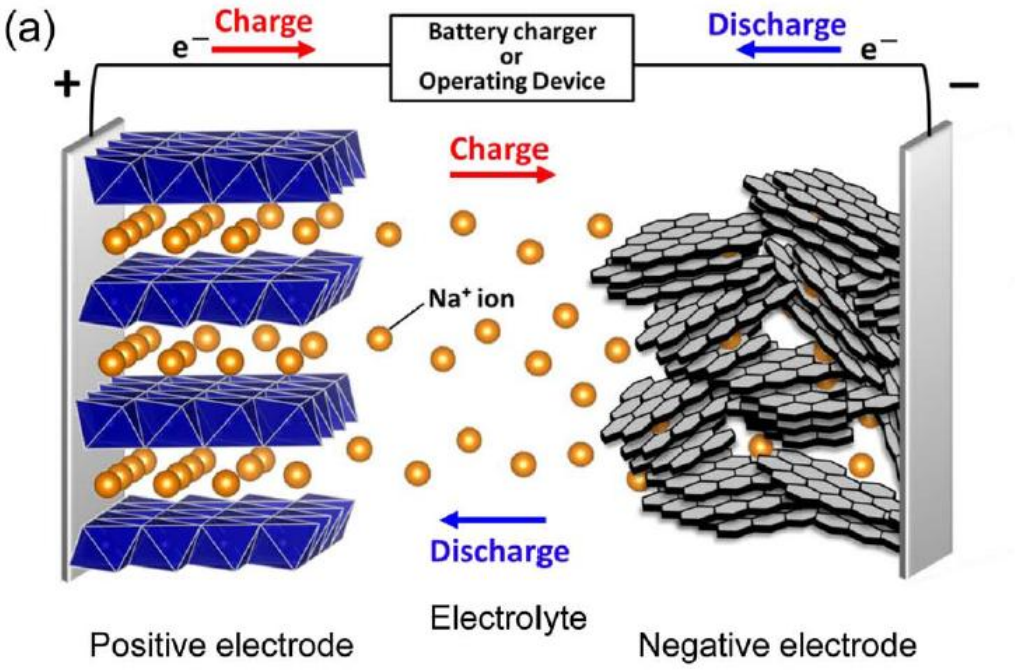

Fig1-2. Schematic illustration of Na-ion batteries. [5]

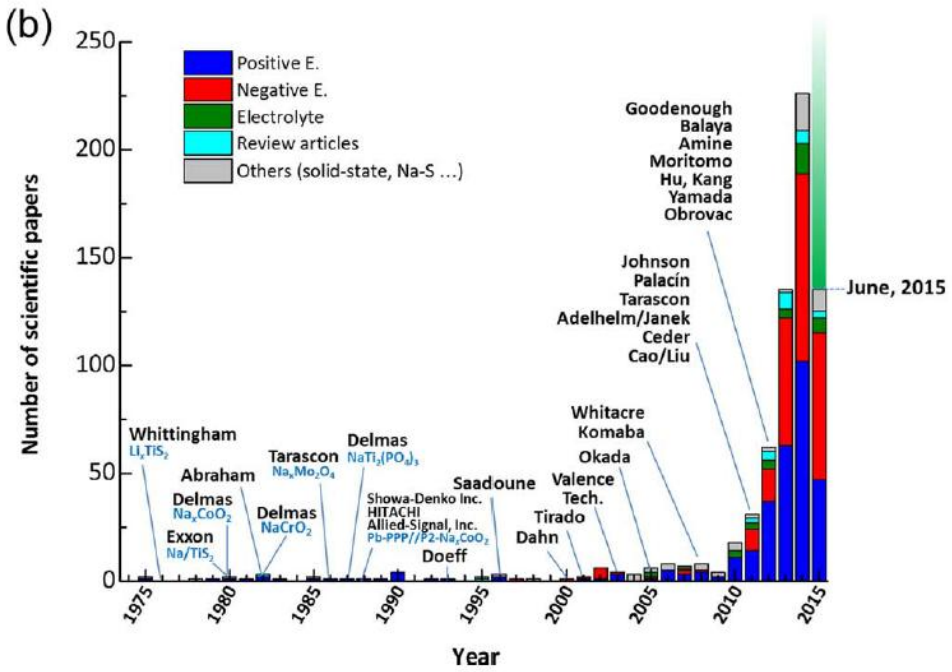

Fig 1-2 The number of publications on the sodium for energy storage devices, published in the past four decades (reproduced from the database of Web of Science, Thomson Reuters). [5]

1-2-1 Cathode materials

In the LIB cathode materials, like the layered oxide $LiMO_2$ materials (M is transition metal Co, Mn, Fe, Ni, *etc.*) are widely studied and achieved large-scale commercial applications. Similarly, layered oxide $NaMO_2$ materials [12, 13] are also intensively studied in the field of cathode materials for sodium-ion batteries. For example, Na_xCoO_2 can form several different structures of the layered oxide as shown in Figure 1-3.

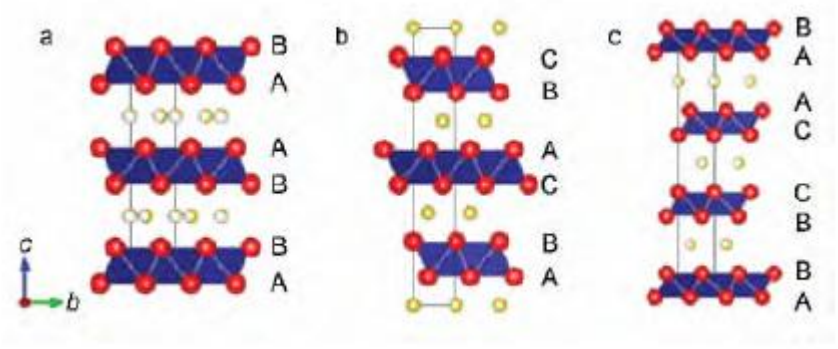

Fig 1-3 Lattice structure of several typical sodium-ion layer structure oxides:

(a) P2-$NaxCoO_2$, (b)O3-$NaxCoO_2$,(c) P3-$NaxCoO_2$. [14]

Even if the cathode materials are very similar in LIBs and NIBs, differences are generally observed on their performances. For example, in LIBs, the electrochemical performances of the $LiCrO_2$ cathode material are poor. However, the contrary performances are observed in SIBs using a cathode material $NaCrO_2$ for which a reversible specific capacity close to 120 $mAh \cdot g^{-1}$ is observed. [15, 16] However, another LIBs cathode material such as $LiMn_{0.5}Ni_{0.5}O_2$ has a reversible specific capacity of 200 $mAh \cdot g^{-1}$ during the charge and discharge cycles, [17] while the corresponding $NaMn_{0.5}Ni_{0.5}O_2$ reversible specific capacity can only reach 120 $mAh \cdot g^{-1}$ in SIB devices. [18]

In 2011, Johnson's research group reported a P_2-type layered oxide material with good electrochemical properties: $Na_{1.0}Li_{0.2}Ni_{0.25}Mn_{0.75}O_{2.35}$ ($Na_{0.885}Li_{0.17}Ni_{0.\ 21}Mn_{0.664}O_2$). [19] In addition to sodium ions in the chemical

formula of this material, one can see that there is a certain amount of lithium ions added as a protective additive in the crystal structure of the electrode material. Using this material, SIB devices can be developed with a specific capacity of 95 ~ 100 $mAh \cdot g^{-1}$ after 50 cycles at a 3.4 V (*vs* Na/Na^{+}) voltage platform.

Lithium salts containing polyanions, such as phosphates, $LiMPO_4$ (M = Fe, Mn, Co, Ni, V) have excellent properties as LIB cathode materials. [20, 21] Likewise, polyanionic sodium salts can also be used as cathode materials for SIBs. For example, the average potential of a fluorophosphate $NaVPO_4F$ is 3.7V (*vs* Na/Na^{+}) with a reversible specific capacity of 80 $mAh \cdot g^{-1}$. [22] Zelang Jian et al. found that another vanadium-containing type oxide $Na_3V_2(PO_4)_3$ also had good electrochemical performances. In a half-cell test, a reversible capacity close to 99.5 $mAh \cdot g^{-1}$ can be maintained (93% of the initial value) even after 80 cycles. [23]

AyukoKitajou et al. found that $NaFeF_3$ can be used as sodium ion battery cathode material. The material charge and discharge capacity is close to 197 $mAh \cdot g^{-1}$ and seems to be maintained even after few charge-discharge cycles. [24]

It can be seen that a number of key cathode materials have emerged with the rapid development of sodium ion battery materials in recent years. There are many similarities between sodium ion batteries and LIBs so that some of the sodium ion electrode materials can be studied from the corresponding lithium-ion electrode materials.

1-2-2 Anode materials

The graphite-type carbon anode material has been widely used in the commercial LIBs, but its irreversible capacity loss is high and there is a potential safety problem with its use. Carbon-based anodes are leading candidates for LIBs due to their low potential, high capacity, abundance, and low-cost. For the same reasons, carbon anodes are also among the most promising choices for SIBs. While graphite, the commercial anode for LIBs, does not function in SIBs due to its extremely low capacity. [25]

Hard carbon, also known as non-graphite carbon, cannot be graphitized by thermal treatment. In earlier studies, the researchers tried to apply graphite to the SIBs as electrode anode materials, but the results showed that the specific volume was very low and the electrochemical reversibility was poor. [26] The size of sodium ion is larger than the lithium ion and it is, therefore, difficult to form reversible intercalation of a high proportion of sodium compounds (such as NaC_6).

In 2000, Stevens and Dahn demonstrated that glucose-derived hard carbon exhibits a dissociation capacity of ~300 $mA \cdot hg^{-1}$. [27, 28] Inspired by their pioneering work, there have been many reports on hard carbon anodes. Luo et al. studied the impact of morphology on cycling performance of hard carbon, where carbon nanofibers derived from cellulose exhibited a stable capacity of 176 $mA \cdot hg^{-1}$ at 200 $mA \cdot hg^{-1}$ over 600 cycles. [29] Yang et al. firstly reported a Sb/C composite by ball-milling commercially available Sb particles with carbon black. After ball-milling, bulk Sb particles become fine Sb nanocrystalline particles embedded in the carbon matrix. Such a Sb/C composite structure shows a reversible capacity as high as 610 $mAh \cdot g^{-1}$, close to the full formation of Na_3Sb (660 $mAh \cdot g^{-1}$,). [30]

Alcántara R et al. reported for the first time that transition metal oxides can be used in SIBs. [31] They found that the spinel structure of $NiCo_2O_4$ has a discharge capacity of 600 $mAh \cdot g^{-1}$, followed by a reversible specific capacity of 200 $mAh \cdot g^{-1}$ and a total reversible specific capacity close to 250 $mAh \cdot g^{-1}$ in the whole cell ($Na_{0.7}CoO_2/NiCo_2O_4$). $Na_2Ti_3O_7$ has the lowest voltage among the reported oxide insertion electrode materials used for SIBs, which has a specific capacity of 178 $mAh \cdot g^{-1}$ at 0.3 V (*vs* Na/Na^+) voltage platform, and its life cycle performances are also excellent. [32]

It should be noted that SIB anode materials have some unique characteristics, not observed in LIBs, which explains the differences between these two devices. In SIBs, research is now focused on the development of novel non-graphite structure type carbon materials to design the anode materials compatible with this technology.

1.3 Outline of thesis

Chapter 1 gives a general introduction of sodium ion batteries including cathode and anode materials and their analogies and differences with those used in LIBs.

Chapter 2 describes the composition of electrolytes for sodium ion batteries and literature finding associated with the interaction between Li^+/Na^+ ion with organic carbonates.

Chapter 3 introduces the density functional theory methodologies and describes the instruments and techniques used during this work.

Chapter 4 depicts the DFT calculation results obtained during this work along with their comparisons with literature data. Then the frequency vibrations and thermodynamic data were further discussed.

In Chapter 5, these theoretical data are also assessed with experimental measurements during this study using Infrared spectroscopy and Nuclear magnetic resonance technique.

Chapter 6 summarizes this research and gives an overall conclusion.

Chapter 2
Literature review

2 Literature review

2-1 Binary/ ternary carbonate properties

Sodium ion battery electrolytes contain two components: nonaqueous solvents and sodium salts. An appropriate choice of these components can minimize the interface reactions and enhance both cell performances and safety aspects. According to Alexandre Ponrouch [33], the properties requirements for a suitable electrolyte are:

(1) Chemical stability: There should be no chemical reactions in the cell operation with the separator, electrodes materials, collectors and packaging materials and itself.

(2) Electrochemical stability: Electrolytes should have a large difference between the high and low onset potential for decomposition of oxidation and reduction, respectively

(3) Thermal stability: It should have a wide liquid range to avoid phase transitions during the operation temperature.

(4) Excellent ionic conductivity: To facilitate the Na^+ ion transport during charge/discharge cycling of the battery.

(5) The electrolyte should have low toxicity and be environmentally friendly.

Table 2.1 Carbonates properties as electrolyte solvents. [34]

Solvent	EC	PC	DMC
Structure	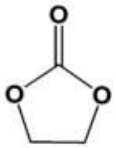	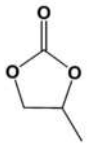	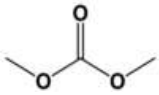
M_w	88	102	90
T_m/^oC	36.4	-48.8	4.6
T_b/^oC	248	242	91
η/mPa·s	1.90(40 ^oC)	2.53 (25 ^oC)	0.59 (20 ^oC)
ε (25^oC)	89.78	64.92	3.107
Dipole moment/ debye	4.61	4.81	0.76
T_f / ^oC	160	132	18
ρ / g·cm^{-3} (25 ^oC)	1.321	1.200	1.063

M_w=molar weight, η= viscosity, ε= dielectric constant, T_m = melting point, T_b= boiling point, T_f= flashing point, ρ= density,

Table 2-1 lists various carbonate solvents including cyclic carbonates such as ethylene carbonate (EC), propylene carbonate (PC) and linear carbonates such as dimethyl carbonate (DMC). Higher dielectric coefficient and lower viscosity are preferred. Higher dielectric coefficient indicates a strong ability to dissolve a high concentration of sodium salts. Lower viscosity facilitates ionic transport. [35] Although EC has the highest dielectric constant among these three solvents, the melting point over room temperature is a drawback. However, EC is still a widely used solvent in mixed electrolytes due to the ability to form the protective layer known as the solid electrolyte interphase (SEI) on graphitic anodes, [36] which prevents excessive electrolyte decomposition and promotes reversible intercalation into and out of the anode. [35]

PC has the second highest dielectric constant among these three solvents and a melting point lower than EC so that it can be potentially used at low temperature. In addition, both EC and PC have a high viscosity, over 1.9 mPa·s, at room temperature while DMC has a much lower viscosity, 0.59 mPa·s. The main shortcoming of DMC is its low dielectric coefficient which limits the salt solubility and also the lower flash point, which may lead to safety concerns. [37]

Since none of the pure solvents is suitable to be used alone in the SIB electrolytes. Hence, it is common to combine them to improve the electrolyte performance and design different electrolytes for different purposes.

A comparative study has been carried out by Ponrouch et al. [33] on solvent mixtures (EC:DMC, EC:DME, EC:PC and EC:Triglyme). Their electrochemical performance was found to be remarkably dependent on the solvent compositions, $NaPF_6$ with EC: PC emerging as clearly optimum with enhanced thermal stability confirmed by differential scanning calorimetry (DSC) study and wider electrochemical potential window in this research. Shinichi Komaba [38] evaluated the battery performances of Na/hard carbon cells with different electrolyte solvents of PC, EC:DEC (50:50 vol%), EC:EMC (50:50 vol%), EC:DMC (50:50 vol%), and PC:VC (98:2 vol%) containing 1 mol dm^{-3} $NaClO_4$. The cells containing the PC and the EC:DEC solutions exhibited better cycle stability over the other electrolytes tested. In 2013 Alexandre et al. [39] formulated electrolytes using EC, PC and DMC as a function of their compositions and it was found that the electrolyte: $EC_{0.45}$:$PC_{0.45}$:$DMC_{0.10}$ with 1 mol·dm^{-3} of Na-salt was the optimal electrolyte formulation for the tested SIBs.

The non-volatility and non-flammability of ionic liquids (ILs) make it suitable as additives to improve safety. The addition of the ILs such as

1-Butyl-3-methylimidazolium bis(trifluoromethylsulfonyl)imide (BMImTFSI), 1-Ethyl-3-methylimidazolium bis(trifluoromethylsulfonyl)imide (EMImTFSI), N-Propyl-N-methylpyrrolidinium bis(trifluoromethylsulfonyl)imide (Pyr_{13}TFSI) in organic carbonate EC: PC SIB electrolytes all show positive trends in several properties such as safety and thermal stability. Although the conductivity decreases due to the increasing viscosity of the electrolytes with the addition of ILs, the flash point will increase thereby improving the safety. [4] It should be pointed out that the electrolytes and additives, which perform well for Li-ion cells do not guarantee their suitability for sodium ion batteries. For example, vinylene carbonate, which is commonly used as an electrolyte additive in LIBs has been found to be detrimental for SIBs. [40]

2-2 Selection of the sodium salts for the electrolyte formulations

Apart from the solvent, the sodium salt is another important component to be carefully selected during the formulation of an electrolyte. Both components affect on the performances of the SIBs dramatically. A good sodium salt should meet the following requirements:

(1) a good salt solubility in selected solvents – to make sure enough charge carriers in the electrolytes,
(2) a good stability *vs*. reduction/oxidation – contributing to the limits of the electrochemical stability window
(3) a good chemical stability – *i.e.* within the electrolytes, the electrodes, and the current collectors,
(4) a low toxicity and other safety aspects. [6]

Both the ionic conductivity and electrochemical stability will be affected by the selection of the sodium salt used. The anion chosen will affect the interaction between sodium cation and solvents in solution. The classic approach is to look for inorganic anions based on a central atom with ligands withdrawing electron density to create a delocalized negative charge and thereby weakly coordinating anions (WCAs). [41] For sodium ion battery electrolytes, we basically find the same perspective anions used in the field of LIB electrolytes for many years: ClO_4^-, BF_4^-, PF_6^-, $CF_3SO_3^-$ (Tf^-), and $[N(CF_3SO_2)_2]^-$ ($TFSI^-$). [42] To briefly summarize, all the above anions have some drawbacks – as already observed in LIB cells; ClO_4^- is a strong oxidant and therefore more or less banned for any practical cell development; BF_4^- produces less conductive electrolytes by virtue of a stronger interaction with the cation and thus fewer charge carriers present; PF_6^- – while being the anion of choice (the best compromise candidate) for LIBs – has severe safety issues, especially at elevated temperatures and in the presence of water, which will lead to the generation of PF_5, POF_3, and HF.

The basic physicochemical properties of the most widely used sodium salts are summarized in Table 2-2. It can be seen that the molar mass of these salts does not vary significantly. Generally, sodium salts have higher melting points compared to lithium salts – which contribute to making them easier to dry than their Li equivalent. Their better thermal stability is also expected to bring in advantages for safety. However, a higher melting point could be also associated to a lower salt solubility in selected solvents. The interaction between Na^+ and the anions is weaker than that in the lithium case. [43] This is due to the sodium volume which is larger than lithium and leads to higher mobility for sodium. Compared with the lithium salts, the conductivities of sodium salts are normally higher, so that SIBs are expected to have a better performance.

Table 2-2 Physicochemical properties for sodium salts[6]

	$NaClO_4$($LiClO_4$)	$NaPF_6$($LiPF_6$)	NaTf(LiTf)	NaTFSI(LiTFSI)	NaFSI(LiFSI)
M_w[g mol^{-1}]	122.4(106.4)	109.8(93.8)	167.9(151.9)	172.1(156.1)	303.1(287.1)
T_m[^oC]	468(236)	384 (293)	300(200)	248(>300)	257(234)
σ[mS cm^{-1}]	6.4(5.6)	(3.4)	7.98(5.8)	(1.7)	6.2(5.1)

1 M NaX (LiX) in PC at 25 ^oC.

One of the most commonly used salts (about 2/3 published for sodium ion batteries paper) is sodium perchlorate ($NaClO_4$). Its popularity is due to both historical reasons and cost considerations. In addition to the safety aspect, a particular problem is that this particular molten salt is difficult to dry. The water content of the electrolytes is rarely reported in the literature. Although the powder was dried overnight at 80^{o}C under vacuum $NaClO_4$-based electrolytes usually exhibit higher levels of water content (>40 ppm) comparing to $NaPF_6$ based electrolytes (<10 ppm). [6] The second most popular salt is $NaPF_6$, which facilitates the comparison with many LIB studies. NaTFSI and NaFSI are also good candidates because their anions can create a suitable ionic medium matrix. Although NaTFSI and NaFSI probably cannot be used as a single salt for SIB electrolytes because of Al corrosion, [44, 45] their non-toxic, high thermal stability and higher conductivity are still promising.

2.3 Molecular interactions in electrolytes

After adding sodium salts into the solvent(s), the crystal lattice of sodium salt will be disrupted by the interaction between sodium salts and the chosen solvent(s). The number of solvent molecules which interact with ions in solution, is still a subject of debate in the literature, along with the nature of interactions between ions and various solvent molecules. [35, 46-52] The molecular interactions in electrolytes play a crucial role in the electrochemical properties of carbonate-based electrolytes. To have a better understanding of solvation behaviors, the DFT approach was used to investigate the molecular

interactions in electrolytes in gas phase.

Based on the computing methods and results reported by Kumar et al. [53] Bhatt et al. [47] and Masia et al. [48], results from DFT calculations are consistent with experimental data. In the research by Kumar et al. , [53] the DFT using B3PW91/6-311++G** approach was used to model sodium cation coordinated with four EC molecules. The inability of the sodium ions to be solvated by four EC molecules in an electrolyte is in sharp contrast to the case of LIBs which are known to form a stable tetrahedral structure with four EC molecules. These papers are highly relevant to the content of this research because similar solvents (EC, PC, DMC) were investigated to describe the optimised solvent structure in electrolytic solutions along with the vibration frequency analysis. [54, 55]

In the previous study, [47, 48, 56] the carbonyl oxygen of the carbonate solvents would be the most likely positions for the lithium atom. Na and Li are both alkali metals and have similar electronegativity values (0.93 for Na^+ and 0.98 for Li^+ on Pauling's electronegativity scale). [57] The Pauling radii for Li^+ and Na^+ are 60 pm and 95 pm, respectively, [58] making Na^+ about 60% larger than Li^+. Because of their alkali metal similarities, the initial assumptions of this study were that Na^+ should exhibit similar solvation characteristics to Li^+. DFT calculations performed on complexes yielded a significantly larger Na^+ carbonate distance of 2.4 – 2.5 Å compared to the Li^+ carbonate distance close to 1.9 Å. [43] Bhatt et al. [41] have carried out DFT with B3LYP functional to investigate electrolyte solvents in the vicinity of a lithium ion in the gas phase. The results are listed in Table 2.3 as a benchmark. In order to keep the number of modes consistent, the same modes were selected from the frequency results for $Li^+(EC)_n$ to compare with the isolated EC. Five modes are chosen to represent the influence on the

frequency shifts with increasing the number of EC molecules surrounding the Li^+ ion, which is demonstrated in Figure 2-1.

Table 2-3. Benchmark for isolated EC. [47]

modes	Wavenumber(cm^{-1})	Assignment
v 1	158.48	Ring C=O bending
v 2	192.8	o.p. ring bending
v 3	536.42	C=O bending
v 4	659.04	i.p. ring distortion
v 5	705.9	Ring stretching
v 6	728.45	o.p. ring C=O bending
v 7	888.6	Ring breathing
v 8	911.15	i.p. CH_2 rocking
v 9	973.34	Ring breathing
v 10	1067.41	O-C asym stretch
v 11	1098.51	O-C sym, C-C stretch
v 12	1116.39	Ring stretching
v 13	1141.05	o.p. CH_2 rocking
v 14	1241.55	i.p. CH_2 twisting
v 15	1250.11	o.p. CH_2 twisting
v 16	1419.59	i.p. CH_2 wagging
v 17	1425.7	o.p. CH_2 wagging
v 18	1508.99	o.p. CH_2 scissoring
v 19	1526.87	i.p. CH_2 scissoring
v 20	1914.81	C=O stretching
v 21	3043.64	o.p. CH_2 sym stretch
v 22	3070.85	i.p. CH_2 sym stretch
v 23	3119.83	o.p. CH_2 asym stretch
v 24	3133.05	i.p. CH_2 asym stretch

Note: *i.p.*: in phase, *o.p.*: out of phase, sym: symmetric, asym: asymmetric.

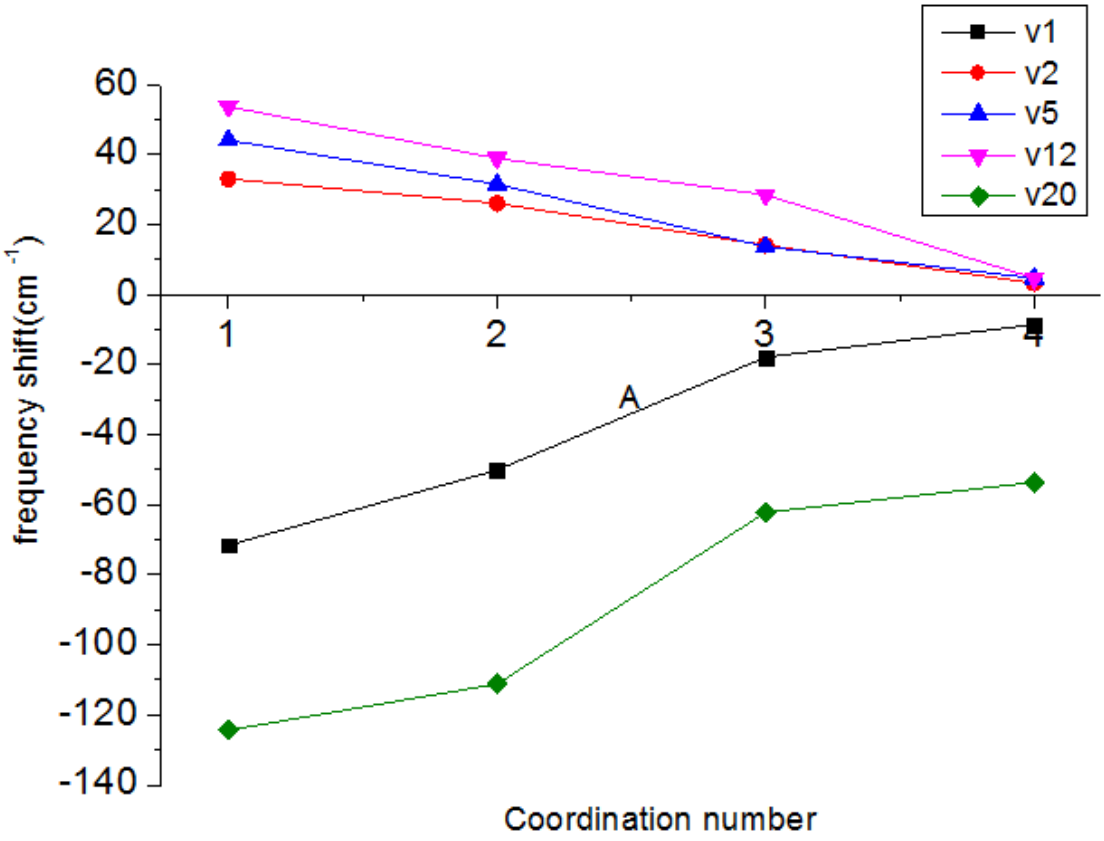

Figure 2-1. Calculated shifts for $Li^+(EC)_n$ (n = 1, 2, 3, 4) complexes as a function of coordination number. [47]

In the frequency shift analysis, the influence of lithium ion decrease with an increase in the coordination number of EC molecules in the gas phase. The thermodynamic data were further analysed to demonstrate the stability of these complexes. For example, the thermodynamic results calculated for $Li^+(EC)_n$ (n = 1, 2, 3, 4, 5) complexes and Gibbs free energy results for $Na^+(EC)_n$ (n = 1, 2, 3, 4) complexes, [53] are reported in the Tables 2-4 and 2-5, respectively. Due to the smaller size of a lithium ion, the charge density at the surface of the ion is higher than a sodium ion, and therefore, a lithium ion can solvate more molecules than a sodium ion, accounting for the larger solvation shell of lithium ions.

Table 2-4. Thermodynamic data reported for $Li^+(EC)_n$ (n = 1, 2, 3, 4, 5)complexes.

Data from reference[47] unit: kcal/mol

Complexes	Δ E	Δ H	Δ G
$Li^+(EC)_1$	51.4	-49.7	-43.5
$Li^+(EC)_2$	34.4	-38.2	-30.4
$Li^+(EC)_3$	21.6	-23.9	-12.5
$Li^+(EC)_4$	13.0	-13.5	-5.6
$Li^+(EC)_5$	11.9	-5.4	9.0

Table 2-5. Thermodynamic data reported for $Na^+(EC)_n$ (n = 1, 2, 3, 4)complexes

Data from reference [53] unit: kcal/mol

		formation free energy
	$Na^+(EC)_1$	
EC + $Na^+(EC)_1$→$Na^+(EC)_2$	$Na^+(EC)_2$	−18.70
EC + $Na^+(EC)_2$→$Na^+(EC)_3$	$Na^+(EC)_3$	−8.22
EC + $Na^+(EC)_3$→$Na^+(EC)_4$	$Na^+(EC)_4$	10.23

Recent computational studies indicate that mixtures of EC and PC have the lowest free energy of Na^+ solvation among investigated candidates. [37, 40] Using similar energetic comparisons, these research groups also find that EC is preferred over PC by Na^+. As seen from Figure 2-2, the lowest ΔG value for the interaction of Na^+ ion with pure carbonate solvents is seen for Na^+(EC) (−71.63 kcal mol^{-1}) complex, indicating EC as a better solvent in comparison with VC, PC, BC, DMC, EMC, and DEC in applications of sodium ion batteries. [37] The calculation of EC preference over PC by Na^+ is opposite to observations of EC: PC preference of Li^+, which means there may be significant differences in the Na^+ *vs*. Li^+ interactions with carbonate solvents. [59]

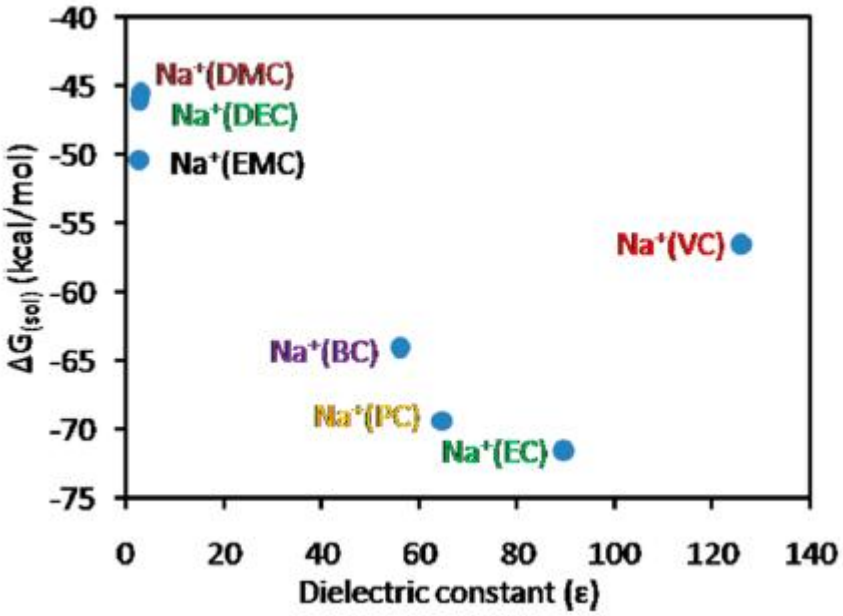

Figure 2-2 Comparison of the free energy of solvation of Na^+ ion in various acyclic/cyclic carbonates. [37]

Chapter 3
Method

3. Method

3-1 Density Functional Theory (DFT) calculation

DFT methods take electron density as a basic variable quantity and take the system energy as the function of electron density. The ground state of a system is only determined by electron density. The advantage of the DFT compared to other computational approaches based on the many-body wave functions is that electron density depends on just three spatial variables, regardless the number of the electrons in the system.

The local density approximation (LDA) can be considered to be the zero-order approximation to the semi-classical expansion of the density matrix in terms of the density and its derivatives. [60]

An improvement in the accuracy can be obtained by using Generalised Gradient Approximation (GGA) functional. In the GGA, a functional form is adopted which ensures the normalization condition and that the exchange hole is negative definite. [61, 62] The functionals depend on not only the value of the density at a point as in the LDA case but also on its gradient.

Functionals that depend explicitly on the semi-local information in the Laplacian of the spin density or of the local kinetic energy density have been developed. [63, 64] Such functionals are generally referred to as meta-GGA functionals. [65]

Hybrid functionals mix the Hartree-Fork exchange integral with GGA exchange functionals at a constant ratio, based on the concept of the adiabatic connection, which makes the Kohn-Sham energies of the

independent electron model link to those of the fully interacting electron one. [66] One of the most successful and accurate examples is the B3LYP [67] exchange-correlation functional:

$$E_{xc}^{B3LYP} = E_x^{LDA} + a_0\left(E_X^{HF} - E_X^{LDA}\right) + a_X\left(E_X^{GGA} - E_X^{LDA}\right) + E_C^{LDA} + a_c\left(E_C^{GGA} - E_C^{LDA}\right)$$

Where a_o=0.20, a_x=0.72, and a_c=0.81.[68] E_X^{GGA} and E_C^{GGA} are generalized gradient approximations: the Becke exchange functional[69] and the correlation functional of Lee, Yang and Parr[70] for B3LYP, E_X^{HF} is the Hartree-Fork exchange functional, and E_C^{LDA} is the Vosko-Wilk-Nusair (VWN) local-density approximation to the correlation functional. [71]

Hybrid functionals of this type are now very widely used in chemical applications with the B3LYP functional being the most notable. Computed binding energies, geometries, and frequencies are systematically more reliable than the GGA functionals. [65]

The computational chemistry package NWChem [72] has been used to perform the DFT calculations in this work. The B3LYP functional has been used as it achieves a good compromise between efficiency and accuracy. [73] A list of the functional and basis set selections in relevant work has been summarized in Table 3-1. Taking into account the limitation of time and computing facilities, B3LYP functional with 6-311++G** basis set has been only used for EC molecule and $Na^+(EC)_1$ complex while 6-31G* basis set has been used for the most demanding calculations.

Table 3-1. The functional and basis set used in literature

Functional	Basis set for EC	Reference
B3PW91	6-311++G**	[53]
B3LYP5	6-31G**	[46]
B3LYP	6-311++G**	[47]
B3LYP	6-31G**	[50]
M06-2X	6-311++G**	[37]

3.1.1 Geometry optimization

The previous studies of analogous systems suggest that four solvent molecules are coordinated with a lithium ion. [47, 48, 54, 55] In this work, we investigate single EC, PC and DMC molecules along with their complexes $Na^+(EC)_n$, $Na^+(PC)_n$, $Na^+(DMC)_n$ (n = 1, 2, 3, 4, 5).

Avogadro has been used to fetch the molecule structures, pre-optimize the geometries, generate the coordinate of single molecules along with their Na^+ complexes, visualize the optimized molecule structures, and molecular vibrations. [74] Thus the first step was to draw the initial geometries in Avogadro. After that, the force field MMFF94 was used to take a preliminary optimization to get more decent initial geometries. MMFF94 is one of the most popular force fields determined from ab initio calculations. The method provides high accuracy including a range of organic and drug-like molecules, across more than 500 test molecular systems. [75] By doing this, the intramolecular bond lengths and angles can be changed slightly close to practical values which relieve the computational burdens in the later geometry optimizations in NWChem. Then the coordinate of single molecules or Na^+ complexes were written in the NWChem input script along with the commands to describe the calculations. The examples of the input scripts for EC

molecule and Na^+ complex can be found in Appendix 7.1. The geometry optimization calculations were run in NWChem and all the post-processing and visualization are done with Avogadro.

3.1.2 Molecular frequencies

For a stable geometry, there should be six zero-frequency indicating three uniform molecule translations and three molecule rotations for the non-linear molecules. The rest of the frequencies should be positive and no negative frequencies are observed, giving us confidence that all the geometries are fully optimized, frequency calculations are meaningful, and the thermodynamic data are trustful.

After the geometries were optimized, the followed frequency calculations were conducted to investigate the internal interactions between the sodium cation and solvent molecules. Because the Na^+ interacts with the solvent molecules, the molecular structures will change, which leads to vibration frequency shifts. Therefore, the first step is to calculate the frequencies for the isolated molecules and Na^+ complexes respectively. The next step is to compare the frequency results between the isolated molecules and Na^+ complexes and assign the vibration modes. Finally, the frequency shifts were calculated and summarized to evaluate the dependence of shifts on the increasing coordination numbers. Avogadro provides the visualization to assign the vibration modes for isolated solvent molecules and their Na^+ complexes. An example of the frequency modes for EC is presented in Appendix 7.1.

3.1.3 Thermodynamic calculations

From the frequency calculations, NWChem provides the thermodynamic potentials at 298.15 K. The stability of Na^+ complex can be quantified using the thermodynamic data Gibbs free energies ΔG obtained through the frequency calculations. The equations which are used to calculate the thermodynamic parameters and the reactions are listed: [76]

Reaction: $ZC + Na^+(ZC)_{n-1} \longrightarrow Na^+(ZC)_n$

ΔH of reaction: $\Delta H_n = H[Na^+(ZC)_n] - H[Na^+(ZC)_{n-1}] - H[ZC]$ Equation 3-1

ΔS of reaction: $\Delta S_n = S[Na^+(ZC)_n] - S[Na^+(ZC)_{n-1}] - S[ZC]$ Equation 3-2

ΔG of reaction: $\Delta G_n = \Delta H_n - T\Delta S_n$ Equation 3-3

ZC indicates solvent molecules EC, PC, and DMC; H and S are the enthalpy and entropy, respectively. An example of the output result for thermodynamic data was presented in Appendix 7.4. Then the Gibbs free energy of the reaction is calculated by Equation 3-3 to determine the stability of the Na^+ complex and the most stable molecular coordination of Na^+.

3.2 Preparation for the electrolytes for NMR and IR measurements

For an experimental point of view, both EC and DMC cannot be used as a single solvent due to the higher melting point and lower dielectric constant for EC and DMC, respectively. Therefore, PC (hereafter, Aldrich, anhydrous, 99.7%) was chosen as a single solvent in this research, which facilitates the comparison with computed results and the data from the literature. $NaClO_4$ (Alfa aesar, anhydrous, 98~102%) was chosen as one of the most commonly used sodium salt to be dissolved in the PC at different solvent: salt molar ratios from 15:1 to 5:1. From our investigation, NaTFSI (Solvionic, anhydrous, 99.9%) is more soluble in PC than $NaClO_4$, and the higher salt concentration can reach a solvent: salt molar ratio to 3:1 at 293 K. The solvent PC was used as received. However, all sodium salts were dried under vacuum at moderate temperature (*i.e.*: 353 K) prior to being used. The sodium salts and solvent PC were then moved into glove box along with some vials and capillary tubes. The procedures for preparing the electrolytes are shown below.

1. Calculate the amount of sodium salts and solvent needed.
2. Transfer the sodium salts and solvent PC with a lab spoon and a pipette respectively into a vial according to the previously calculated molar ratio.
3. Add a clean stir bar into the vial and put the vial on the magnetic stirrer.
4. Close the lid and open the magnetic stirrer to speed up the dissolution process.
5. Wait until the solution turns to clear and transparent.
6. Transfer about 1 ml solution into a capillary for ^{1}H, ^{13}C NMR, and 1 ml solution into another capillary for ^{23}Na NMR. The rest of solvent in the vial is prepared for IR measurement.
7. Seal the capillaries and vial with both lids and parafilm.

8. Clean the table and move the waste out of the glove box.

Repeat the procedures and prepare the electrolytes at different concentrations. The detailed composition of the electrolytes can be found in Appendix 7.5. It only takes no more than half an hour to dissolve NaTFSI in PC. However, it takes more than five days to dissolve $NaClO_4$ in PC at a high concentration such as 1.7 mol/kg. All electrolytes were made in a dry glove box (with an oxygen and water content lower than 1 ppm; which is filled with pure argon) to avoid water contamination.

3.3 Infrared spectroscopy

Infrared spectroscopy is used to study some characteristic vibrational frequencies of a molecule from the analysis of the fingerprint frequencies. The user can confirm the bond length, bond angle and the stereochemical structure of the molecules. The strength of the chemical bond can be also obtained and the thermodynamic data can be quantified from the vibrational frequencies.

One of the advantages of infrared spectroscopy is that only a little amount of samples are needed, which can be as low as 50 picograms. [77] All the solid, liquid or gaseous state are possible to be studied using this technique. The identification of the substance is possible due to the unique absorption frequency of each functional group. Although Infrared spectroscopy is powerful in identifying functional groups of a particular structure, it still needs to be combined with other techniques such as Raman spectroscopy to present a complete image of the chemical structure of the system. There are some limitations; for example, some vibrational modes are not IR active. Moreover, some inorganic substances such as metal oxides cannot be measured because they are beyond normal frequency range. [78]

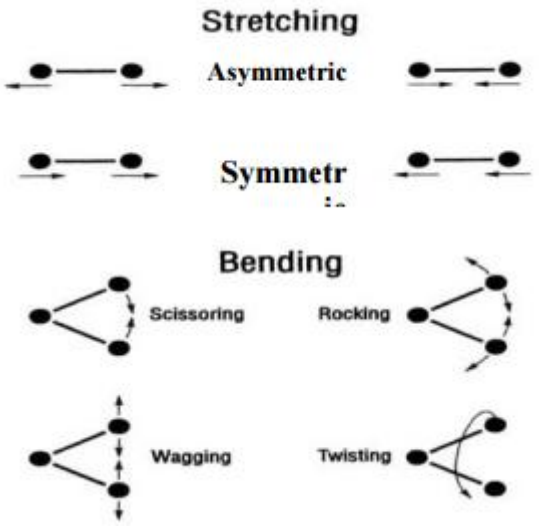

Figure 3-1: Typical stretching and bending vibrational modes. [79]

Figure 3-1 shows the stretching and bending modes. The IR method was performed in this research as a complementary method to validate the functional group in the electrolytes and compare the vibrations with the computed Infrared spectroscopy. Infrared spectra were recorded in the 500–4000 cm^{-1} range on a PerkinElmer Spectrum 100 FT-IR Spectrometer.

The software package PerkinElmer Spectrum is installed on the computer connected to an FT-IR spectrometer, which is used to collect data and analyze the spectra. The procedures for scanning the infrared spectrum are shown below.

1. Make sure the FT-IR spectrometer is on.
2. Open and log in the software Spectrum.
3. Check the basic state of the instrument by observing the energy level of the instrument and the single beam background spectrum.
4. Set the scanning conditions with scanning region: 500–4000 cm^{-1}, accumulation: 4 times, resolution: 2cm^{-1}

5. Use acetone to clean the sample disk and scan the background.
6. Take a drop from the vial containing the electrolytes with a dropper and drop it in the middle of the sample disk.
7. Scan the spectrum and save it as the .asc file.
8. Use acetone to clean the sample disk for next measurement.
9. After completing all measurements, clean the table, discard waste, and turn off the power.

It is important to confirm that the basic state of the instrument is normal before starting the measurement. If the energy value suddenly changes (10% or more) or a continuous decline occurs, check the instrument status before testing. The purpose of scanning the background is to minimize the influence of the environment and get more accurate results. It is required to scan the background once every 5 measurements. All the post-processing and visualization are done with Orginal 8.1.

3.4 Nuclear magnetic resonance

Nuclear magnetic resonance (NMR) is a widely-used method to determine chemical structures, molecular interactions as well as configurational information in details. [40] NMR measurements are mainly classified into two different types: in solution (mostly in deuterated solvents) and in solid-state. The measurements in solution are preferred because they require a smaller amount of substance and give a larger signal than in solid state.

Nuclear magnetic resonance is caused by the nuclear spin. Different nuclei give different NMR signals. In NMR spectroscopy, the chemical shift expresses the difference in the resonance frequency of a given nucleus compared to internal standards. In practice, this difference is divided

by the operating radio-frequency of the instrument and the Chemical shift δ is expressed in parts per million (ppm), downfield from Tetramethylsilane (TMS) : [80]

$$\delta = \frac{\nu\text{sample} - \nu_{\text{TMS}}}{operating\ frequency}$$

where νsample is the absolute resonance frequency of the sample and ν_{TMS} is the absolute resonance frequency of the standard TMS, measured in the same applied magnetic field B_0.

The chemical shift is influenced by the inductive effect, van der Waals deshielding effect, anisotropic effect, and hydrogen bonding effect. The different chemical environments give different chemical shifts, from which the user can infer the chemical structure and bonding to a certain extent. In this thesis, proton, carbon, and sodium NMR spectra were recorded at room temperature on a Bruker-Spectrospin B-ACS 60 spectrometer and Bruker ASCEND 600 MHz NMR magnet system at 300 MHz and 600 MHz, respectively. This method has been used in the experiment of this thesis to validate the structures and interactions in the electrolytes. The samples were prepared in the capillaries and submitted to NMR measurements. All the post-processing and visualization are done with software MestReNove.

Chapter 4 DFT
Results and discussion

4 DFT results and discussion

4.1 Structure results from ab initio calculations

The geometry of a single EC molecule in the gas phase was optimized using NWCHEM at the B3LYP level with the 6-311++G** basis set. To depict the accuracy of the selected software and method, we present a comparison of our findings against the benchmark calculations and experimental data in Table 4-1. Our calculations are consistent with both benchmark results and experimental data available in the literature. In fact, our determined bond angle values (*ie*: O4-C2-O1) and the dihedral angles (*ie:* O3-C2-O1-C6) are closer to the experimental data than the reported simulation data. After this preliminary validation, we are confident that the software NWChem and method DFT/B3LYP used are accurate and could be then used to optimize the structure of all the selected pure solvents: EC, PC and DMC and their complexes with Na^+.

Concerning the geometry of the EC molecule, Angell et al. suggested a planar configuration for EC at early experimental results; Here the dihedral angle of C2-O3-C5-C6 and O3-C5-C6-O1 showed a nonplanar ring structure, which is consistent with Wang et al., [81] Fortunato et al., [82] and Matias et al., [83] who also suggested that EC has a nonplanar ring geometry. [48] It is worth noting that the coordination with Na^+ changes the EC conformation slightly toward a more planar geometry: the C2-O3-C5-C6 dihedral angle reduces from 20.1°to 15.2° and the O3-C5-C6-O1 dihedral angle decreases from 23.7°to 17.7° for the same level of theory. (Table 4-1, second and third column). The bond distortion induced by the coordination is also evident in the internal coordinates. Namely, the optimized carbonyl bond length increases from 1.19 Å in the isolated EC molecule to 1.21 Å in the complex. The C5-C6

and the C-H bond lengths do not undergo any significant distortions. This is easily explained by the proximity of sodium to the carbonyl oxygen and the distance from C5 and C6.

Table 4.1 Comparison of EC structural parameters against benchmark calculations and experimental data (distances unit in Å, angles unit in degree).

	EC (6-311++G**)	$Na^+(EC)_1$ (6-311++G**)	Benchmark (6-311++G**)	Experiment data [47]
Bond length				
O4-C2	1.19	1.21	1.19	1.20
C2-O3/C2-O1	1.36	1.33	1.36	1.34
O1-C6/O1-C5	1.43	1.46	1.44	1.46
C5-C6	1.53	1.53	1.53	1.52
C-H	1.09	1.09	1.09	1.09
Bond angle in degree				
O4-C2-O1	124.9	123.5	124.95	124.17
C2-O3-C5	109.4	109.2	109.43	108.71
O3-C5-H10	108.7	107.6	108.78	108.30
O3-C2-O1	110.1	113.0	110.10	111.67
H9-C5-H10	109.9	110.3	109.81	110.82
C5-C6-H7	112.6	113.5	112.55	113.94
Dihedral angle in degree				
O4-C2-O3-C5	171.6	173.7	171.78	N/A
C2-O3-C5-C6	20.1	15.2	19.70	21.25
C2-O3-C5-H9	141.0	136.1	140.66	141.81
O3-C5-C6-O1	-23.7	-17.7	-23.21	-24.80
O3-C2-O1-C6	-8.4	-6.3	-6.18	-8.73
O3-C5-C6-H8	-141.0	-134.3	-140.56	-154.32

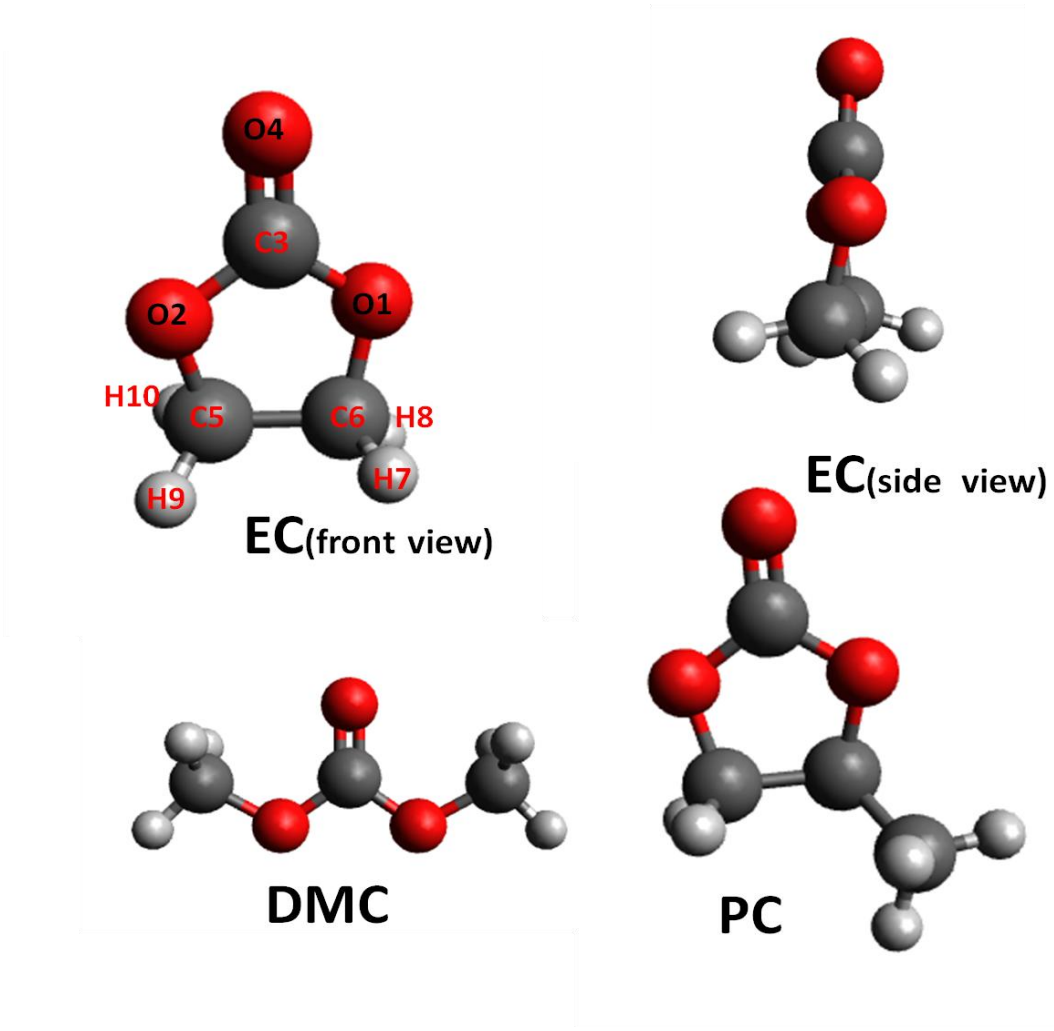

Fig. 4-1. Optimized geometry of single EC, PC and DMC molecule.

In which oxygen, carbon, and hydrogen are rendered in red, black and gray, respectively.

To have a look at how the single EC molecule is affected by the coordination with sodium ion, the optimized geometry of the $Na^{+}(EC)_n$ (n = 1, 2, 3, 4, 5) complexes have been obtained starting from the configurations where the sodium ion is close to the carbonyl oxygen. This configuration was suggested by a previous study, [54] which is also validated by the experimental spectroscopies from this research. Because of high demanding of computational resource for 6-311++G**, a relatively smaller basis set 6-31G* was used instead to optimize the geometry of the complexes. Our results are summarized in Table 4.2.

The complexes mentioned above are highly symmetrical for $Na^+(EC)_n$ (n = 1, 2, 3), which leads to an identical value of the internal coordinates. However, the geometry for $Na^+(EC)_4$ and $Na^+(EC)_5$ are less symmetrical, which results in slightly different internal coordinates. For example, the biggest difference observed in bond length is O4-C2 in $Na^+(EC)_5$ complex, which varies from 1.206 Å to 1.213 Å for different EC molecules. Here the average values are reported. The most affected internal coordinate occurs in $Na^+(EC)_1$ complex where the O3-C5-C6-O1 dihedral angle achieves its minimum and the O4-C2 bond is maximally stretching. With the increasing number of EC molecules, the distance between sodium and carbonyl oxygen increases and its geometry seems to approach the isolated EC molecule. The O1-C2-O3-O4 group remains its planarity.

Table 4.2 Geometry Results for EC and Its Complexes with Sodium at B3LYP/6-31G* level (distances unit in Å, angles unit in degree)

	EC	$Na^+(EC)_1$	$Na^+(EC)_2$	$Na^+(EC)_3$	$Na^+(EC)_4$	$Na^+(EC)_5$
Bond length						
Na-O4	N/A	2.102	2.137	2.188	2.251	2.356
O4-C2	1.194	1.222	1.217	1.212	1.208	1.210
C2-O3/C2-O1	1.364	1.328	1.333	1.339	1.345	1.131
O1-C6/O3-C5	1.434	1.454	1.451	1.447	1.444	1.444
C5-C6	1.535	1.539	1.538	1.537	1.536	1.536
C-H	1.092	1.09	1.09	1.093	1.094	1.09
Bond angle in degree						
O4-C2-O1	124.9	123.4	123.6	123.9	123.9	124.1
C2-O3-C5	109.5	109.3	109.3	109.3	109.3	109.5
O3-C5-H10	108.9	107.7	107.9	108.3	108.4	108.3
O3-C2-O1	110.2	113.2	112.8	112.2	111.8	111.9
H9-C5-H10	109.5	110.1	110	109.9	109.9	109.9
C5-C6-H7	112.6	113.6	113.5	113.3	113.1	114
Dihedral angle in degree						
O4-C2-O3-C5	172.1	174.6	174.1	173.5	173.1	175.1
C2-O3-C5-C6	18.9	13	14.1	15.4	16.4	17
C2-O3-C5-H9	139.9	133.9	135	136.4	137.4	137.8
O3-C5-C6-O1	-22.3	-15.1	-16.5	-18.1	-19.2	-22.3
O3-C2-O1-C6	-7.9	-5.4	-5.9	-6.4	-6.7	-6.8
O1-C2-O3-O4	180	180	180	180	179.9	180
O3-C5-C6-H8	-139.8	-131.8	-133.2	-135	-136.3	-136.4

4.2 Geometry optimizations

We used Avogadro [74] to generate and pre-optimize the geometry of each complex using MMFF94 force field. [75] Then the complex geometry was refined using NWCHEM. [72] All the post-processing and visualization are done with Avogadro. Figures 4-2, 4-3, 4-4 and 4-5 illustrate the geometries of $Na^+(ZC)_n$ (n = 1, 2, 3, 4, 5) complexes which are fully optimized and investigated in this work. Their geometry coordinates are given in Appendix 7.2.

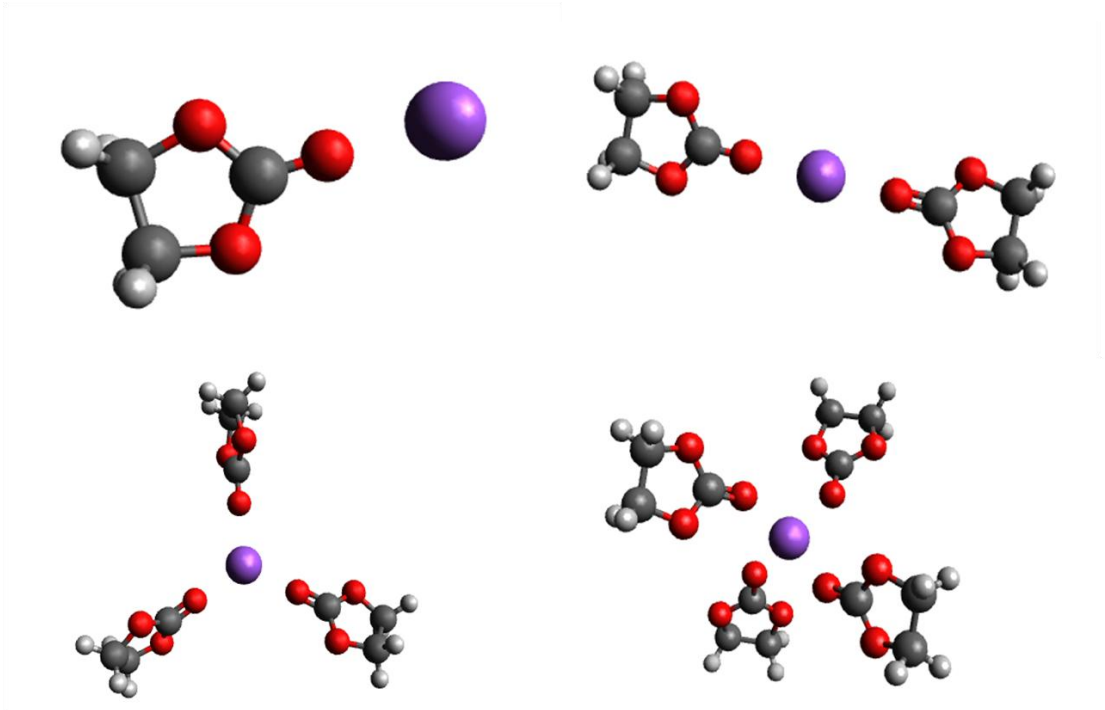

Fig. 4-2 Geometries of Na^+ with 1-4 EC molecule(s) at B3LYP/6-31G* level

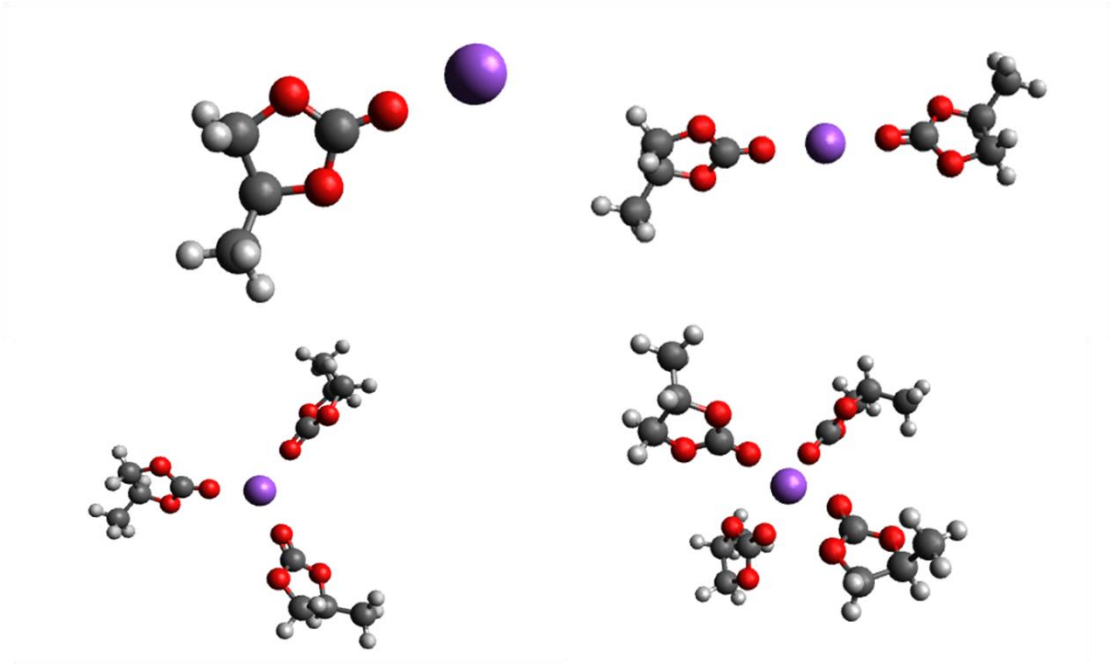

Fig. 4-3 Geometries of Na^+ with PC 1-4 molecule(s) at B3LYP/6-31G* level

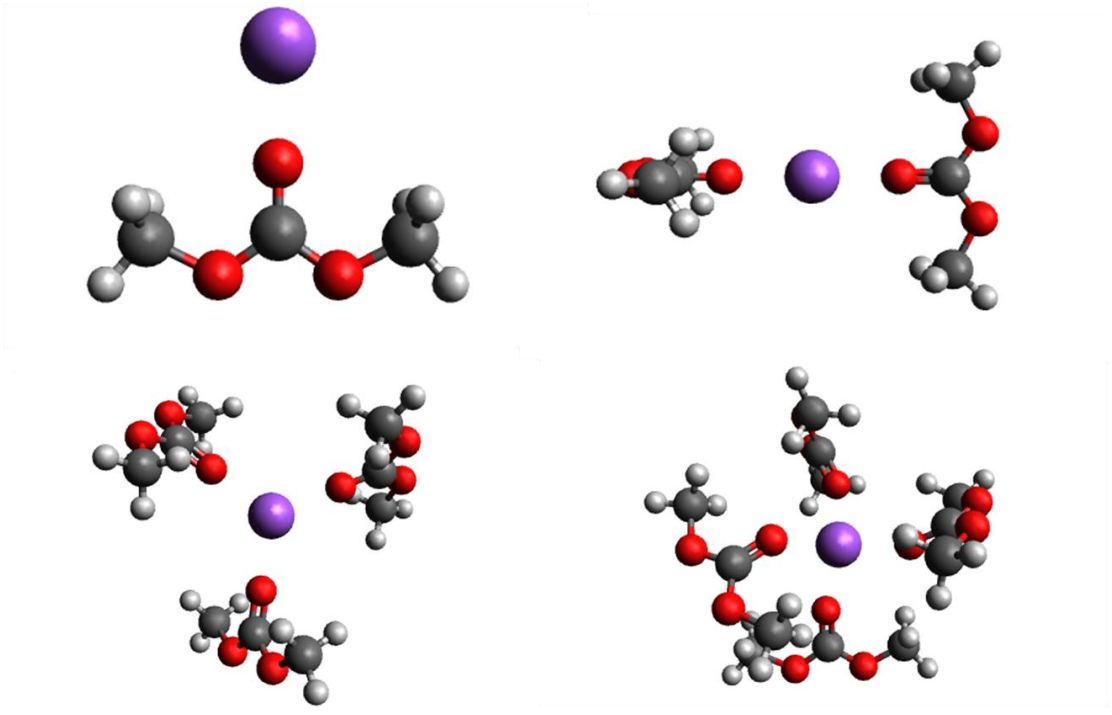

Fig. 4-4 Geometries of Na^+ with1-4 DMC molecule(s) at B3LYP/6-31G* level

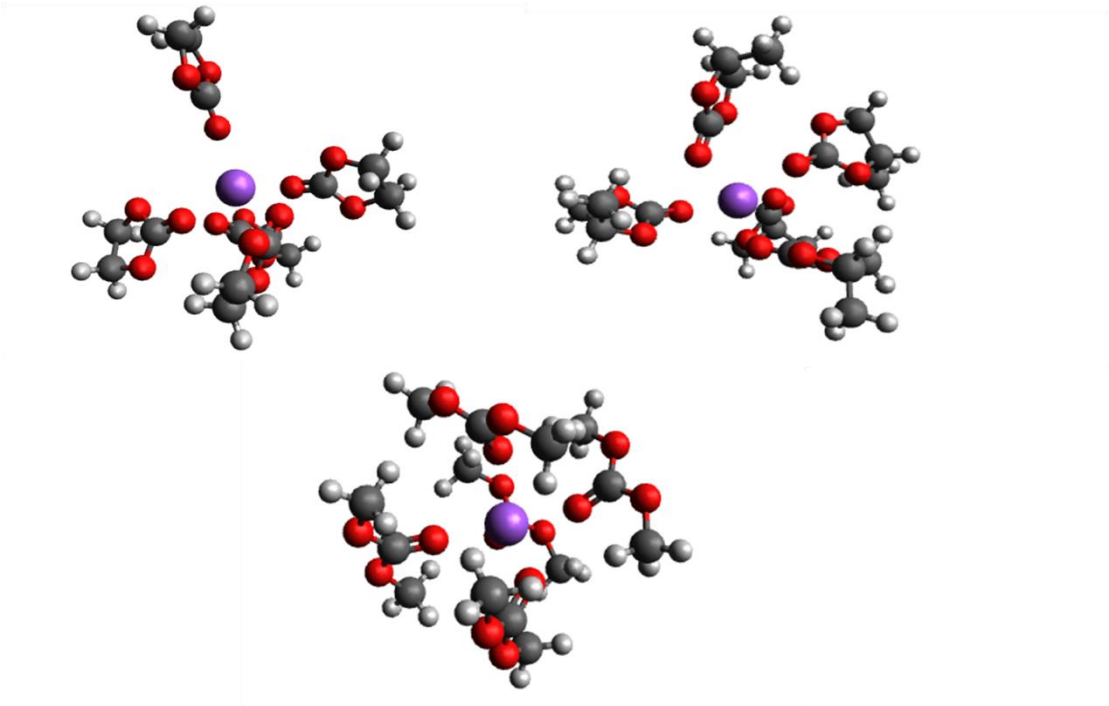

Fig. 4-5 Geometries of Na^+ with 5 EC (top left), 5 PC (top right), 5 DMC (bottom) at B3LYP/6-31G* level.

All the geometries are fully optimized at B3LYP functional with the 6-31G* basis set. According to the Figure 4-2, 4-3 and 4-4, the Na^+ complexes give similar structures for similar coordination. In the $Na^+(DMC)_1$ and $Na^+(EC)_1$ complexes, the sodium, oxygen, and carbon connected by the double bond are in a straight line while the value of the Na-O=C angle in the $Na^+(PC)_1$ complex is 178.2°. This small difference can be explained by the asymmetry of PC molecule.

In the case of the $Na^+(ZC)_2$ complexes, the molecular planes of the two PC are nearly perpendicular to each other, while the two DMC are strictly perpendicular to each other. However, two EC is neither perpendicular to each other or in the same plane. The dihedral of O-Na-O was found to be 179.2°, 178.3° and 180.0° in $Na^+(EC)_2$, $Na^+(PC)_2$ and $Na^+(DMC)_2$ complexes, respectively.

In all the $Na^+(ZC)_3$ complexes, three molecules formed a triangle. The $Na^+(ZC)_4$ complexes demonstrate tetrahedral complexations. Although the geometry optimization for $Na^+(ZC)_5$ complexes are converged, their structures are less regular. In the case of $Na^+(ZC)_2$ and $Na^+(ZC)_3$ complexes, the differences of the distance between Na^+ and carbonyl oxygen are negligible. However, for $Na^+(ZC)_4$ and $Na^+(ZC)_5$, the differences of the distance between Na^+ and carbonyl oxygen have been changed to a greater degree. The distance summary is shown in Table 4-3. Arthur V. Cresce et al. [43] pointed that Na^+–carbonate distance can be yielded as larger as 2.4–2.5 Å, which also gives us confidence that they are still coordinated together when increasing the coordinated molecules to five.

Table 4-3 Distances between Na^+ or Li^+ [52] and carbonyl oxygen

Complex O_c - Na distance (Å)					
	$O_{c,1}$	$O_{c,2}$	$O_{c,3}$	$O_{c,4}$	$O_{c,5}$
$Na^+(EC)_1$	2.102	N/A	N/A	N/A	N/A
$Na^+(EC)_2$	2.137	2.137	N/A	N/A	N/A
$Na^+(EC)_3$	2.188	2.188	2.190	N/A	N/A
$Na^+(EC)_4$	2.250	2.250	2.251	2.251	N/A
$Na^+(EC)_5$	2.238	2.376	2.376	2.396	2.396
$Na^+(PC)_1$	2.097	N/A	N/A	N/A	N/A
$Na^+(PC)_2$	2.134	2.134	N/A	N/A	N/A
$Na^+(PC)_3$	2.186	2.186	2.186	N/A	N/A
$Na^+(PC)_4$	2.239	2.254	2.254	2.256	N/A
$Na^+(PC)_5$	2.268	2.326	2.350	2.369	2.449
$Na^+(DMC)_1$	2.104	N/A	N/A	N/A	N/A
$Na^+(DMC)_2$	2.137	2.137	N/A	N/A	N/A
$Na^+(DMC)_3$	2.186	2.186	2.187	N/A	N/A
$Na^+(DMC)_4$	2.242	2.245	2.247	2.273	N/A
$Na^+(DMC)_5$	2.314	2.318	2.322	2.362	2.384
$Li^+(EC)_4$	1.947	1.947	1.947	1.947	N/A
$Li^+(PC)_4$	1.938	1.947	1.947	1.951	N/A
$Li^+(DMC)_4$	1.940	1.941	1.953	1.978	N/A

Both of the sodium and lithium complexes are optimized at B3LYP 6-31G* level by NWCHEM. The structure and distances are visualized by Avogadro. Since the complex of $Li^+(ZC)_5$ were not converged in a previous MPhil student thesis, only the biggest distances observed in $Li^+(ZC)_4$ complex were presented here. [52] The distances between sodium ion and carbonyl oxygen are larger than those in lithium complexes in all the cases, which indicate that the sodium ion had weaker interaction with organic carbonates compared to lithium ion. [43]

4.3 Frequency calculations

The motivation of the frequency calculation was to have a better understanding of the interactions between the Na ion and the coordinated molecules. Moreover, the frequency calculation was studied in order to quantify the stability of the complexes. First of all, the result of single EC frequency calculation was compared with data from literature in Table 4-4. In order to validate the computational approach and its accuracy, the vibration assignments and the values for the frequency were further discussed. The vibration assignments and the frequency shifts comparison have been visualized with Avogadro. Some of the vibrations (*e.g.*:v1, v2, v20) are closer to the experimental data, which were presented in Table 4-5. [48] The frequency values are not identical because the optimized geometries of EC are slightly different which affect the intermolecular vibrations. Given the consistency of data reported in Table 4-4, the same approach was used to determine the behaviour of all the complexes.

In Table 4-4, the different vibration frequencies were observed in our calculation against the benchmark results. The biggest difference was the ring C=O bending, which shifted from 199.31 cm^{-1} in our calculation to 158.48 cm^{-1} in the benchmark. These different results were caused by the different internal molecular structures reported in Table 4-1 (*ie*: the dihedral angles O3-C2-O1-C6). The Gaussian 09 software was used in the benchmark. [84] The Gaussian implementation of B3LYP used VWN 3 local correlation functional. While in NWChem, it used VWN formula 1 RPA local correlation in B3LYP. In addition, the grid sizes, coordinate systems, geometry optimizers, and convergence criteria were different in these two calculations. So the results turned out to be slightly different, even though both of the calculation were using B3LYP/6-311++G** basis set

Table 4-4 Frequencies and mode assignments

compared against benchmark results [47]

	This work 6-311++G**		Reference 6-311++G**	
modes	$\tilde{\nu}$ (cm^{-1})	assignment	$\tilde{\nu}$ (cm^{-1})	assignment
v1	196.58	Ring bending	158.48	Ring C=O bending
v2	199.31	Ring C=O bending	192.80	o.p. ring bending
v3	526.85	C=O bending	536.42	C=O bending
v4	691.87	i.p. ring distortion	659.04	i.p. ring distortion
v5	719.53	Ring stretching	705.90	Ring stretching
v6	774.67	o.p. ring C=O bending	728.45	o.p. ring C=O bending
v7	890.55	Ring breathing	888.60	Ring breathing
v8	891.38	i.p. CH_2 rocking	911.15	i.p. CH_2 rocking
v9	964.59	Ring breathing	973.34	Ring breathing
v10	1052.42	O–C asym stretch	1067.41	O–C asym stretch
v11	1091.59	O–C sym, C–C stretch	1098.51	O–C sym, C–C stretch
v12	1114.67	Ring stretching	1116.39	Ring stretching
v13	1153.83	o.p. CH_2 rocking	1141.05	o.p. CH_2 rocking
v14	1238.23	i.p. CH_2 twisting	1241.55	i.p. CH_2 twisting
v15	1245.64	o.p. CH_2 twisting	1250.11	o.p. CH_2 twisting
v16	1387.58	i.p. CH_2 wagging	1419.59	i.p. CH_2 wagging
v17	1400.56	CH_2 wagging	1425.70	o.p. CH_2 wagging
v18	1521.81	o.p. CH_2 scissoring	1508.99	o.p. CH_2 scissoring
v19	1530.19	i.p. CH_2 scissoring	1526.87	i.p. CH_2 scissoring
v20	1893.55	C=O stretching	1914.81	C=O stretching
v21	3051.05	o.p. CH_2 sym stretch	3043.64	o.p. CH_2 sym stretch
v22	3055.54	i.p. CH_2 sym stretch	3070.85	i.p. CH_2 sym stretch
v23	3120.34	o.p. CH_2 asym stretch	3119.83	o.p. CH_2 asym stretch
v24	3132.20	i.p. CH_2 asym stretch	3133.05	i.p. CH_2 asym stretch

Table 4-5 Comparison between Computed results and Experiment data

		This work 6-311++G**	Reference 6-311++G**[47]		IR Experiment data [48]	
modes	$\tilde{\nu}$ (cm^{-1})	assignment	$\tilde{\nu}$ (cm^{-1})	assignment	$\tilde{\nu}$ (cm^{-1})	assignment
v 1	196.58	Ring bending	158.48	Ring C=O bending	215	Ring puckering
v 2	199.31	Ring C=O bending	192.80	o.p. ring bending	230	Ring puckering
v 20	1893.55	C=O stretching	1914.81	C=O stretching	1868	C=O stretching

The $Na^+(EC)_1$ has three modes compared to a single EC because the sodium ion is involved. Therefore, those three additional vibrations represent the interactions between sodium ion and the coordinated molecules. To make it easier to compare the computed vibrational frequencies of the single EC with $Na^+(EC)_n$ complexes, the notation ν_n present the 24 modes of EC to keep the same number of vibrations as before and ϖ_n present those three modes where sodium is involved. The frequency comparison between the interacted $Na^+(EC)_1$ and isolated EC was displayed in Table 4-6.

TABLE 4-6: Comparison between EC and $Na^+(EC)_1$ at B3LYP/6-31G* level

	EC	$Na^+(EC)_1$	Assignment	Shift (cm^{-1})
ν1	160.08	112.10	Ring C=O bending	-47.98
ν2	189.78	220.16	ring bending	30.38
ν3	519.92	513.52	C=O bending	-6.40
ν4	697.23	724.44	i.p. ring distortion	27.21
ν5	720.81	752.33	Ring stretching	31.52
ν6	759.62	773.16	o.p. ring C=O bending	13.53
ν7	896.14	921.80	ring breathing	25.66
ν8	897.05	878.04	i.p. CH_2 rocking	-19.00
ν9	970.97	989.57	Ring breathing	18.60
ν10	1069.01	1029.03	O–C asym stretch	-39.98
ν11	1109.30	1124.17	O–C sym, C–C stretch	14.87
ν12	1144.82	1253.20	Ring stretching	108.38
ν13	1168.80	1160.44	o.p. CH_2 rocking	-8.36
ν14	1247.43	1239.36	i.p. CH_2 twisting	-8.08
ν15	1255.58	1255.60	o.p. CH_2 twisting	0.02
ν16	1404.09	1406.94	i.p. CH_2 wagging	2.85
ν17	1421.58	1467.15	CH_2 wagging	45.57
ν18	1547.60	1546.42	o.p. CH_2 scissoring	-1.18
ν19	1556.57	1554.69	i.p. CH_2 scissoring	-1.88
ν20	1934.91	1833.69	C=O stretching	-101.22
ν21	3073.12	3117.45	o.p. CH_2 sym stretch	44.33
ν22	3076.32	3118.78	i.p. CH_2 sym stretch	42.45
ν23	3140.75	3177.67	o.p. CH_2 asym stretch	36.93
ν24	3152.59	3191.42	i.p. CH_2 asym stretch	38.84
ϖ1		112.10	C-O-Na^+ bending	
ϖ2		220.16	ring O-Na^+ bending	
ϖ3		513.52	ring O-Na^+ stretching	

Some of the frequencies for the isolated EC are affected after coordinating with the sodium ion. Both red and blue shifts are observed in Table 4-6. The most affected frequency shifts occur in the ring stretching and carbon-oxygen double bond stretching modes; a blue shift of up to 108.4 cm^{-1} for the (ν12) ring stretching mode and a red shift up to 101.2 cm^{-1} for the C=O stretching mode (ν20) are found.

Interestingly, the substantial shift of some modes may lead to a reordering of frequencies. Two crossing of frequencies were observed. ν12 and ν13 modes for single EC molecules were assigned as CH_2 rocking and the ring stretching vibrations respectively, which showed an inverted order when introducing a sodium cation in the system. v7 mode was assigned as ring breathing, which shifted to a higher frequency in the sodium complex. On the other hand, the v8 assigned as in the plane CH_2 rocking was shifted to lower frequencies, leading to the crossing of their frequencies.

All the frequencies for $Na^+(EC)_n$ complexes were obtained with the same approach and presented in Table 4-7 keeping the same number of vibrations as those in an isolated EC molecule after selection.

Table 4-7 Results of small basis set (6-31G*) frequencies calculations for EC and its complexes with sodium

modes	EC	$Na^+(EC)_1$	$Na^+(EC)_2$	$Na^+(EC)_3$	$Na^+(EC)_4$	$Na^+(EC)_5$
v1	160.08	220.16	216.44	212.10	206.80	197.20
v2	189.78	112.10	120.72	131.23	139.68	151.98
v3	519.92	513.52	515.55	516.22	521.96	523.53
v4	697.23	724.44	720.28	715.08	710.80	706.73
v5	720.81	752.33	748.94	743.70	736.58	731.10
v6	759.62	773.16	772.08	769.24	767.42	772.40
v7	896.14	921.80	921.86	920.63	917.54	918.32
v8	897.05	878.04	881.80	886.26	889.42	893.32
v9	970.97	989.57	986.41	982.71	979.50	978.37
v10	1069.01	1029.03	1036.40	1044.30	1050.24	1050.43
v11	1109.30	1124.17	1121.20	1117.62	1114.09	1111.40
v12	1144.82	1253.20	1232.09	1217.84	1204.66	1204.01
v13	1168.80	1160.44	1161.80	1163.27	1164.38	1164.74
v14	1247.43	1239.36	1248.76	1247.39	1247.10	1247.92
v15	1255.58	1255.60	1255.91	1256.20	1256.28	1258.11
v16	1404.09	1406.94	1406.59	1406.24	1405.81	1406.37
v17	1421.58	1467.15	1458.29	1448.62	1441.70	1441.90
v18	1547.60	1546.42	1546.55	1546.74	1546.76	1544.01
v19	1556.57	1554.69	1555.14	1555.50	1555.60	1553.13
v20	1934.91	1833.69	1850.86	1869.94	1878.95	1863.32
v21	3073.12	3117.45	3111.99	3104.79	3098.83	3096.81
v22	3076.32	3118.78	3113.59	3106.78	3101.14	3107.08
v23	3140.75	3177.67	3173.23	3167.48	3162.79	3163.88
v24	3152.59	3191.42	3186.74	3180.70	3175.69	3177.60

From the Table 4-7, all the main vibration modes in different Na^+ complexes were summarized to compare with the single EC molecules. It is expected frequency shifts will uniformly decrease as the distortion of EC decreases with the increasing coordination number of EC because the charge density will be shared by more EC molecules, some of the frequencies remain stable, and no obvious shifts were observed from v14 to v19 modes.

Those above v14 to v19 modes and those from v21 to v24 modes were CH_2 vibrations, which were less analysed here. In order to have a straightforward observation, five modes were chosen to represent the behaviour of Na^+ complexes. These are two low-frequency molecule bending modes, two most affected molecule stretching modes and C=O stretching mode.

With respect to the explanation of Table 4-7, the number of modes increased noticeably with the growth of coordination number of EC molecules. For example, there are four C=O stretching modes and more than one hundred modes in total in $Na^+(EC)_4$ complex. Thanks to the assigned mode found in a single EC molecule, which helped to identify the corresponding frequency quickly in the n-coordination complex (n = 1, 2, 3, 4, 5). It can be seen in the output file that most of these frequencies did not make many differences (difference less than 2 cm^{-1}), so the data reported here were average values after calculation. On the contrary, two modes showed a wider dispersion as n increases (see Table 4-8). It is interesting to discover further whether this dispersion could be observed in the liquid phase.

Table 4-8 Non-negligible dispersion of frequency in EC complex (6-31G*)

	$Na^+(EC)_1$	$Na^+(EC)_2$	$Na^+(EC)_3$	$Na^+(EC)_4$	$Na^+(EC)_5$
v20	1934.907	1842.567	1861.108	1870.676	1849.834
		1859.145	1861.304	1871.874	1851.268
			1887.393	1871.91	1861.724
				1901.337	1862.013
					1891.748
v11	1109.296	1120.592	1116.313	1112.653	1107.628
		1121.807	1116.403	1112.691	1107.949
			1120.145	1112.739	1111.872
				1118.286	1112.539
					1117.007

The influence of sodium ion will be expected to decrease with an increase in the coordination number of EC molecule. Figure 4-6 illustrates the observed shifts for the five chosen vibration modes corresponding to the coordination number of EC molecule. Table 4-9 presents observed shifts for the five chosen vibration modes for $Na^+(EC)_n$ (n = 1, 2, 3, 4, 5) complexes. In the Figure 4-6, the frequency shifts seem to change uniformly as a function of coordination number for $Na^+(EC)_n$ (n = 1, 2, 3, 4) complexes. In the case of $Na^+(EC)_5$ complex, the C=O stretching mode showed an opposite tendency.

Table 4-9 Computed shifts for $Na^+(EC)_n$ n = (1, 2, 3, 4, 5)

modes	assignment	$Na^+(EC)_1$	$Na^+(EC)_2$	$Na^+(EC)_3$	$Na^+(EC)_4$	$Na^+(EC)_5$
v1	Ring C=O bending	-47.979	-39.360	-28.853	-20.405	-8.100
v2	ring bending	30.382	26.665	22.319	17.028	7.422
v5	Ring stretching	31.520	28.130	22.885	15.775	10.293
v12	Ring stretching	108.383	87.268	73.022	59.840	59.187
v20	C=O stretching	-101.22	-84.051	-64.972	-55.958	-71.590

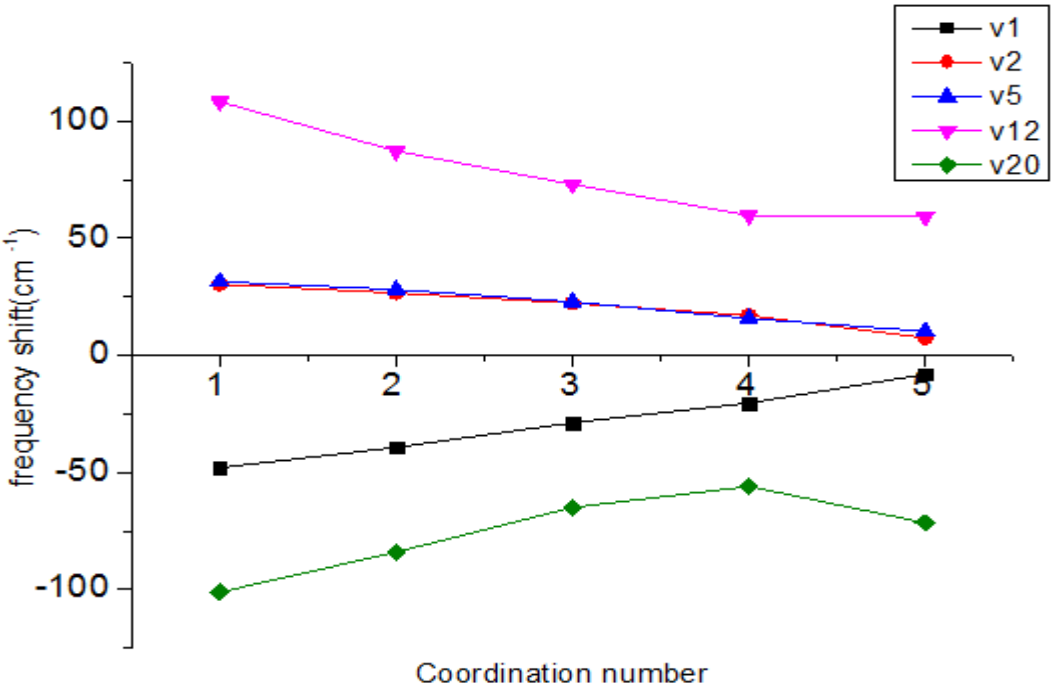

Figure 4-6 Computed shifts for $Na^+(EC)_n$ n = (1, 2, 3, 4, 5) as a function of the coordination number

In the case of the PC and DMC molecules, the coordination number of $Na^+(PC)_n$ and $Na^+(DMC)_n$ (n = 1, 2, 3, 4, 5) complexes are evaluated by the same approach. Due to the different structures and vibrations for PC and DMC molecules, those chosen frequency modes which used to be analysed in EC are not appropriate here. But the strategy to select frequency modes is still the same which is to choose the C=O stretching vibration alone with two most affected stretching vibrations and one low-frequency molecule bending vibration. Another low-frequency molecule bending mode is not reported here because its shift is relatively small and the tendency is therefore not obvious. Computed frequency vibrations and assignments were summarized in appendix 6.4. Computed frequency shifts for $Na^+(PC)_n$ and $Na^+(DMC)_n$ complexes are demonstrated in Table 4-10 and Table 4-11 respectively as well as in Figure 4-7 and Figure 4-8, which provides a better visualization.

Table 4-10 Computed shifts for $Na^+(PC)_n$ n = (1, 2, 3, 4, 5)

mode	assignment	$Na^+(PC)_1$	$Na^+(PC)_2$	$Na^+(PC)_3$	$Na^+(PC)_4$	$Na^+(PC)_5$
v2	Ring bending	21.126	19.1305	16.40167	1.385	5.006
v8	Ring stretching	25.242	22.8845	18.97933	3.699333	-1.5084
v18	Ring stretching	58.478	56.059	43.88767	21.532	16.7702
v27	C=O stretching	-104.843	-86.633	-66.4883	-58.5175	-67.2984

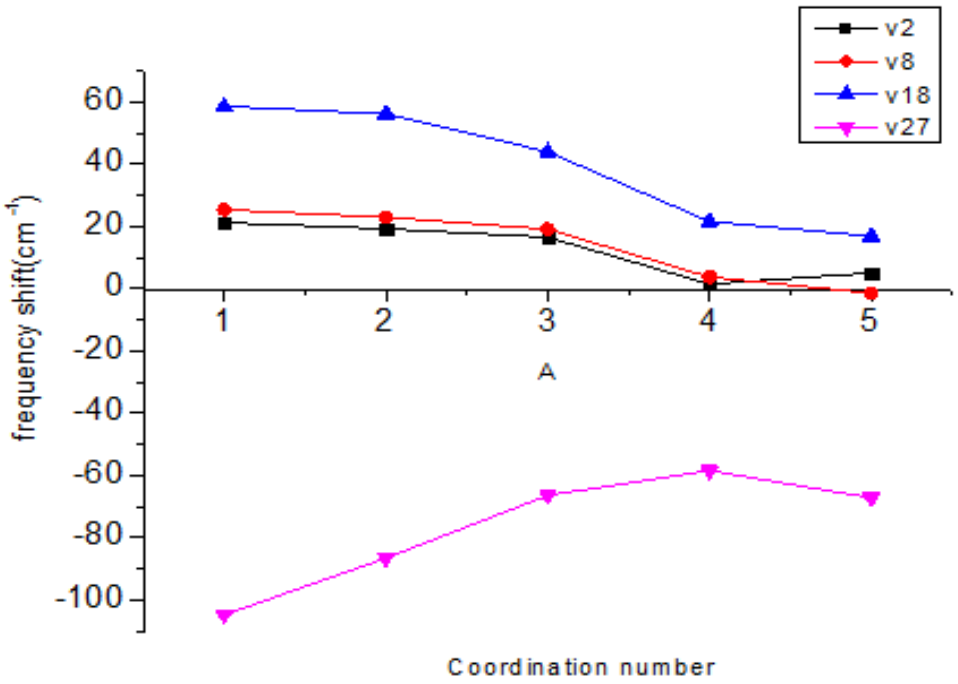

Figure 4-7 Computed shifts for $Na^+(PC)_n$ n = (1, 2, 3, 4, 5) as a function of the coordination number

Table 4-11 Computed shifts for $Na^+(DMC)_n$ n = (1 ,2, 3, 4, 5)

mode	Assignment	$Na^+(DMC)_1$	$Na^+(DMC)_2$	$Na^+(DMC)_3$	$Na^+(DMC)_4$	$Na^+(DMC)_5$
v5	molecule bending	22.134	21.344	18.544	12.888	7.866
v10	molecule stretching	76.147	68.953	58.739	48.895	39.638
v17	molecule stretching	-100.936	-87.158	-71.507	-69.267	-70.455
v24	C=O stretching	-30.673	-14.406	-10.156	-2.142	-1.002

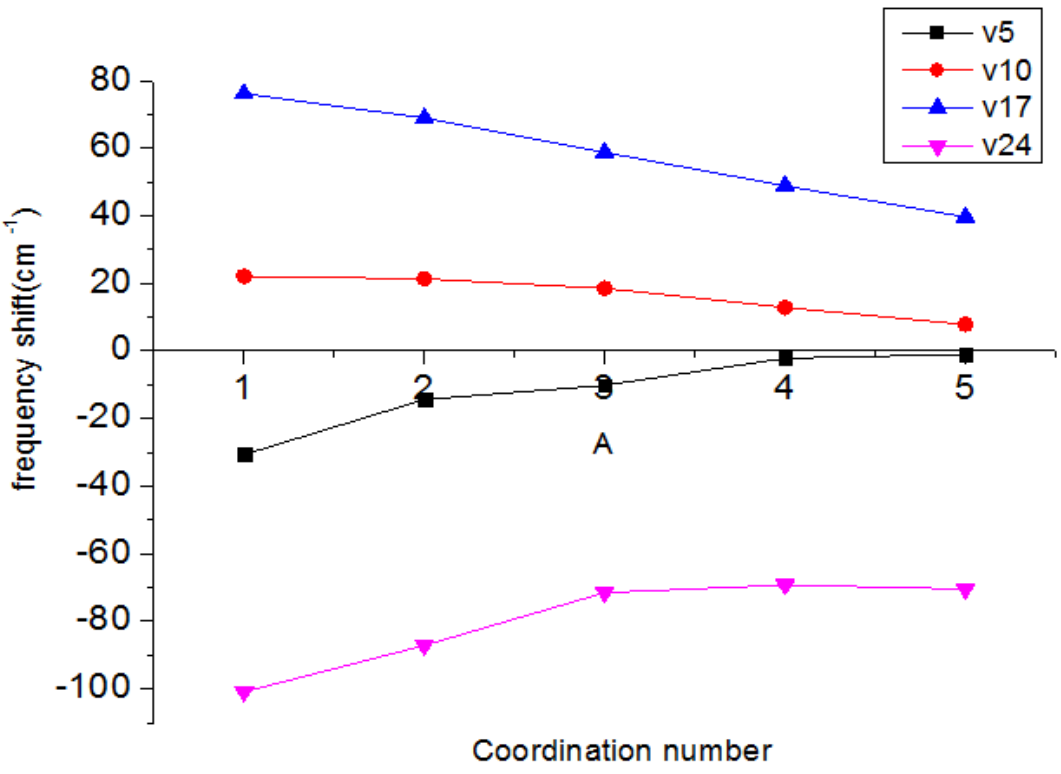

Figure 4-8 Computed shifts for $Na^+(DMC)_n$ n = (1, 2, 3, 4, 5) as a function of the coordination number

4.4 Discussion of the thermodynamic data

The stability of Na^+ complex can be quantified using the thermodynamic data Gibbs free energies obtained through the frequency calculations. Table 4-12 summarizes all of the parameters included in the frequency output files.

Table 4-12 Thermodynamic data output at the B3LYP/6–31G* level

	H_{corr} (kcal/mol)	E_0 (kcal/mol)	TS (kcal/mol)
Na	1.481	-101706.459	10.531
EC	50.949	-214856.075	21.478
$Na^+(EC)_1$	53.174	-316603.383	25.785
$Na^+(EC)_2$	105.672	-531493.225	39.477
$Na^+(EC)_3$	158.017	-746373.200	51.180
$Na^+(EC)_4$	210.239	-961246.635	62.987
$Na^+(EC)_5$	262.614	-1176115.088	70.964
PC	69.353	-239530.415	23.556
$Na^+(PC)_1$	71.539	-341278.920	27.733
$Na^+(PC)_2$	142.422	-580843.825	42.529
$Na^+(PC)_3$	213.172	-820398.353	55.582
$Na^+(PC)_4$	283.853	-1059944.951	69.202
$Na^+(PC)_5$	354.567	-1299486.381	80.019
DMC	65.211	-215614.896	24.306
$Na^+(DMC)_1$	67.201	-317355.800	28.074
$Na^+(DMC)_2$	133.796	-533000.051	43.652
$Na^+(DMC)_3$	200.285	-748636.390	58.464
$Na^+(DMC)_4$	266.845	-964266.576	70.366
$Na^+(DMC)_5$	333.494	-1179891.222	81.528

Here in table 4-12, the T= 298.15K, H_{corr} is the enthalpy correction at 298.15 K, E_0 is the DFT ground state energy. S is the total entropy. The zero-point energy has been taken into account in the E_0. The enthalpy of the complex at 298.15K is the sum of DFT ground state energy and a thermal correction to the enthalpy. [76] In addition, the equations which are used to calculate the thermodynamic parameters and the reactions are listed in chapter 3-1-3.

Table 4-13 Calculated thermodynamic data at B3LYP/6–31G* level

	ΔH(kcal/mol)	TΔS(kcal/mol)	ΔG(kcal/mol)
$Na^+(EC)_1$	-40.105	-6.224	-33.881
$Na^+(EC)_2$	-32.219	-7.785	-24.433
$Na^+(EC)_3$	-22.504	-9.775	-12.729
$Na^+(EC)_4$	-16.087	-9.670	-6.417
$Na^+(EC)_5$	-10.952	-13.501	2.550
$Na^+(PC)_1$	-41.342	-6.354	-34.987
$Na^+(PC)_2$	-32.960	-8.760	-24.200
$Na^+(PC)_3$	-22.716	-10.504	-12.212
$Na^+(PC)_4$	-14.856	-9.936	-4.920
$Na^+(PC)_5$	-9.654	-12.740	3.086
$Na^+(DMC)_1$	-33.936	-6.763	-27.173
$Na^+(DMC)_2$	-27.972	-8.729	-19.243
$Na^+(DMC)_3$	-20.164	-9.494	-10.670
$Na^+(DMC)_4$	-13.941	-12.404	-1.537
$Na^+(DMC)_5$	-8.312	-13.144	4.832

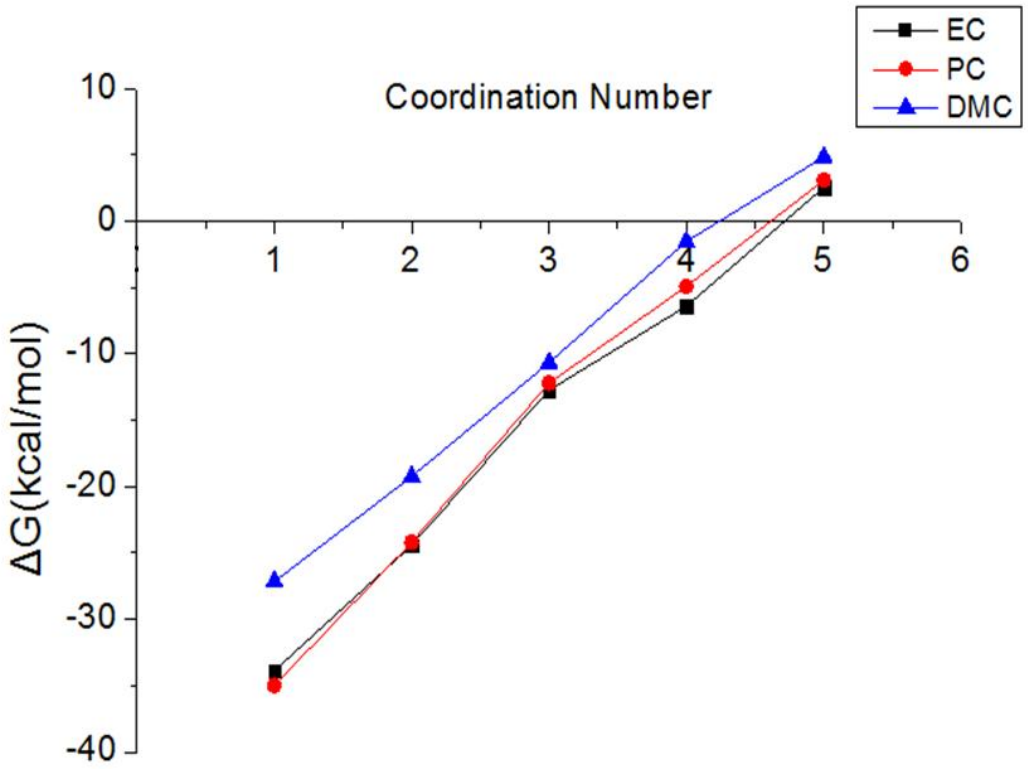

Fig 4-9 ΔG *vs.* Coordination number at B3LYP/6–31G* level

The calculated thermodynamic data are presented in Table 4-13 and the ΔG changes corresponding to the coordination number are illustrated in Fig 4-9. The ΔH values are negative in all cases, which indicates that all the reactions are exothermic. In the case of $Na^+(EC)_5$, even though the reaction is exothermic, its Gibbs free energy change (ΔG) turns out to be positive. Hence, we can draw the conclusion that the four-coordinated complex $Na^+(EC)_4$ is the most stable structure. The same conclusions can be drawn for Na^+ with PC and DMC complex that the most stable structure is the four-coordinated complex. It is notable that the Gibbs free energy for $Na^+(EC)_n$ complexes are smaller than those for $Na^+(PC)_n$ and $Na^+(DMC)_n$ complexes, which indicates that EC could be a better electrolyte solvent compared to PC and DMC for sodium-ion batteries. [46] The larger basis set def2-svp was used to compare the results of thermodynamic data in the following Table 4-14.

Table 4-14 Calculated thermodynamic data at B3LYP/def2-svp level

	ΔH(kcal/mol)	TΔS (cal/mol)	ΔG(kcal/mol)
$Na^+(EC)_1$	-32.361	-6.324	-26.037
$Na^+(EC)_2$	-26.370	-5.934	-20.436
$Na^+(EC)_3$	-16.364	-6.549	-9.816
$Na^+(EC)_4$	-9.822	-7.985	-1.836
$Na^+(PC)_1$	-41.254	-6.450	-34.804
$Na^+(PC)_2$	-33.229	-6.021	-27.209
$Na^+(PC)_3$	-23.074	-6.927	-16.147
$Na^+(PC)_4$	-15.330	-6.764	-8.565
$Na^+(DMC)_1$	-26.781	-6.898	-19.882
$Na^+(DMC)_2$	-22.878	-7.449	-15.429
$Na^+(DMC)_3$	-14.722	-8.337	-6.385
$Na^+(DMC)_4$	-8.485	-10.427	1.943

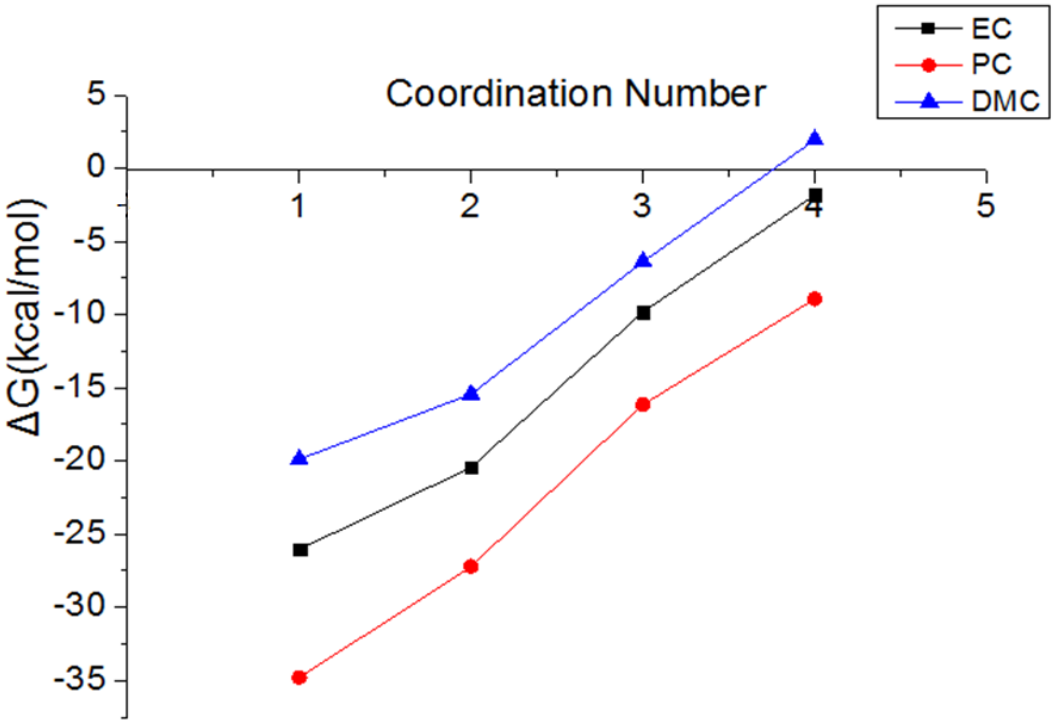

Fig 4-10 ΔG *vs.* Coordination number at B3LYP/def2-svp level

The geometries of all the complexes were optimized again and the same procedures were applied to calculate the Gibbs free energy of formation. The most stable $Na^+(EC)_n$ and $Na^+(PC)_n$ complex are still the four-coordinated complex while for $Na^+(DMC)_n$ complex the most stable structure has changed to three-coordinated complexes in this research. In the case of DMC, although the free energy difference for the path going from $Na^+(DMC)_3$ to $Na^+(DMC)_4$ is 1.943 kcal/mol, the $Na^+(DMC)_3$ complex has still been predicted to be the most favourable one.

The optimization in the DFT module is to iterate on the Kohn-Sham (SCF) equations. Convergence of the total energy is defined to be when the total DFT energy at iteration N and at iteration N-1 differ by a value less than a specific value (the default is 10^{-6} Hartree). The thermodynamic data obtained from frequency calculations are calculated based on the optimized geometries. In this study, by setting the convergence criteria as ‘tight’, the figure of the total energy is precise to eight decimals. Therefore, all the thermodynamic data calculated at both B3LYP/6-31G* and B3LYP/def2-svp levels are significant. The larger the chosen basis set, the more accurate the results.

Chapter 5 Spectroscopy results and discussion

5 Spectroscopy results and discussion

5.1 ^{23}Na NMR

^{23}Na NMR allows us to examine solvation from the perspective of the Na^+ ion. The reference compound used is 3 mol NaCl in D_2O. ^{23}Na has a spin 3/2 nucleus and is therefore quadrupolar. As a result, the signal width increases with asymmetry of the environment. Hence, in the spectra in Fig.5-1, the NaCl signal is narrower than the NaClO4 signal. The negative shifts indicate higher shielded compounds compared to the reference. Fig.5-2 plots ^{23}Na shifts with different sodium salts in PC on the y-axis and tracks how the concentration of the solution affects that chemical shifts. In both of these two cases, the sodium NMR peaks shift to upfield with the increasing concentrations, which indicates lower deshielding effect. In addition, ^{23}Na is more downfield in $NaClO_4$/PC than in NaTFSI/PC at the same concentration due to the anion effect.

Providing that the sodium is at the position of deshielding area of the C=O double bond. The lower the concentration of $NaClO_4$ in PC, the more PC surrounding around the sodium, the more deshielding effect. Therefore, the sodium NMR peak shifted to the downfield with decreasing concentrations in the experiments which are consistent with the assumption of initial complex structures in the simulation.

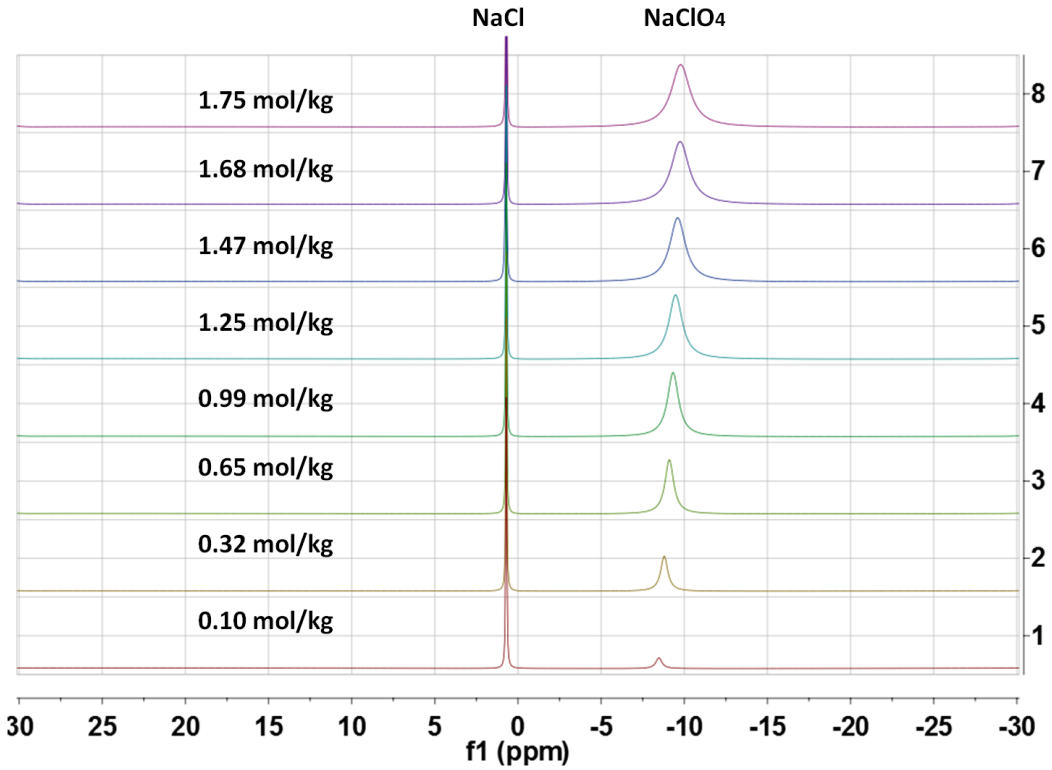

Fig. 5-1 Sodium NMR for $NaClO_4$ in PC(concentration increases from bottom to top)

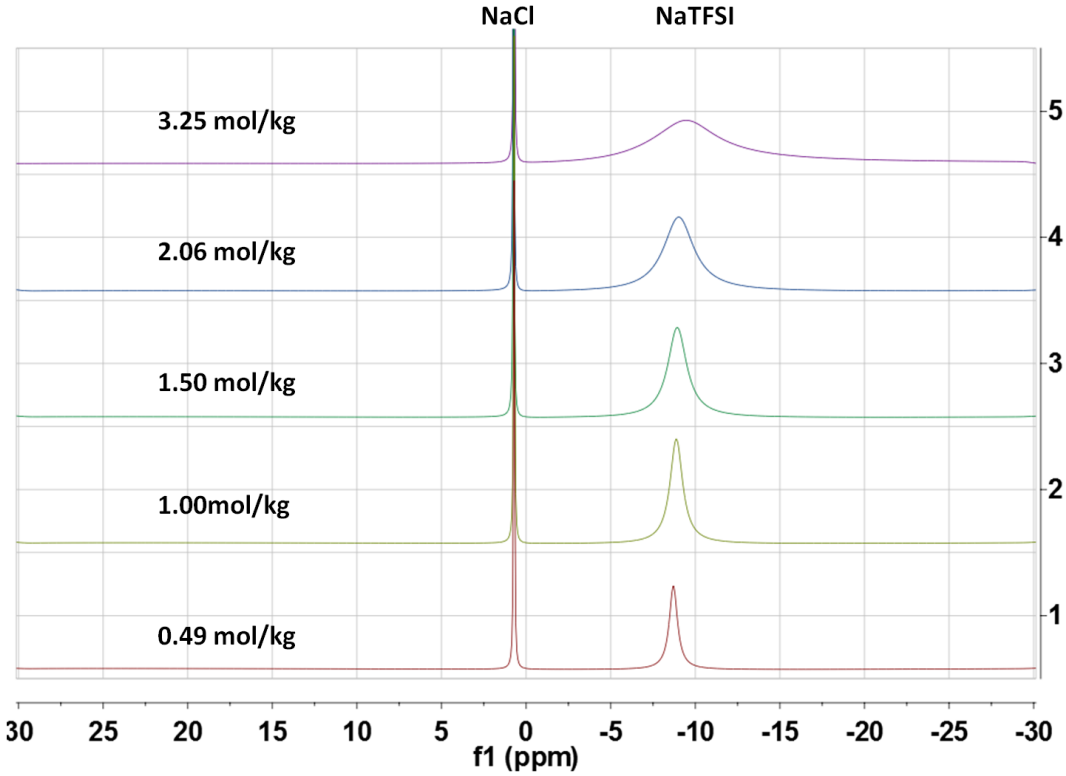

Fig. 5-2 Sodium NMR for NaTFSI in PC(concentration increases from bottom to top)

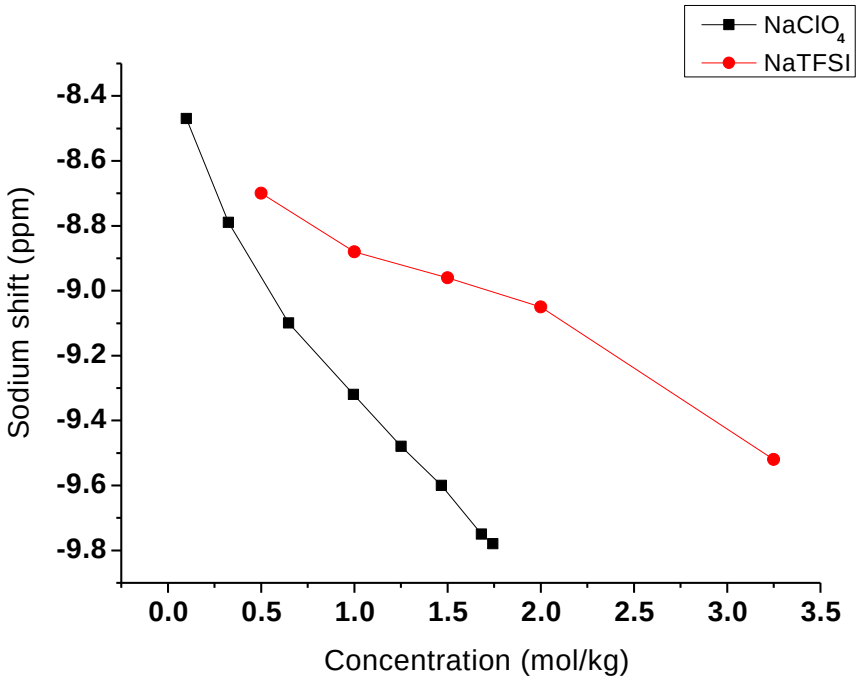

Fig. 5-3 Sodium NMR shifts for $NaClO_4$ and NaTFSI in PC

5.2 ^{13}C NMR

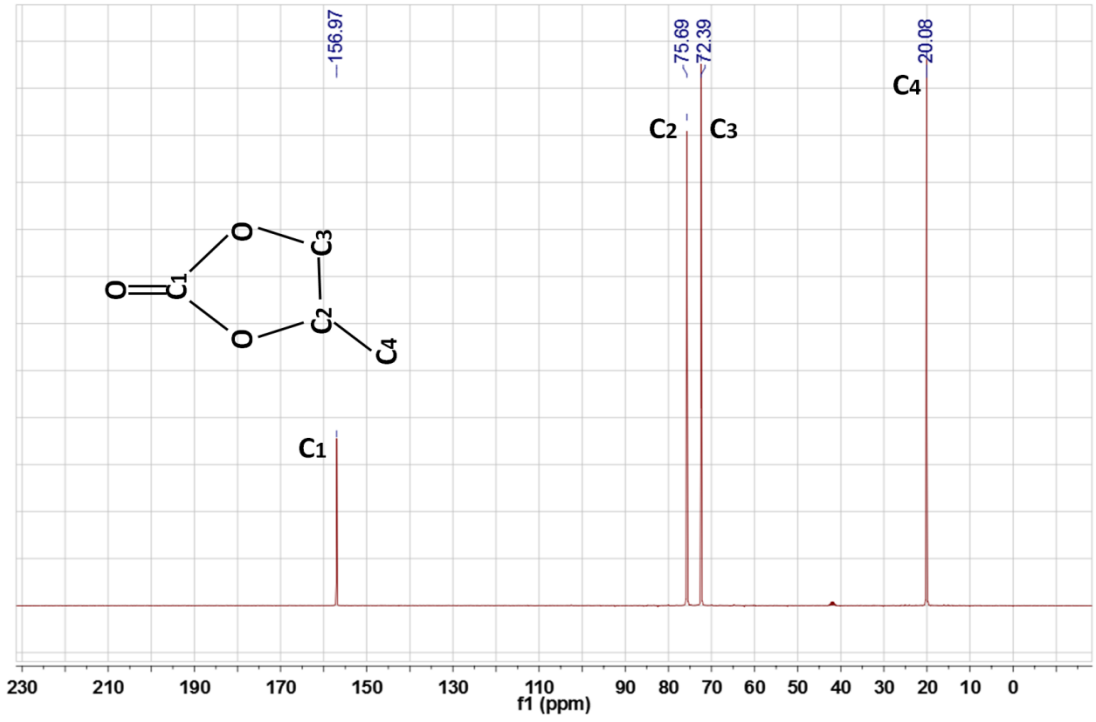

Fig. 5-4 PC ^{13}C-NMR example

Fig.5-4 presented the structure of PC and the label of different carbon in PC. The electronegativity of an oxygen atom is higher than a carbon atom. Electronegative atoms present in the molecule tend to draw the electron density towards themselves, resulting in a decrease of the electron density and an increase in chemical shift values for the surrounding atoms due to the deshielding of the nucleus. Therefore, C_1, C_2, C_3, C_4 can be assigned due to different chemical environments respectively, which is also consistent with Yang's assignment. [85]

The reference compound used in ^{13}C NMR is dimethyl sulfoxide (DMSO). In Fig 5-5 to 5-8, it can be seen there is an increasing tendency for a downfield change in the chemical shift with increasing concentration for C_1, $C_{2,}$ and C_3. While the chemical shift for C_4 in different concentrations of NaClO4/PC solutions remains constant, which indicates that the C-H_3 in PC has significantly lower interactions with Na^+ compared to the others, for example, the C=O bond. This has also been verified by simulation showing that Na^+ has stronger interactions with the C=O double bond compared to the CH_3 group. The similar behaviours were observed in the case of NaTFSI/PC.

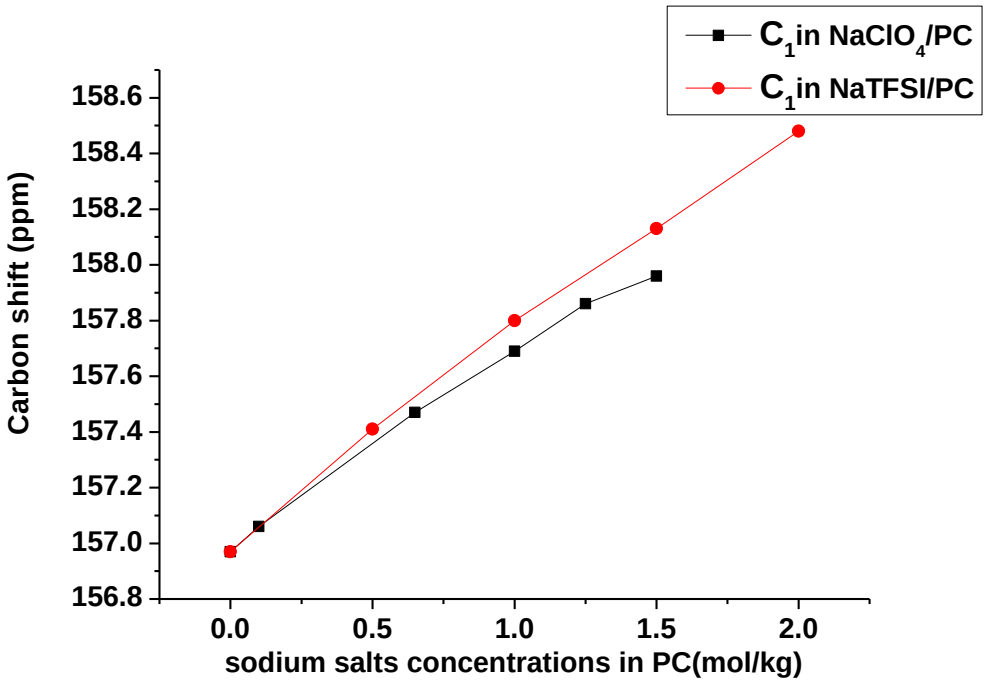

Fig. 5-5 The C_1 carbon shift with increasing concentrations

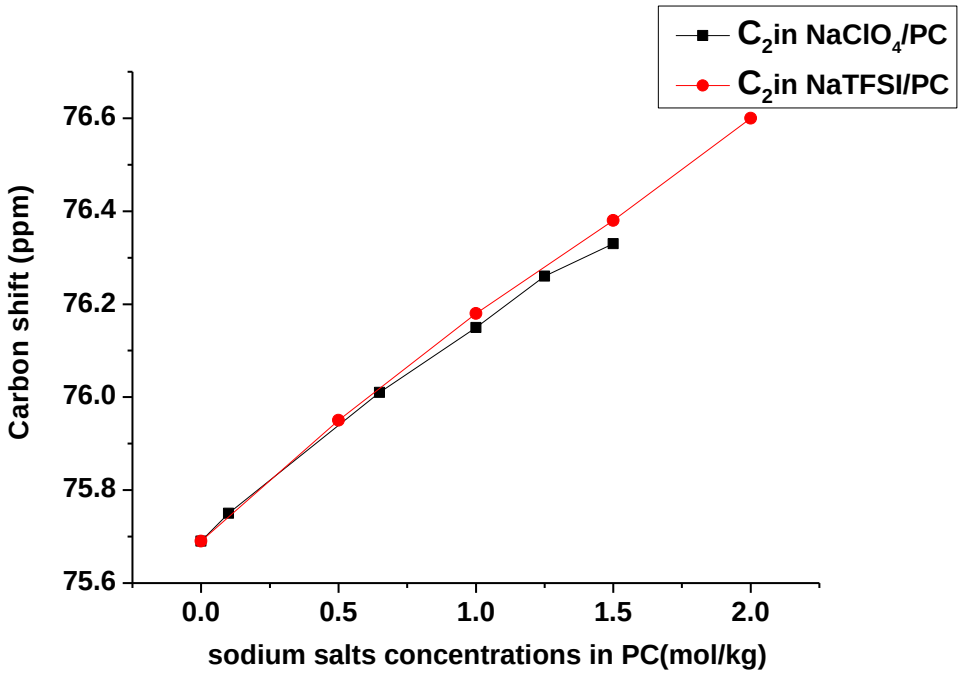

Fig. 5-6 The C_2 carbon shift with increasing concentrations

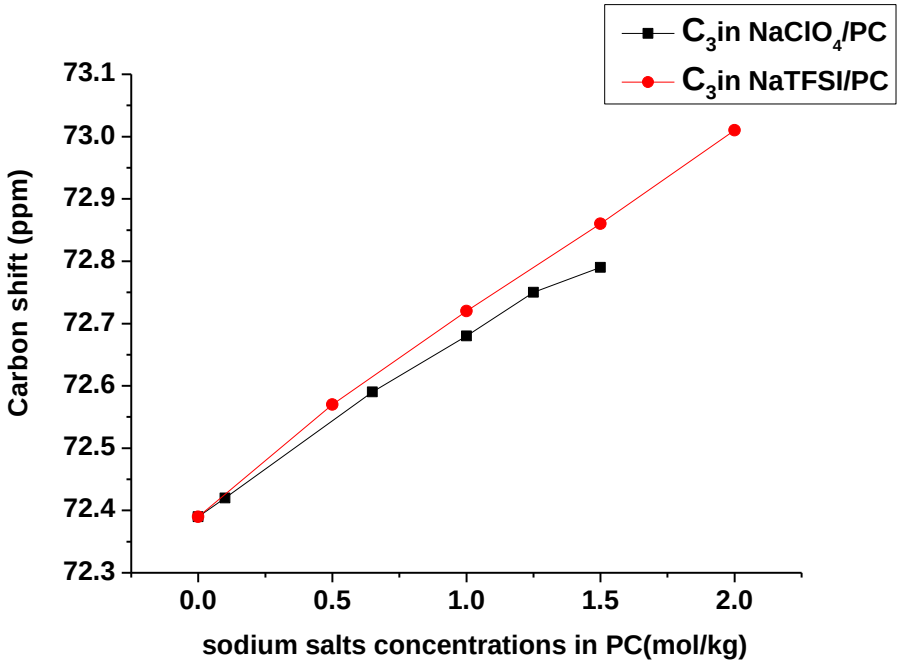

Fig. 5-7 The C_3 carbon shift with increasing concentrations

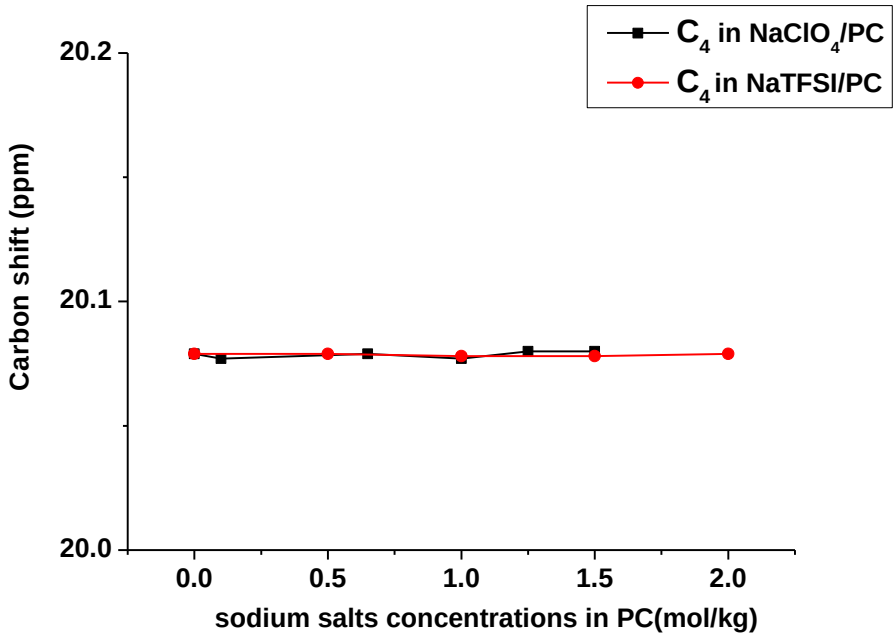

Fig. 5-8 The C_4 carbon shift with increasing concentrations

5.3 ^{1}H NMR

The reference compound used in ^{1}H NMR is dimethyl sulfoxide (DMSO). The different protons in PC were assigned in the example in Fig 5-9.

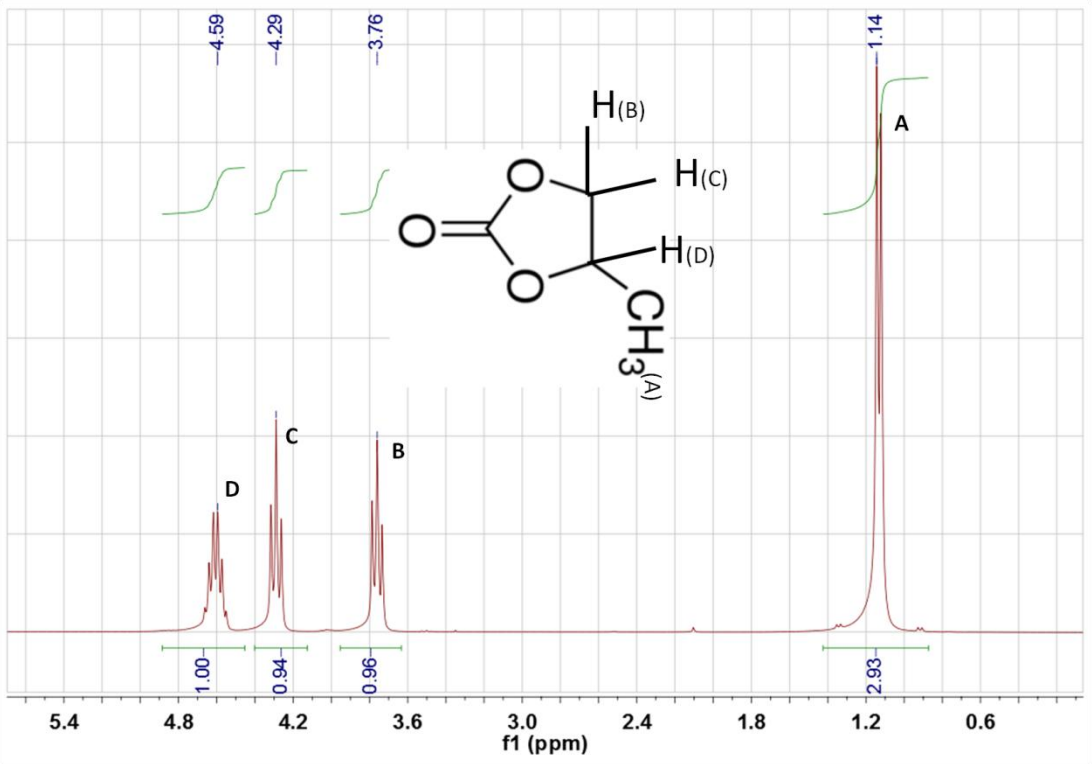

Fig. 5-9 PC ^{1}H-NMR example

Table. 5-1 Proton shifts

Sample	Concentration (mol/kg)	H(D) H(C) H(B) H(A)
PC	0	δ 4.59 (s, 1H), 4.29 (s, 1H), 3.76 (s, 1H), 1.14 (s, 3H).
NaTFSI/PC	0.5	δ 4.58 (s, 1H), 4.28 (s, 1H), 3.74 (s, 1H), 1.12 (s, 3H).
NaTFSI/PC	1	δ 4.57 (s, 1H), 4.26 (s, 1H), 3.73 (s, 1H), 1.09 (s, 3H).
NaTFSI/PC	1.5	δ 4.58 (s, 1H), 4.27 (s, 1H), 3.73 (s, 1H), 1.09 (s, 3H).
NaTFSI/PC	2	δ 4.55 (s, 1H), 4.24 (s, 1H), 3.70 (s, 1H), 1.06 (s, 3H).

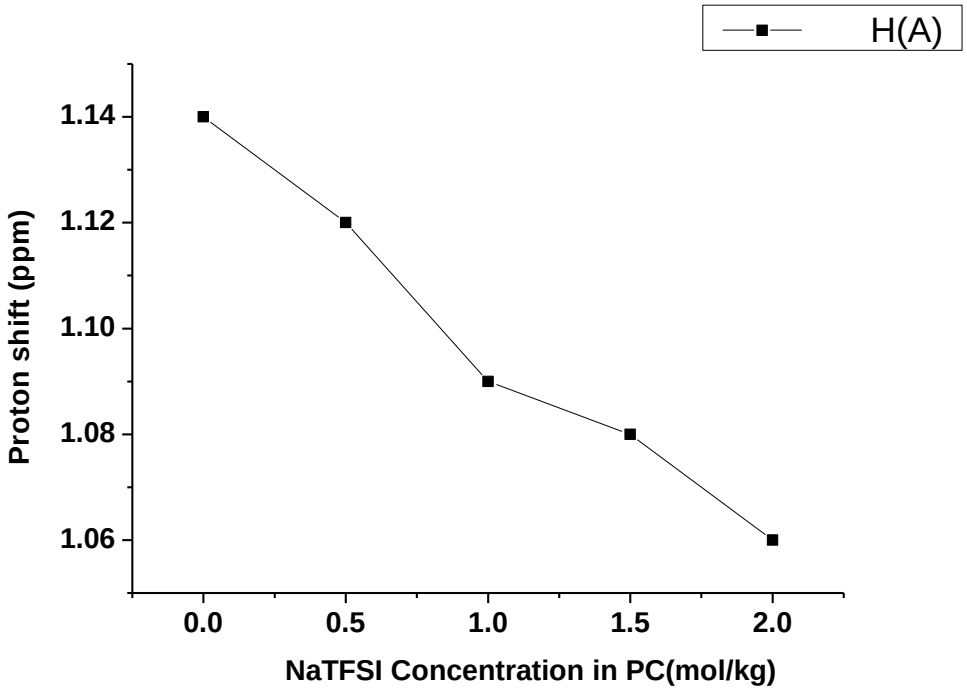

Fig. 5-10 PC ^{1}H-NMR shift example

It can be seen from Table 5-1 and Figure 5-10 that all the protons are shifted to upfield with respect to the increasing salt concentrations. Although the chemical shift range for proton is much smaller with respect to carbon, we can still notice a 0.08 ppm chemical shift from lower to higher concentrations. However, unlike the carbon shifts, all the proton signals are shifted. This difference in the proton and carbon shifts is probably due to the mesomeric effect caused by the positioning of the sodium salt within the PC structure. For example, assuming the electron density within C-H bond is constant then if the corresponding C experiences an electron deshielding effect (downfield shift) then the corresponding H will experience an electron shielding effect resulting in an upfield shift.

5-4 IR spectroscopy

Figures 5-11 illustrates the infrared spectroscopy data obtained from experiment and simulation. Experimental infrared spectra were recorded in the middle-infrared region of 500–4000 cm^{-1}. The computed infrared spectroscopy has 33 frequency vibrations for the isolated PC, which can be found in Appendix 7.3. The main reason that these two spectra are not comparable directly is due to the fact that the experimental and computed spectra are in condensed phase and gas phase respectively. In order to get a more comparable result, hundreds of PC molecules need to be simulated in condensed phase instead of one isolated PC, which requires more demanding calculations. Here we aim to compare the tendency of the frequency shift in both experimental and computed spectra.

Table 5-2 summarizes the results of ab initio (B3LYP 6-31G* level) calculations of the PC, as well as a description of the vibrational modes obtained experimentally. PC has a relatively large permanent dipole moment (4.94 D) which would suggest considerable self-association in the pure liquid phase would exist. [86] However, the isolated PC molecule in the simulation does not have self-association, which cause the different frequency shifts for the same vibration. For example, C=O was observed at 1781.6 $cm^{-1}$and 1931.7 cm^{-1} in experimental and computed IR spectroscopy respectively. Due to the limited solubility of $NaClO_4$ in PC, NaTFSI was used to get achieve experimental data at higher Na^+ concentration.

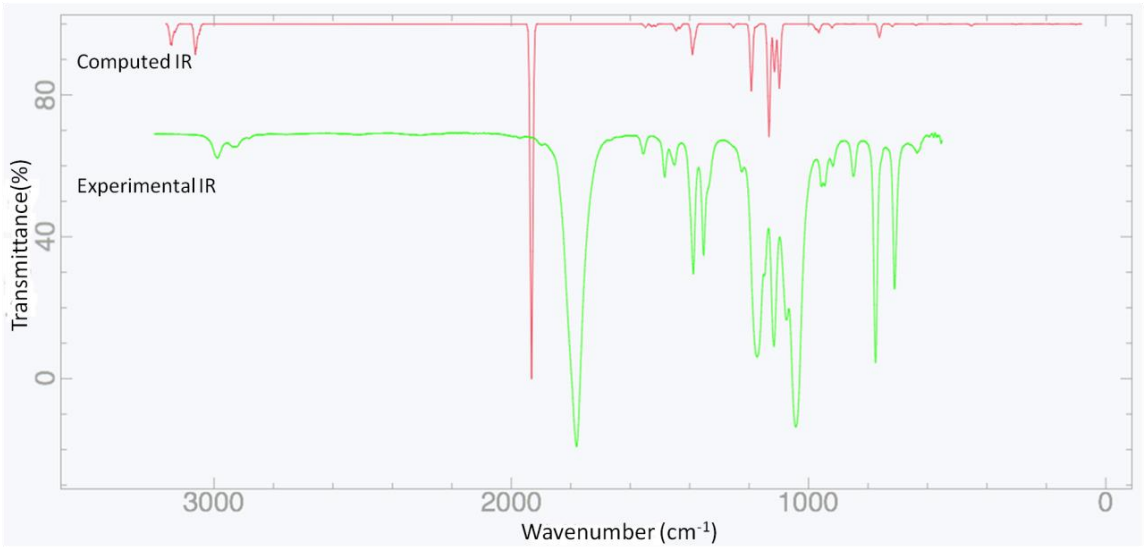

Fig. 5-11 Experimental and Computed IR spectroscopy for PC rendered in green and red respectively.

Table 5-2 Comparison of Infrared spectroscopy from this work with literature

DFT calculations		Experiment data		
Description of vibration	B3LYP /6-31G*	This work $\tilde{\nu}$ (cm^{-1})	Reference[86] $\tilde{\nu}$ (cm^{-1})	Assignment[86]
ring distortion	637.512	630.1	711.9	Ip. ring (O=COO) str.
Ring stretching	717.956	711.2	755.6	Ip. asym. ring str.
o.p. ring C=O bending	761.792	774.47	776.6	Op. ring bend ring (O=COO)
ring breathing	863.814	849.9	849.2	CH_3 stretch + ring str.
O-C-O stretching & C-C-C stretching	920.961	918.5	917.9	Ip. O-C-O str.
H-C-O asymmetrical stretching & all C-H rocking	964.975	945.6	945.5	CH_3/CH rock
C-H i.p. rocking &	976.356	955.92	956.5	Ip. ring str. +CH_3

ring breathing				bend
CH_2-O stretching	1098.1	1043	1052.4	Ip.asym.ring str.+CHbend +C-C twist
asymmetrical ring stretching	1114.692	1074	1076.8	Ip. asym. ring str.
Ring stretching	1133.031	1117	1120.3	Ip. ring +CO str. (O=COO)
CH_3 & CH_2 wagging	1176.501	1148	1148.2	CH bend/wag
ring stretchingg & CH_2, CH_3 twisting	1192.175	1172.9	1184.4	CH_2 rock
CH_2-CH stretching & CH_2 twisting	1252.776	1224.6	1255.1	CH_2 scissor
CH_2,CH,CH_3 wagging	1381.652	1335	1354.1	HC-CH bend
CH-CH_2 scissoring	1390.822	1353	1388.9	CH bend/rock
CH_2,CH,CH_3 asymmetrical wagging	1432.615	1387	1400	CH sym. bend
CH_2,CH,CH_3 symmetrical wagging	1445.928	1449	1450.9	C -CH bend (CH_3)
CH_3 scissoring	1514.76	1456	1457.5	CH bend (CH_3)
CH_3 scissoring	1527.512	1484	1484.3	CH bend (CH_3)
CH_2 scissoring	1548.937	1555.9	1556.1	CH def. (CH_3)
C=O stretching	1931.763	1780.6	1795	C=O str.

From the previous DFT calculation, several PC vibrational bands are good candidates for studying ion-solvent interactions because they clearly exhibit relatively larger frequency shifts due to the sodium cation association with PC.

For this reason, the ring stretching vibrations at 711 cm^{-1}, 1172 cm^{-1} and the carbonyl stretching vibration at 1780 cm^{-1} have been examined further. The frequency shifts observed at 711 cm^{-1}, 1172 cm^{-1}, and 1780 cm^{-1} are illustrated in the Fig.5-12, Fig. 5-13 and Fig. 5-14 respectively. All the results along with DFT calculations are summarized in Table 5-3. The vertical arrows are plotted from the peak of pure PC to higher concentration of the solution to provide a better observation of frequency shifts.

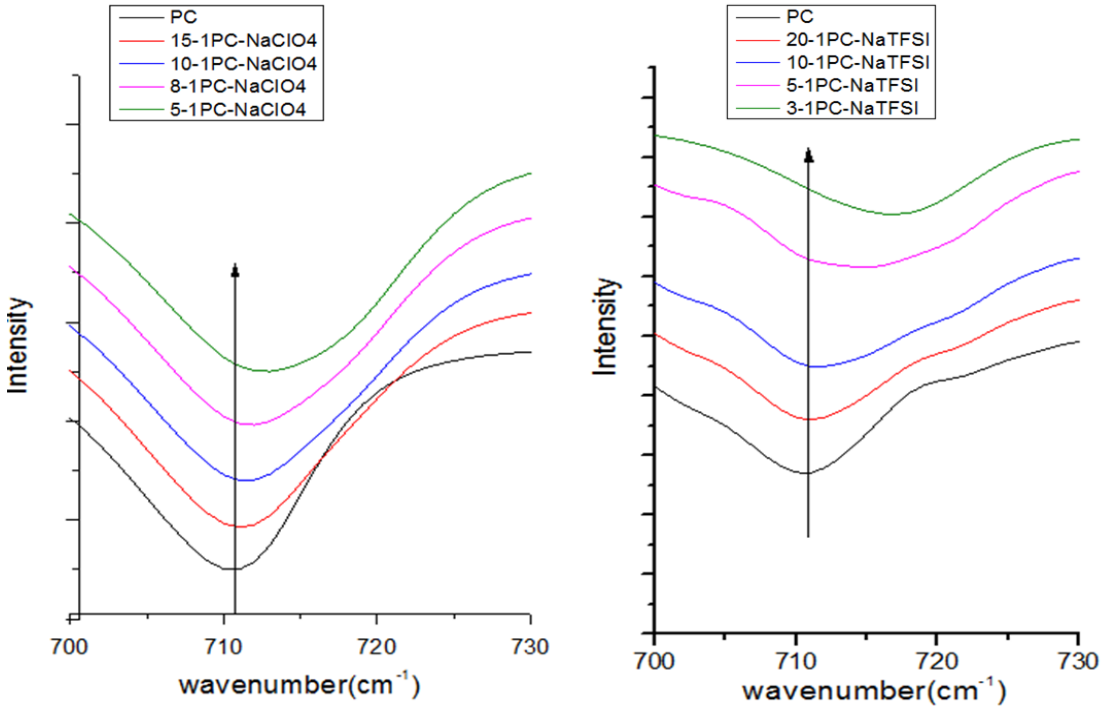

Fig. 5-12 IR spectra of PC ring stretching

with different concentrations of $NaClO_4$ and NaTFSI

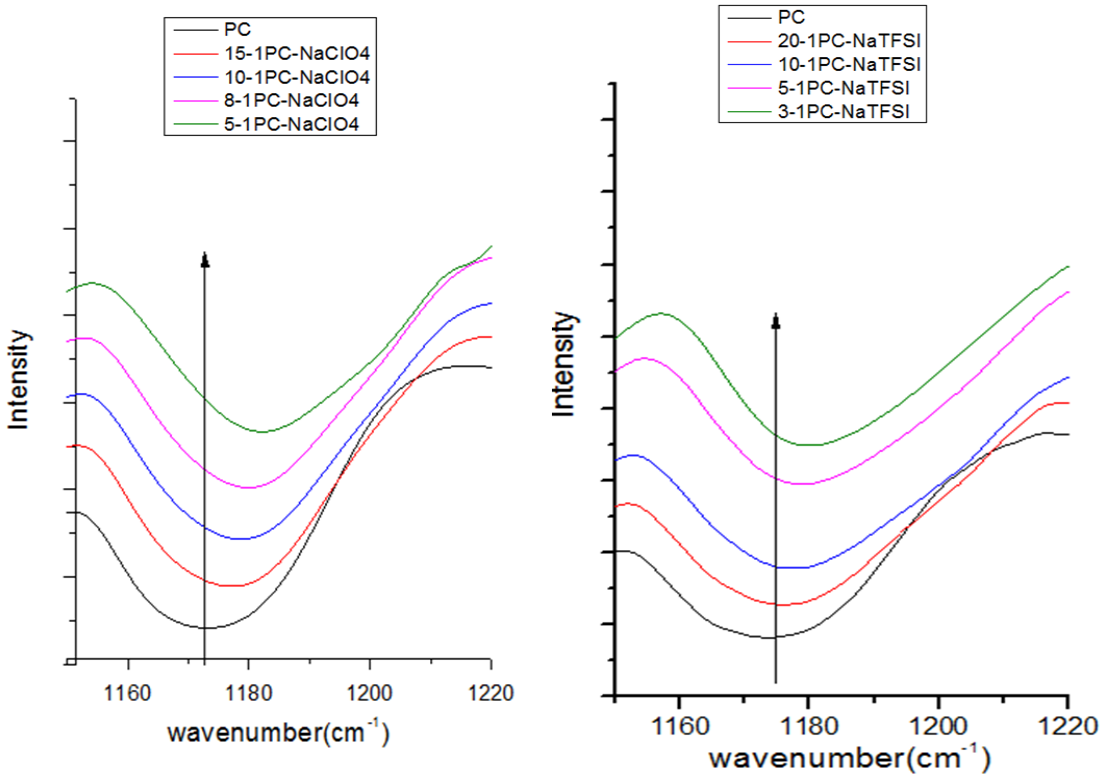

Fig. 5-13 IR spectra of PC ring stretching

with different concentrations of $NaClO_4$ and NaTFSI

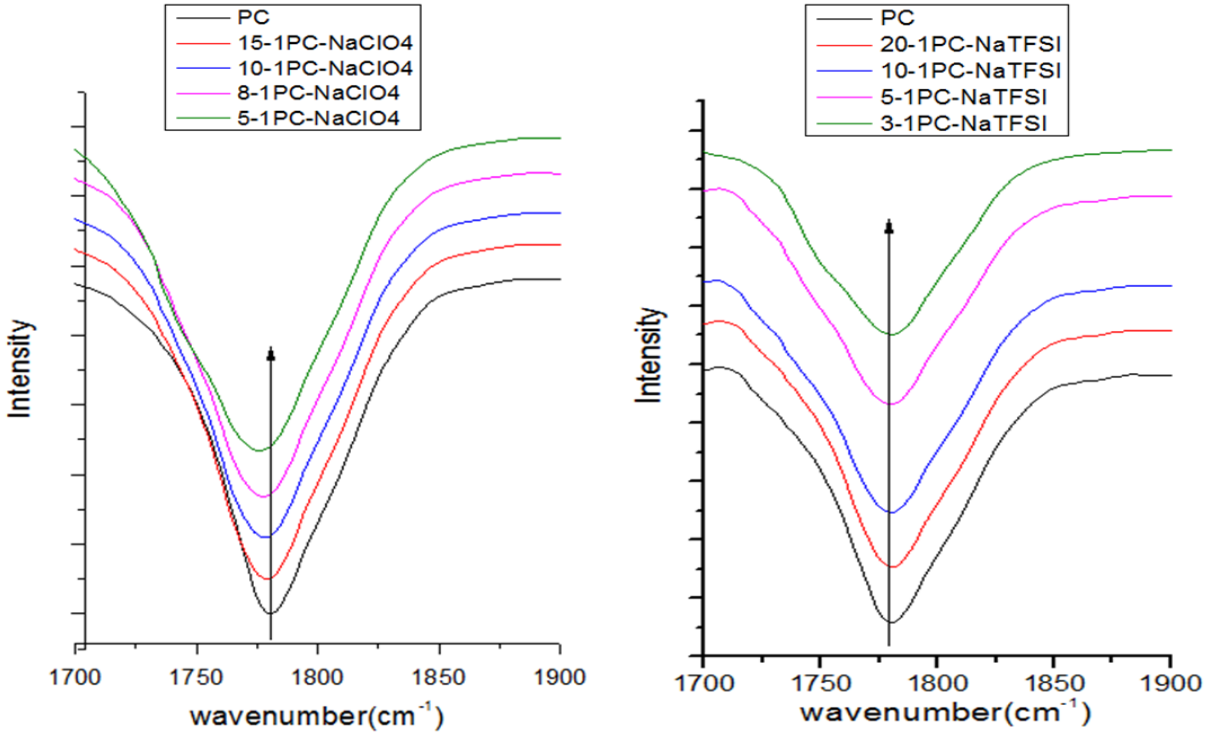

Fig. 5-14 IR spectra of PC carbonyl stretching

with different concentrations of $NaClO_4$ and NaTFSI

Table 5-3 IR frequency shift for both DFT calculation and Experiment

DFT	PC	5:1 PC:Na	4:1 PC:Na	3:1 PC:Na	2:1 PC:Na	1:1 PC:Na
Ring stretching	718.0	716.4	721.7	736.9	740.8	743.2
Ring stretching	1192.2	1208.9	1213.7	1236.1	1248.2	1250.7
C=O stretching	1931.8	1864.5	1873.2	1865.3	1845.1	1826.9
Experiment	PC	15:1 PC:$NaClO_4$	10:1 PC:$NaClO_4$	8:1 PC:$NaClO_4$	5:1 PC:$NaClO_4$	
Ring stretching	710.4	711.2	711.5	711.9	712.9	
Ring stretching	1172.9	1176.8	1179.5	1180.2	1182.2	
C=O stretching	1780.6	1779.0	1777.9	1777.2	1774.6	
Experiment	PC	15:1 PC:NaTFSI	10:1 PC:NaTFSI	5:1 PC:NaTFSI	3:1 PC:NaTFSI	
Ring stretching	710.4	710.7	711.5	714.4	716.5	
Ring stretching	1172.9	1175.5	1177.6	1178.4	1180.1	

The PC carbonyl stretching and ring stretching vibrations are plotted in Fig. 5-15 and Fig. 5-16 to have an intuitive observation. In Fig. 5-14, the carbonyl stretching vibrations seem consistent in different concentrations of NaTFSI/PC but they are actually shifted and hidden under the curves. One needs to do deconvolution analysis on these peaks and these peaks are not further investigated here due to the complicated anion $TFSI^-$. It has been found that the stretching frequencies of C=O bonds become red-shifted after binding with Na^+ ion, indicating that C=O bonds are weakened. As mentioned before, the position of the assigned absorption peaks from experimental and DFT calculations are not exactly the same, but the tendency of shift will be similar. In Fig. 5-15, the C=O stretching band showed an opposite tendency when increasing the molar ratio of PC: Na^+ from 4 to 5. This can be explained by the fact that the distance of Na^+ with PC is larger in the 5-coordinated

complex rather than the 4-coordinated complex and the PC is not tightly connected to Na^+, which indicates a favour of the four-coordinated complex for $Na^+(PC)_n$ complex. In addition, the shift tendency of ring stretching mode from DFT calculations are consistent with both those shifts observed in $NaClO_4$/PC and NaTFSI/PC solutions.

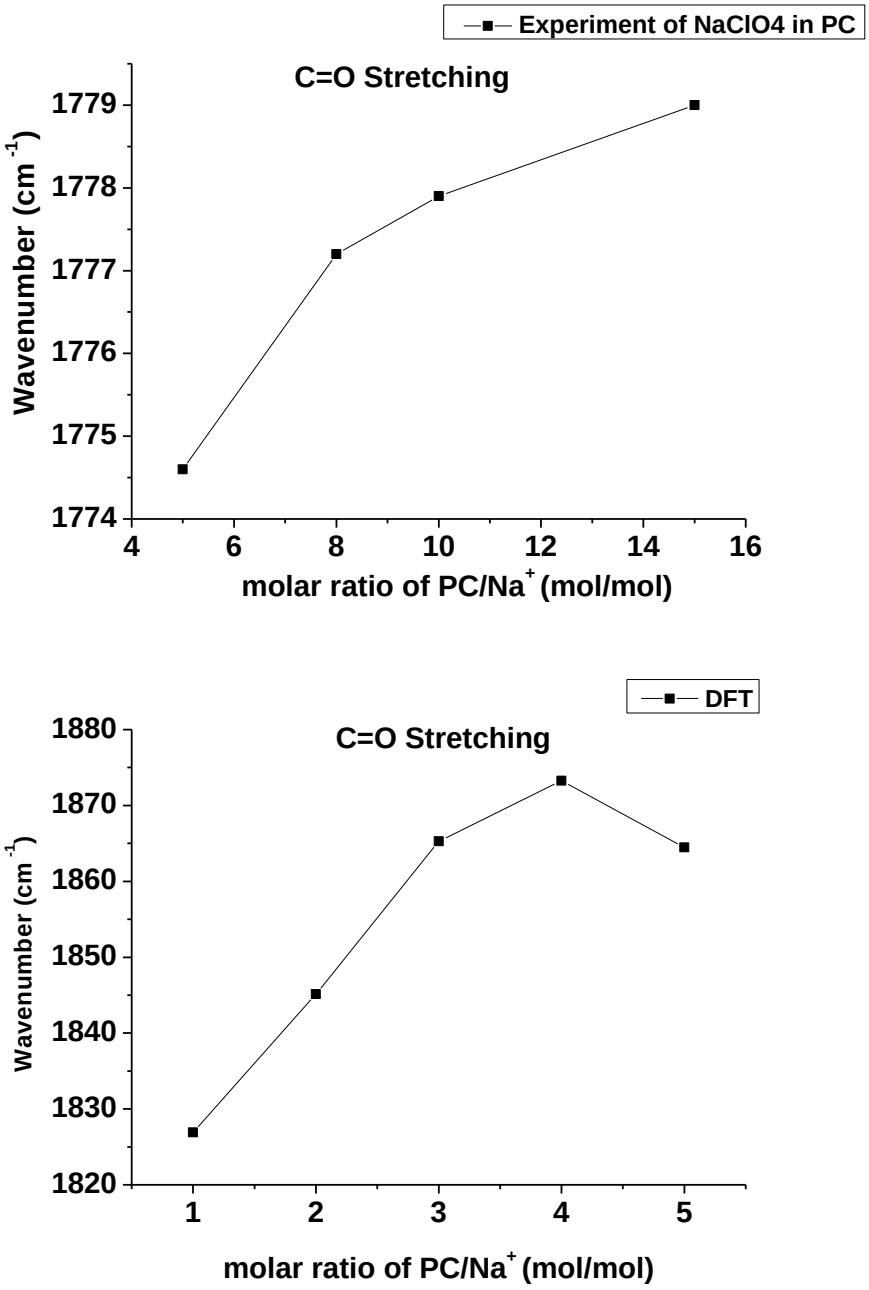

Fig. 5-15 Comparison of IR frequency shifts for C=O stretching using experimental and computational data

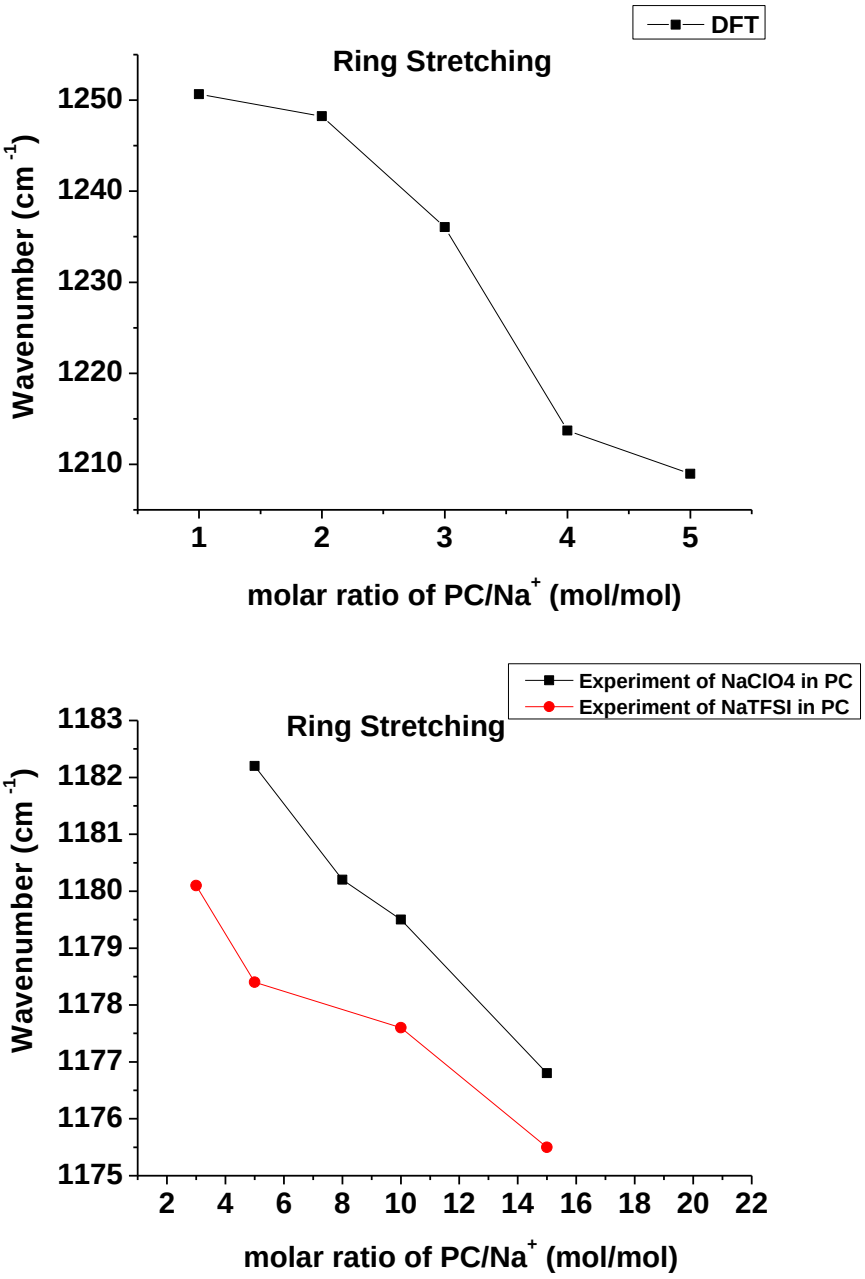

Fig. 5-16 Comparison of IR frequency shifts for C=O stretching using experimental and co[mputational data

Chapter 6 Conclusions and Future work

6. Conclusions and Future work

Structures and thermodynamic properties of EC, PC, DMC with sodium cation in the gas phase have been studied. The distances between sodium cation and carbonyl oxygen are larger than those in lithium complexes. This indicates that the sodium cation has weaker interactions with organic carbonates compared to the lithium cation. The sodium cation coordination causes significant red or blue shifts in some vibrational frequencies in the gas phase, which leads to a few cases of reordering modes. These most affected shifts are mainly observed in the ring stretching and carbonyl stretching modes. Most of the vibrations are blue shifted to higher wavenumbers, while the carbonyl stretching and bending modes exhibit red shifts. The influence of sodium ion decreases when increasing the coordination number on the vibrational frequency shifts.

To further investigate the stability of the Na^+ complexes, the thermodynamic data such as enthalpy, entropy, and Gibbs free energy are calculated and compared using different basis sets. It is notable that the Gibbs free energy for $Na^+(EC)_n$ complexes are smaller than those for $Na^+(PC)_n$ and $Na^+(DMC)_n$ complexes, which indicates that EC could be a better electrolyte solvent compared to PC and DMC for sodium-ion batteries. At B3LYP/6-31G* level, the most stable structure is found to be four-coordinated complex. A larger basis set, B3LYP/def2-svp, was used to verify the thermodynamic results. Using a larger basis set, the most stable structure for $Na^+(DMC)_n$ complex is changed to three-coordinated complex. Although both of the calculations at different levels are significant, the larger basis set brings in more accurate results. This thermodynamic calculation method can be utilized to predict the maximum solvation number of the complex, but it requires a higher accuracy of the basis set. The fewer molecules coordinated to Na^+, the smaller the first

solvation shell. This is beneficial for battery operation because a small complex of molecules can be transported more easily in the electrolyte solution resulting in faster charge/discharge rates.

The ^{23}Na NMR and ^{13}C NMR further validated the complex structures found in the simulation. The infrared spectroscopy of $NaClO_4$ and NaTFSI in PC solutions were performed to compare with the results from DFT calculations. The experimental and computed infrared spectra are not comparable directly is due to the fact that they are in condensed phase and gas phase respectively. However, the tendency of experimental frequency shifts in the most affected carbonyl stretching and ring stretching modes are consistent with the computed IR spectra.

One of the further work is to determine the solvation number of the Na^+ ion in PC by Raman spectroscopy. The intensity of free PC and associated PC can be obtained by band fitting and then it is possible to estimate the solvation number. In addition, classical molecule dynamic simulations can be performed in condensed phase corresponding to the concentration achievable in the laboratory to further investigate the solvation shell, the surrounding behavior and thermodynamic properties. A mixture of DMC, EC, and PC associated with Na^+ ion can be used to design the target sodium ion battery electrolytes and the same approach can be used to study their properties.

Chapter 7
Appendixes

7. Appendixes

7.1 Example of the input file and part of the output file from NWChem software.

Example of isolated EC molecule input script:

```
start EC

title "EC rpbe opt + freq"

echo

charge 0

geometry units angstroms print xyz noautosym noautoz

  load format xyz EC-opt.xyz

end

basis

   * library 6-31G*

end

dft

  direct

  xc B3LYP

  mult 1

end

driver

  clear

  tight

  maxiter 80

  print low

end

task dft optimize ignore

task dft freq
```

Example of the $Na^{+}EC_1$ complex input script:

```
start Na_1EC

title "Na_1EC rpbe opt + freq"

echo

charge 1

geometry units angstroms print xyz noautosym noautoz

  load format xyz Na_1EC-opt.xyz

end

basis

   * library 6-31G*

end

dft

  direct

  xc B3LYP

  mult 1

end

driver

  clear

  tight

  maxiter 80

  print low

end

task dft optimize ignore

task dft freq
```

Example of frequency result of isolated EC output:

```
Normal Eigenvalue ||           Projected Infra Red Intensities
  Mode    [cm**-1]   || [atomic units] [(debye/angs)**2] [(KM/mol)]
[arbitrary]
 ------  ----------  || --------------  -----------------  ----------
-----------
    1        -0.000 ||     0.000009            0.000          0.009
0.002
    2        -0.000 ||     0.000033            0.001          0.033
0.008
    3         0.000 ||     0.004586            0.106          4.471
1.045
    4         0.000 ||     0.009070            0.209          8.842
2.067
    5         0.000 ||     0.001840            0.042          1.793
0.419
    6         0.000 ||     0.000014            0.000          0.013
0.003
    7       160.083 ||     0.000412            0.010          0.402
0.094
    8       189.777 ||     0.001600            0.037          1.560
0.365
    9       519.918 ||     0.000399            0.009          0.389
0.091
   10       697.231 ||     0.001126            0.026          1.097
0.257
   11       720.810 ||     0.004097            0.095          3.994
0.934
   12       759.623 ||     0.024085            0.556         23.480
```

5.489

13 896.141 || 0.003042 0.070 2.965

0.693

14 897.047 || 0.000949 0.022 0.925

0.216

15 970.970 || 0.016487 0.380 16.072

3.757

16 1069.005 || 0.014552 0.336 14.186

3.316

17 1109.296 || 0.203703 4.700 198.580

46.421

18 1144.820 || 0.264301 6.098 257.654

60.230

19 1168.803 || 0.004506 0.104 4.393

1.027

20 1247.431 || 0.005898 0.136 5.750

1.344

21 1255.575 || 0.012973 0.299 12.647

2.956

22 1404.091 || 0.002986 0.069 2.911

0.681

23 1421.579 || 0.044305 1.022 43.191

10.096

24 1547.598 || 0.004374 0.101 4.264

0.997

25 1556.570 || 0.001904 0.044 1.856

0.434

26 1934.907 || 0.581317 13.411 566.697

132.474

27	3073.121	0.026295	0.607	25.633	5.992
28	3076.322	0.039821	0.919	38.820	9.075
29	3140.747	0.012160	0.281	11.855	2.771
30	3152.585	0.029605	0.683	28.861	6.747

Example of frequency result of $Na^{+}(EC)_1$ output:

Mode	Normal Eigenvalue [cm**-1]	Projected Infra Red Intensities [atomic units]	[(debye/angs)**2]	[(KM/mol)]	[arbitrary]
1	-0.000	0.000850	0.020	0.828	0.161
2	-0.000	0.010978	0.253	10.702	2.084
3	0.000	0.009234	0.213	9.002	1.753
4	0.000	0.009334	0.215	9.099	1.772
5	0.000	0.002930	0.068	2.857	0.556
6	0.000	0.001208	0.028	1.178	0.229
7	37.260	0.030526	0.704	29.759	5.796
8	64.267	0.037398	0.863	36.458	

7.101

9 112.104 || 0.000186 0.004 0.182

0.035

10 220.159 || 0.000362 0.008 0.353

0.069

11 272.321 || 0.052316 1.207 51.000

9.933

12 513.517 || 0.001683 0.039 1.640

0.319

13 724.443 || 0.005007 0.116 4.881

0.951

14 752.330 || 0.046857 1.081 45.678

8.896

15 773.156 || 0.028566 0.659 27.848

5.424

16 878.044 || 0.002035 0.047 1.984

0.386

17 921.801 || 0.031160 0.719 30.376

5.916

18 989.566 || 0.002063 0.048 2.011

0.392

19 1029.030 || 0.002930 0.068 2.857

0.556

20 1124.165 || 0.148876 3.435 145.132

28.266

21 1160.443 || 0.000695 0.016 0.678

0.132

22 1239.356 || 0.073253 1.690 71.410

13.908

23 1253.203 || 0.146983 3.391 143.286
27.907
24 1255.595 || 0.012043 0.278 11.741
2.287
25 1406.938 || 0.000214 0.005 0.208
0.041
26 1467.149 || 0.098037 2.262 95.571
18.614
27 1546.420 || 0.020713 0.478 20.192
3.933
28 1554.687 || 0.000747 0.017 0.728
0.142
29 1833.692 || 0.937612 21.631 914.030
178.019
30 3117.454 || 0.009238 0.213 9.006
1.754
31 3118.776 || 0.008893 0.205 8.670
1.689
32 3177.674 || 0.000767 0.018 0.748
0.146
33 3191.421 || 0.004386 0.101 4.276
0.833

7.2 Optimized coordinates for pure solvents and Na^+ complexes.

EC:

10

geometry

C	-1.47631518	-0.30161992	-0.09618279
C	-0.45539504	-1.43892152	0.04315417
O	-0.68970236	0.86646209	0.17224203
H	-2.29203205	-0.35053185	0.62764978
H	-1.88868975	-0.22728587	-1.10854337
O	0.79534097	-0.77128164	-0.16931701
H	-0.56641510	-2.22502622	-0.70613529
H	-0.45480154	-1.88429062	1.04420231
C	0.63215489	0.56959495	0.01735335
O	1.51926709	1.36891949	0.04168296

Na^+(EC):

11

geometry

C	-2.08199099	-0.84413147	-0.11101687
C	-1.05782194	-1.98497328	0.02480181
O	-1.26710892	0.34552661	0.07500978
H	-2.85418415	-0.84666437	0.65802586
H	-2.53882234	-0.78258278	-1.10116482
O	0.21481358	-1.29378900	-0.10399250
H	-1.11693902	-2.73144822	-0.76702876
H	-1.07383455	-2.47254717	1.00198728
C	0.01685918	0.01511073	0.00040507
O	0.92466697	0.83307808	0.02530470

Na	2.48570031	2.23989255	0.06840698

$Na^+(EC_2)$: 21

geometry

H	1.00185899	-6.07522137	-1.03253027
H	1.37823622	-5.79086457	0.69217454
H	-1.00989907	-6.05070182	1.08745480
H	-1.38713145	-5.81204568	-0.64395961
C	0.74576939	-5.49285431	-0.14747305
C	-0.75547833	-5.49065185	0.18763326
C	-0.00777487	-3.35412683	-0.00729515
O	1.01395709	-4.09615596	-0.43344044
O	-1.02756906	-4.08778772	0.43755007
O	-0.00931916	-2.13725965	-0.02263139
H	-0.99203846	6.08100681	-1.02785036
H	-1.36645713	5.79849730	0.69758003
H	1.02395586	6.04479725	1.08795260
H	1.39619663	5.80435064	-0.64430149
C	-0.73740801	5.49706340	-0.14341002
C	0.76449938	5.48636328	0.18856565
C	0.00443283	3.35411428	-0.00537021
O	-1.01404084	4.10194329	-0.42906939
O	1.02923237	4.08194213	0.43762179
O	-0.00076139	2.13726104	-0.02119991
Na	-0.00551263	0.00008644	-0.03647256

$Na^+(EC_3)$:

31

geometry

C	5.43653422	1.10403073	-0.53236531
C	5.54687670	-0.00991042	0.52097516
O	4.01138565	1.34732572	-0.59378200
H	5.77113627	0.79402607	-1.52583513
H	5.92998785	2.03348224	-0.24736207
O	4.19867869	-0.53255879	0.57748268
H	5.80951555	0.36020659	1.51550994
H	6.21674536	-0.82219969	0.23801624
C	3.36249955	0.33252637	-0.00953787
O	2.15702135	0.21097061	-0.01190116
H	-3.18093972	-5.02184536	-1.26379094
H	-3.32215333	-5.22509553	1.15746599
Na	-0.02155828	-0.00924249	-0.01500782
C	-2.21503363	-5.10907464	-0.75928659
C	-1.40737324	-3.11241550	-0.03147252
C	-2.32045077	-5.03329280	0.77223120
O	-1.98454615	-3.65323985	1.04874466
O	-0.92047539	-2.00317990	-0.05304059
O	-1.43039534	-3.93779718	-1.08506386
H	-1.68378682	-5.98855454	-1.12381757
H	-1.59533225	-5.66900367	1.28717405
H	-4.35752240	4.45439941	-0.99761734
H	-3.92427501	4.39167596	1.39672760
C	-3.30237930	4.46077616	-0.72332055
C	-3.04958156	4.62500009	0.78387574
O	-2.75399366	3.15048084	-0.99943029
O	-2.03566873	3.62729504	1.04937133

C	-1.97643992	2.77099270	0.02208719
O	-1.29749059	1.76752035	0.01758764
H	-2.76327070	5.19001878	-1.33377735
H	-2.65043457	5.60053860	1.06243305

$Na^{+}(EC_{4})$:

41

geometry

C	4.15363429	-0.73279608	3.30324142
C	4.13636906	0.73069319	3.77022550
O	2.91158882	-0.85013916	2.57566441
H	4.14522055	-1.45736267	4.11812228
H	4.97538836	-0.95522418	2.61673785
O	3.17311508	1.33851489	2.88252479
H	5.08969668	1.24562112	3.64752809
H	3.77933119	0.85016889	4.79704986
C	2.44541067	0.37826782	2.28969439
O	1.48695147	0.59513604	1.58678575
H	0.14458098	-3.58362314	-4.42880079
H	2.57345201	-3.66316370	-4.54597708
C	0.62058522	-2.62012335	-4.63162312
C	1.24371557	-1.53675365	-2.72962281
C	2.14964948	-2.66012765	-4.48827046
O	2.35907672	-2.15355172	-3.15227441
O	1.16690515	-0.91476968	-1.69667431
O	0.22724036	-1.69387411	-3.59566307
H	0.27607617	-2.23117501	-5.59033276
H	2.66480785	-1.99847937	-5.19039569
H	-2.52981271	5.81304591	-0.69843465

C	-2.09868019	5.05593264	-1.35411851
O	-2.32209420	3.75868542	-0.76033556
H	-2.59881976	5.07854164	-2.32648678
C	-1.20770396	3.01831385	-0.87493297
H	-0.10218530	5.66502382	-0.63324466
C	-0.56760620	5.12230155	-1.46082619
O	-1.14011688	1.85008520	-0.57427476
Na	0.00567262	0.00010589	0.00001614
O	-0.18080920	3.73397261	-1.36613185
H	-3.88595783	-3.96145631	2.68490238
O	-1.50118849	-1.52442323	0.68506197
O	-3.23103760	-2.92830055	1.01909752
H	-0.20694942	5.51618004	-2.41154475
C	-2.47687143	-1.85740659	1.31503951
C	-4.21257220	-3.12561971	2.05972939
H	-4.20816192	-1.86963815	3.88489142
O	-2.93802801	-1.20514035	2.39666131
C	-4.20121532	-1.77851729	2.79827466
H	-5.16740879	-3.36514908	1.59075466
H	-5.00097075	-1.10538666	2.47679584

$Na^{+}(EC_{5})$:

51

geometry

C	3.53759406	-1.46092275	4.81301148
C	2.91319712	-0.14501522	5.30175522
O	2.78803581	-1.74445910	3.61284646
H	3.40973774	-2.29476823	5.50409880
H	4.59299309	-1.36153493	4.54352565

O	2.25999168	0.35844023	4.11731792
H	3.64287868	0.59439286	5.63356700
H	2.15506876	-0.29109564	6.07652058
C	2.14277408	-0.63362047	3.21678013
O	1.53306611	-0.53974839	2.18007569
H	-1.60710948	-2.95869919	-2.81617246
H	0.31998439	-4.42089163	-3.05528255
C	-0.85294026	-2.60178278	-3.52138397
C	0.76305902	-1.43135754	-2.44056901
C	0.44256898	-3.42623966	-3.48481684
O	1.28835828	-2.65401869	-2.60602023
O	1.29386419	-0.54608655	-1.80423539
O	-0.41140914	-1.30107791	-3.07727223
H	-1.28325426	-2.49728851	-4.51792682
H	0.93590186	-3.49969200	-4.45840276
H	-1.78161863	5.03967543	0.13670791
C	-2.36609125	4.19614112	-0.23169230
O	-2.15840984	3.07776236	0.65735151
H	-3.43041243	4.44875128	-0.22227426
C	-1.95398922	1.96575436	-0.06400563
H	-0.85051869	3.92093563	-1.81137882
C	-1.88407491	3.64979484	-1.58382933
O	-1.81920013	0.86089351	0.41677736
Na	0.36216647	-0.07656147	0.33032758
O	-1.93341845	2.22126206	-1.38175525
H	-4.37290125	-3.61885594	0.74533236
O	-0.80600225	-2.12248228	-0.10336040
O	-3.01972514	-2.49435613	-0.34425630
H	-2.53617365	3.90154826	-2.42083469

C	-1.92136981	-2.16893472	0.36325405
C	-4.15447507	-2.56500078	0.54918905
H	-3.93637586	-2.27194099	2.73370991
O	-2.21626725	-1.91264532	1.64715171
C	-3.64937992	-1.81305589	1.78737509
H	-5.00681521	-2.09255998	0.06019766
H	-3.91411181	-0.75247870	1.78228248
H	3.76217131	0.91534639	-2.54094607
H	4.88196950	2.04970841	-1.71991519
C	3.84360205	1.85546077	-1.98926718
O	3.07327149	1.72478217	-0.77556325
C	3.15050001	3.02842821	-2.69447690
C	1.87387336	2.29857085	-0.95763862
H	3.03595240	2.89403553	-3.77039144
H	3.62049418	3.99411035	-2.48618039
O	0.94133202	2.18825155	-0.19464356
O	1.83600014	3.02308975	-2.09198856

PC:

13

geometry

C	-0.40833635	-0.84939967	-0.61524362
C	-0.17478954	0.52158841	-1.26852749
O	-0.00563458	-0.60245686	0.74921755
O	0.77927171	1.14667851	-0.40147289
H	-1.08860509	1.12821101	-1.29110490
H	0.24814687	0.46218515	-2.27342249

C	0.76908440	0.51567553	0.80762652
O	1.35725169	0.89244762	1.77712431
C	-1.83613770	-1.35825250	-0.65657216
H	0.28107106	-1.59714902	-1.02764043
H	-2.51885562	-0.62716336	-0.21137242
H	-1.92613266	-2.29876282	-0.10553991
H	-2.14174365	-1.53839799	-1.69371782

$Na^+(PC_1)$:

13

geometry

C	-0.40833635	-0.84939967	-0.61524362
C	-0.17478954	0.52158841	-1.26852749
O	-0.00563458	-0.60245686	0.74921755
O	0.77927171	1.14667851	-0.40147289
H	-1.08860509	1.12821101	-1.29110490
H	0.24814687	0.46218515	-2.27342249
C	0.76908440	0.51567553	0.80762652
O	1.35725169	0.89244762	1.77712431
C	-1.83613770	-1.35825250	-0.65657216
H	0.28107106	-1.59714902	-1.02764043
H	-2.51885562	-0.62716336	-0.21137242
H	-1.92613266	-2.29876282	-0.10553991
H	-2.14174365	-1.53839799	-1.69371782

$Na^+(PC_2)$:

27

geometry

C	0.06137793	-5.55457101	-0.47045558
C	-0.91325328	-5.39674744	0.71050891
O	0.54838197	-4.18171561	-0.63853228
O	-1.17112459	-3.97067973	0.74803514
H	-0.46940028	-5.68452596	1.66829430
H	-1.86455916	-5.91046676	0.57094429
C	-0.24770573	-3.34322402	0.01793876
O	-0.14900509	-2.13040504	-0.03807632
C	1.22489555	-6.49557534	-0.24218285
H	-0.47073035	-5.79913556	-1.39518122
H	1.78485388	-6.21542561	0.65564521
H	1.90290260	-6.48595293	-1.09969346
H	0.85123268	-7.51773168	-0.11633826
H	-1.73227950	6.25805580	0.66117762
H	0.50524564	5.66820062	1.67753734
Na	-0.03293770	0.00024939	-0.07169997
C	-1.16313508	6.52837983	-0.23387584
O	1.16710176	3.94128115	0.75215680
C	0.94464442	5.37343024	0.71982516
O	0.10225688	2.13001024	-0.04468330
C	0.23061430	3.33978578	0.01666450
H	-0.76482183	7.54047635	-0.10242792
O	-0.54249013	4.20034684	-0.63854275
C	-0.02241405	5.56009316	-0.46316640
H	-1.83877393	6.53922960	-1.09323866
H	1.90874207	5.86406318	0.58503402
H	0.51811261	5.79548925	-1.38538092

$Na^+(PC_3)$:

40

geometry

C	-2.42901358	5.03179297	-0.53574226
C	-1.86860089	5.17999227	0.88935082
O	-2.21455431	3.60947552	-0.79250876
O	-1.03216447	4.01094797	1.04574995
H	-2.64975104	5.14597708	1.65552416
H	-1.24883047	6.06598859	1.03032592
C	-1.34602509	3.11908769	0.09628721
O	-0.89086775	1.99616305	0.05260675
C	-3.89354217	5.37757819	-0.70472793
H	-1.81046440	5.56976019	-1.26189956
H	-4.51288539	4.80148359	-0.00992314
H	-4.22336158	5.17054953	-1.72634402
H	-4.04627666	6.44444865	-0.50767677
H	-1.90883651	-6.30960500	0.09780998
H	-3.20980047	-4.80711397	1.65365981
C	-2.68506207	-6.08548825	-0.64073862
O	-3.00266609	-2.86232331	0.98143935
C	-3.59265846	-4.17540809	0.84573010
O	-1.28143463	-1.77148001	0.02567189
C	-2.03025128	-2.72403809	0.06988328
H	-3.54252620	-6.74246718	-0.45768549
O	-1.98282082	-3.75312901	-0.78055292
C	-3.12072689	-4.63853666	-0.54338321
H	-2.29634924	-6.30493971	-1.63877493
H	-4.67489929	-4.07549400	0.93381948
H	-3.86111764	-4.39700702	-1.31330808
H	6.41614976	1.50061749	0.15277055

H	5.77088635	-0.41916570	1.65695270
Na	-0.00002272	-0.00015377	0.04563980
C	6.60962062	0.73755755	-0.60783338
O	3.98266702	-1.19575098	0.96719662
C	5.41438462	-1.04491899	0.83251636
O	2.17441701	-0.22684497	0.04132756
C	3.37399750	-0.39910896	0.07819040
H	7.60825287	0.31990514	-0.43851455
O	4.23914488	0.18012405	-0.75892563
C	5.57605093	-0.36696957	-0.53900411
H	6.60260970	1.21159736	-1.59300746
H	5.87024393	-2.03361659	0.89295106
H	5.73682089	-1.10737821	-1.32972109

$Na^{+}(PC_4)$:

53

geometry

H	-5.05308054	3.32249242	1.18905010
H	-5.39690058	2.45919990	-0.33778841
H	-6.20463140	0.65031508	1.00420688
H	-4.63819065	1.86178862	3.36257232
H	-5.66245676	0.40996177	3.44668216
H	-6.39283945	1.99166980	3.10771833
C	-4.91145978	2.38997642	0.63962717
C	-5.33021492	1.13817117	1.44014297
C	-3.16778997	0.92825574	0.70918204
C	-5.51314687	1.36279703	2.93141756
O	-3.49650082	2.20148119	0.43041376
O	-4.20460030	0.24335145	1.21114481

O	-2.06845465	0.45962478	0.52972151
H	4.35618981	-1.05623155	4.43133950
H	3.12820811	-0.06010478	5.26467437
H	1.71153366	-1.98896997	5.21827430
H	3.48950741	-3.09198108	2.95836355
H	2.09586969	-3.93400219	3.67356585
H	3.53608041	-3.60865409	4.65905161
C	3.31741057	-0.72154814	4.41462851
C	2.30210423	-1.87898823	4.30625412
C	1.94789879	-0.34845284	2.63674380
C	2.89107613	-3.20916290	3.86856377
O	3.10654651	0.02898724	3.20088013
O	1.39086238	-1.38321846	3.28422028
O	1.47002405	0.18588410	1.66274634
H	3.19014435	4.24675582	-3.69533034
H	1.48186579	4.76041108	-3.80765058
H	1.70295912	5.55431060	-1.56003911
H	4.15155440	3.70777144	-1.27729535
H	3.53951920	4.80237398	-0.01646566
H	4.20380074	5.46793381	-1.52229099
C	2.21094106	4.20044975	-3.21536673
C	2.23627032	4.61647194	-1.72935652
C	1.29280617	2.54017983	-1.96013209
C	3.61688233	4.64673057	-1.09607120
O	1.79582050	2.81957564	-3.17342668
O	1.43348302	3.57015932	-1.11188409
O	0.77665075	1.48450183	-1.67441088
H	-1.81374108	-3.84949430	-4.08061063
H	-0.36123466	-3.04517534	-4.74318510

H	0.90002700	-4.89454483	-3.89753328
H	-1.47436759	-5.50713519	-2.03431651
H	0.02054160	-6.46460631	-2.14319445
H	-1.08061321	-6.37992445	-3.53247709
C	-0.80268807	-3.50551113	-3.85494634
C	0.08988641	-4.59776304	-3.22806201
C	0.05881366	-2.73435068	-1.89395537
C	-0.65701138	-5.80991350	-2.69816357
O	-0.88834841	-2.50372506	-2.82047638
O	0.71224949	-3.88137879	-2.12367832
O	0.29039599	-1.99665923	-0.96419857
Na	0.04860847	0.06532760	-0.08190056

$Na^+(PC_5)$:

66

geometry

H	-2.21389916	-3.06748401	2.64554715
H	-1.12688294	-3.09417180	4.06728537
H	-2.67327023	-1.63579333	5.16445486
H	-3.89329027	-1.09194595	2.39431463
H	-4.51556164	-0.44601019	3.93247472
H	-4.56312527	-2.19350290	3.62254162
C	-1.68434446	-2.45506525	3.37729911
C	-2.60209883	-1.43726167	4.09263377
C	-0.87184906	-0.34700760	3.05793255
C	-3.97882738	-1.27893576	3.46999290
O	-0.74520699	-1.62803954	2.66547748
O	-1.85800986	-0.19605204	3.95244155
O	-0.17280386	0.55177478	2.64891534

H	-2.13347225	2.74414439	-4.30770170
H	-3.00263355	1.73359595	-3.11186885
H	-3.60000373	3.79272439	-2.03717331
H	-1.18904764	5.08947988	-3.44839285
H	-2.31184612	5.93085578	-2.35663325
H	-2.89413083	5.29564279	-3.90873880
C	-2.26664027	2.53127849	-3.24528526
C	-2.57114437	3.78684168	-2.40340229
C	-0.80139836	2.63874821	-1.51034803
C	-2.21657900	5.10645233	-3.06867606
O	-1.00851130	2.07151831	-2.71497796
O	-1.72215969	3.57734256	-1.24160800
O	0.10801395	2.34401890	-0.77185409
H	4.51977779	-1.19106652	-3.04055328
H	4.65982489	-2.05025306	-1.47829099
H	3.71120760	-3.94611245	-2.59566643
H	2.59220622	-1.99339659	-4.69862429
H	2.38825762	-3.76133132	-4.72757952
H	4.00332722	-3.05183706	-4.91438653
C	3.98586335	-1.78610015	-2.29782472
C	3.25091543	-3.00279027	-2.89678706
C	1.80916562	-1.72888055	-1.64857544
C	3.04137614	-2.94731916	-4.40062158
O	2.91634158	-0.98082881	-1.76171386
O	1.96372039	-2.93799166	-2.21540538
O	0.78786915	-1.36182204	-1.11166318
H	3.49085189	1.68902441	5.14034601
H	4.87962707	2.06121889	4.07905265
H	3.58499058	3.87718823	3.22092750

H	1.05631550	2.47114998	4.27218270
H	1.11337604	4.07184104	3.51118046
H	1.89289447	3.82073840	5.08723895
C	3.80129631	1.88099656	4.11151138
C	2.97885009	2.99090900	3.42149147
C	2.92221957	1.06598052	2.17658808
C	1.67882183	3.35816143	4.11702565
O	3.51374648	0.70493091	3.32853546
O	2.69053498	2.38812866	2.13010424
O	2.63432600	0.29409316	1.29073695
Na	0.49862055	0.43004622	0.38036498
C	-2.95823976	-2.27796969	-2.45984852
C	-3.17997600	-3.07696129	-1.15727615
O	-2.60626634	-0.96059679	-1.95198150
O	-2.57686765	-2.25219793	-0.14039782
H	-2.67370939	-4.04419913	-1.15678069
H	-4.23677627	-3.21212683	-0.90999384
C	-2.30056866	-1.03194179	-0.64546824
O	-1.85940694	-0.11615251	0.00630399
C	-1.84497006	-2.80359505	-3.34975648
H	-3.88793298	-2.15438866	-3.02016140
H	-0.91259684	-2.90879209	-2.78615037
H	-1.67366494	-2.12090686	-4.18708106
H	-2.12723610	-3.78143864	-3.75635620

DMC:

12

geometry

111

C	-0.00000018	2.33447857	-0.01113449
O	-0.00000101	1.08452607	-0.71706027
H	0.00000264	3.10204706	-0.78546569
H	0.89052706	2.42317469	0.61685951
H	-0.89052945	2.42317825	0.61685621
C	-0.00000017	0.00000001	0.07252557
O	-0.00000104	-1.08452618	-0.71706015
O	0.00000185	-0.00000000	1.28437920
C	0.00000014	-2.33447870	-0.01113445
H	0.00000007	-3.10204706	-0.78546573
H	-0.89052759	-2.42317737	0.61685857
H	0.89052895	-2.42317604	0.61685718

$Na^{+}(DMC_{1})$:

13

geometry

C	0.00000018	2.36469678	-0.67510898
O	-0.00000065	1.07550415	-1.32338247
H	0.00000044	3.08657717	-1.48965672
H	0.89943787	2.48213729	-0.06558675
H	-0.89943713	2.48213825	-0.06558636
C	-0.00000009	0.00000003	-0.56799285
O	-0.00000065	-1.07550405	-1.32338256
O	0.00000119	0.00000007	0.67227241
C	0.00000015	-2.36469667	-0.67510912
H	0.00000065	-3.08657691	-1.48965699
H	-0.89943728	-2.48213837	-0.06558671
H	0.89943772	-2.48213708	-0.06558673
Na	-0.00000015	-0.00000016	2.77672846

$Na^+(DMC_2)$:

25

geometry

Na	0.00000087	0.00000009	0.00000003
H	2.38931126	1.10359030	-2.86354662
H	-2.38931219	-1.10359440	-2.86354315
C	-1.67646101	-1.66165814	-3.47578037
C	1.67646087	1.66165814	-3.47578139
C	-0.00000515	0.00000510	-3.37273818
O	0.00000170	-0.00000149	-2.13705363
O	0.76460035	0.75784979	-4.13215601
O	-0.76460146	-0.75784927	-4.13215559
H	2.19371603	2.17424325	-4.28484470
H	-1.12472749	-2.37952195	-2.86366127
H	-2.19371577	-2.17424421	-4.28484333
H	1.12473189	2.37952316	-2.86366001
H	-2.17424613	2.19371373	4.28484342
H	2.17424627	-2.19371309	4.28484475
C	-1.66166761	1.67645158	3.47578038
O	-0.75788663	0.76456432	4.13215554
H	-1.10358064	2.38929159	2.86355143
C	-0.00000181	-0.00000180	3.37273806
O	0.00000207	0.00000170	2.13705348
O	0.75788225	-0.76456824	4.13215595
C	1.66166768	-1.67645152	3.47578143
H	2.37954173	-1.12473717	2.86365696
H	-2.37954238	1.12474135	2.86365307
H	1.10358532	-2.38929281	2.86354974

$Na^+(DMC_3)$:

37

geometry

Na	0.00004186	-0.00112202	-0.00510186
H	1.49932428	-2.54288438	-2.57208030
H	2.14792408	-1.96844352	2.60036763
C	3.10354663	-1.99646202	2.07046891
C	1.32266922	-3.47728480	-2.03311197
C	2.14903233	-2.65804900	0.01804922
O	1.37440041	-1.70143168	0.00907321
O	2.22425405	-3.59027071	-0.91542850
O	3.03664069	-2.91473747	0.96279546
H	1.55419106	-4.33032575	-2.66878953
H	3.37147933	-0.99625772	1.72054951
H	3.88375229	-2.39304728	2.71806167
H	0.28532968	-3.52709526	-1.69242829
H	0.11374721	4.56993941	2.69604619
H	2.98976380	3.49741011	-2.66818756
C	0.16455958	3.69301233	2.05277951
O	1.00047752	4.08906534	0.94869110
H	-0.83334081	3.42337156	1.69761707
C	1.22739325	3.18800006	0.00910389
O	0.78567430	2.03905129	0.00206324
O	2.00328734	3.71499947	-0.92168099
C	2.36253480	2.87319316	-2.03391471
H	1.46809736	2.55746362	-2.57712898
H	0.61458333	2.85385184	2.58954183
H	2.92176456	2.00072334	-1.68652287

H	-2.57444933	-2.42618378	1.68190998
C	-3.30981475	-1.69346308	2.02394482
O	-2.15997006	-0.34031044	-0.01899233
H	-2.91660396	-0.01820364	-2.60922918
H	-4.05281032	-2.17099927	2.66057389
C	-3.37613302	-0.53040436	-0.02645211
O	-4.05587703	-1.17203434	0.90760739
H	-2.81319709	-0.88220889	2.56248248
C	-3.64333556	0.60168794	-2.07783163
O	-4.20798750	-0.12505201	-0.96977668
H	-4.48897975	0.83138856	-2.72397383
H	-3.17057391	1.52296096	-1.72798611

$Na^{+}(DMC_{4})$:

49

geometry

C	-1.60121297	-3.85095215	-0.93863383
O	-2.25839269	-2.90965557	-1.80938938
H	-2.27991886	-4.70016527	-0.87718253
H	-1.44439419	-3.41384522	0.05059490
H	-0.64515648	-4.15935635	-1.36832579
C	-1.64352096	-1.75547827	-2.01666263
O	-2.36771151	-1.03072416	-2.86167817
O	-0.57994011	-1.41036361	-1.50877795
C	-1.81697683	0.23777395	-3.26631533
H	-2.51376165	0.62316554	-4.00940519
H	-0.82697130	0.09948264	-3.70704756
H	-1.75809168	0.91554019	-2.41088824
Na	0.17262542	0.09550789	0.01848487

H	-0.57272924	-1.42644388	3.75646369
H	1.63990129	-2.78968796	-0.44377735
C	2.50318568	-2.96970296	0.20217645
C	0.40371080	-1.63666886	4.19996948
C	1.40977451	-2.22778855	2.15415657
O	1.09940305	-1.15632107	1.63775872
O	1.12726570	-2.58903205	3.39516685
O	2.08010988	-3.20399460	1.55962740
H	0.28653038	-2.11871288	5.16918975
H	3.01962355	-3.88202619	-0.09280820
H	3.18785022	-2.11848109	0.15945272
H	0.97525495	-0.71095712	4.29947166
H	-0.57763084	3.49984136	0.14130317
H	2.47170087	2.61011787	1.83319833
H	1.73859065	2.78112859	-3.03185495
H	-3.98228664	0.05138431	-0.73262495
C	-1.15306384	3.71535334	1.04485540
O	-2.50661030	3.24409638	0.91326149
H	-1.24175550	4.79014651	1.19631964
C	-2.67034985	1.96339149	0.61687118
O	-1.76643249	1.15498086	0.41691092
C	3.30001184	1.94832405	1.56567663
O	-3.96452999	1.69457408	0.56366511
O	1.74442766	1.56300725	-0.61662003
C	2.88280837	2.00526060	-0.75363535
C	2.64118062	2.16795630	-3.09069724
O	3.74718859	2.22671169	0.22563321
C	-4.33985812	0.33645746	0.25969502
O	3.44172403	2.33941396	-1.90571894

H	4.16300560	2.15117453	2.19821022
H	3.27564005	2.50204163	-3.91015531
H	-5.42838544	0.33374964	0.28468100
H	-0.67480771	3.24983883	1.91130695
H	2.98870187	0.90523453	1.66090514
H	2.37265211	1.11634956	-3.22000850
H	-3.93972959	-0.34565738	1.01395934

$Na^+(DMC_5)$:

61

geometry

C	-1.86538525	-3.14571168	-1.52371900
O	-2.12587613	-2.25797798	-2.62552958
H	-2.68640254	-3.86167318	-1.53843338
H	-1.85650998	-2.59198680	-0.58089632
H	-0.91156517	-3.66037172	-1.66423876
C	-1.21666464	-1.31682292	-2.85806355
O	-1.57916802	-0.63375912	-3.93172393
O	-0.20654290	-1.12349759	-2.18624853
C	-0.71647551	0.44761842	-4.33440449
H	-1.17859666	0.85552045	-5.23247570
H	0.28310593	0.06887379	-4.56243985
H	-0.67229346	1.20060350	-3.54522417
Na	0.01073603	0.05826810	-0.20815723
H	1.19483014	-2.03593725	3.38712616
H	1.95416723	-2.25864029	-1.55102436
C	3.00300913	-2.25936339	-1.24667421
C	2.28641231	-2.04322750	3.40775935
C	2.50398037	-2.10787061	1.05456226

O	1.73646131	-1.16244114	0.89500370
O	2.82438852	-2.65355103	2.22167102
O	3.14917394	-2.75819205	0.09680504
H	2.64517470	-2.66072373	4.23013526
H	3.58281235	-2.94426429	-1.86418746
H	3.41654940	-1.24933821	-1.31535744
H	2.66337004	-1.02269759	3.51338777
H	-1.05727465	4.00357478	-1.97072900
H	2.32970138	3.03602059	2.26860274
H	2.11431395	2.55779485	-2.53018534
H	-3.96448724	0.10753103	-1.69763119
C	-1.19596748	4.04845086	-0.88698680
O	-2.45723711	3.44964209	-0.52726494
H	-1.27500353	5.08545082	-0.56298260
C	-2.57905902	2.14497636	-0.74306579
O	-1.68951801	1.40247539	-1.14655364
C	2.92781706	2.12139091	2.25177409
O	-3.81848980	1.77758822	-0.44591850
O	1.49943457	1.82467440	-0.01612424
C	2.72552371	1.82084554	-0.06986512
C	2.72114337	1.65579291	-2.42078490
O	3.54522057	1.95170494	0.96218403
C	-4.14809182	0.38910283	-0.65821490
O	3.44837944	1.68986349	-1.17801186
H	3.75662523	2.19919696	2.95419225
H	3.48775332	1.61835299	-3.19384928
H	-5.20993830	0.31561148	-0.42667091
H	-0.36695220	3.54339554	-0.38722789
H	2.30130688	1.25767375	2.48530080

H	2.08245319	0.76992547	-2.47288911
H	-3.56133806	-0.24088550	0.01370155
H	-1.43944607	2.37470127	3.83408450
C	-1.42819555	1.69939643	2.97971490
H	-0.54339648	1.88115842	2.36304702
H	-2.33521617	1.82654642	2.38400512
O	-1.38381987	0.37682445	3.55170570
C	-1.43721934	-0.64109533	2.70409930
O	-1.46090763	-0.55435557	1.48040825
O	-1.46050099	-1.77479539	3.39649553
C	-1.59141335	-2.99208998	2.63666543
H	-2.53960259	-2.99775365	2.09361247
H	-0.75776322	-3.09809192	1.93827247
H	-1.57561067	-3.79079004	3.37686813

7.3 Frequency mode assignment (for PC and DMC):

Table 7-1. Assignments for isolated PC molecule.

Modes	PC	Assignment
v 1	100.8	Ring C=O bending
v 2	178.885	o.p. ring bending
v 3	231.822	CH_3 twisting
v 4	302.346	CH_3 rocking & CH_2 rocking
v 5	451.47	C-C-C stretching
v 6	540.732	O=C-ring i.p. bending
v 7	637.512	ring distortion
v 8	717.956	Ring stretching
v 9	761.792	o.p. ring C=O bending
v 10	863.814	ring breathing
v 11	920.961	O-C-O stretching & C-C-C stretching
v 12	964.975	H-C-O asymmetrical stretching & all C-H i.p. rocking
v 13	976.356	C-H i.p. rocking & ring breathing
v 14	1098.1	H_2C-O stretching
v 15	1114.692	o.p. asymmetrical ring strecting
v 16	1133.031	Ring stretching
v 17	1176.501	CH_3 & CH_2 wagging & ring stretching
v 18	1192.175	CH_3-C stretching & CH_2, CH_3 twisting
v 19	1252.776	CH_2-CH stretching & CH_2 twisting
v 20	1381.652	CH_2,CH,CH_3 wagging
v 21	1390.822	CH-CH_2 scissoring
v 22	1432.615	CH_2,CH,CH_3 asymmetrical wagging
v 23	1445.928	CH_2,CH,CH_3 symmetrical wagging
v 24	1514.76	CH_3 scissoring
v 25	1527.512	CH_3 scissoring
v 26	1548.937	CH_2 scissoring

v 27	1931.763	C=O stretching
v 28	3051.138	H_3-C symmetrical stretching, H_2-C & H-C symmetrical stretching
v 29	3059.211	H-C & H_3-C symmetrical stretching
v 30	3063.209	H-C & H_2 symmetrical stretching
v 31	3130.145	H_3-C asymmetrical stretching
v 32	3141.778	H_3-C asymmetrical stretching
v 33	3146.414	H_2-C asymmetrical stretching

Table 7-2. Assignments for isolated DMC molecule

Modes	DMC	Assignment
v 1	115.335	CH_3 asym wagging
v 2	120.892	molecule bending
v 3	137.3	CH_3 sym wagging
v 4	203.056	o.p. O-C-O twisting
v 5	237.861	molecule bending
v 6	351.115	C-O-C asym bending
v 7	518.009	molecule stretching
v 8	697.516	i.p. O-C-O twisting
v 9	785.139	o.p. O=C-O bending
v 10	936.701	molecule stretching
v 11	1015.571	O-C-O rockingz
v 12	1159.245	O-C stretching
v 13	1187.284	CH_3 asym stretching
v 14	1191.819	CH_3 sym stretching
v 15	1215.608	CH_3 asym stretching
v 16	1242.545	CH_3 sym stretching
v 17	1336.234	molecule stretching
v 18	1487.846	CH_3 sym bending
v 19	1510.563	CH_3 asym bending

v 20	1513.83	asym H-C-H rocking & i.p. C-H wagging
v 21	1514.327	sym H-C-H rocking & i.p. C-H wagging
v 22	1526.587	H-C-H asym bending
v 23	1527.606	H-C-H sym bending
v 24	1833.666	C=O stretching
v 25	3074.426	CH_3 asym stretching
v 26	3075.435	CH_3 sym stretching
v 27	3149.296	asym H-C-H asym stretchging
v 28	3149.86	sym H-C-H asym stretchging
v 29	3182.895	asym H-C-H sym stretchging & C-H stretching
v 30	3183.154	sym H-C-H sym stretchging & C-H stretching

7.4 Example of thermodynamic parameters

```
Output file for EC:

Temperature                        =   298.15K

frequency scaling parameter        =   1.0000

Zero-Point correction to Energy  =   47.316 kcal/mol  (  0.075403 au)

 Thermal correction to Energy     =   50.357 kcal/mol  (  0.080248 au)

 Thermal correction to Enthalpy   =   50.949 kcal/mol  (  0.081192 au)

 Total Entropy                     =   72.037 cal/mol-K

   - Translational                 =   39.320 cal/mol-K (mol. weight =
88.0160)

   - Rotational                  =   25.757 cal/mol-K (symmetry =1)

   - Vibrational                 =    6.960 cal/mol-K

 Cv (constant volume heat capacity) =   16.409 cal/mol-K

   - Translational                   =    2.979 cal/mol-K

   - Rotational                      =    2.979 cal/mol-K

   - Vibrational                     =   10.450 cal/mol-K
```

7.5 Composition of the electrolytes

Table 7-3 Composition of $NaClO_4$/PC

Sample reference	$mNaClO_4$(g)	mPC(g)	Concentration(mol/kg)
A1	0.0269	2.1926	0.100
A2	0.0886	2.2345	0.324
A3	0.3199	4.0277	0.649
A4	0.4972	4.0783	0.996
A5	0.3543	2.3133	1.251
A6	0.3683	2.0491	1.468
A7	0.5070	2.4605	1.683
A8	0.3457	1.6192	1.744

Table 7-4 Composition of NaTFSI/PC

Sample reference	mNaTFSI(g)	mPC(g)	Concentration(mol/kg)
B1	0.3738	2.4942	0.494
B2	0.6661	2.2008	0.998
B3	1.0082	2.2250	1.495
B4	1.3148	2.1066	2.059
B5	0.7935	0.8040	3.256

Reference

1. Li, H.W., Chuana,b Wu, Fenga,b Bai, Ying*,a,b, *Sodium Ion Battery: A Promising Energy-storage Candidate for Supporting Renewable Electricity.* ACTA CHIMICA SINICA, 2014. **72**: p. 21-29.
2. Huang, H., J. Zhang, and G. Xie. *RESEARCH on the future functions and MODALITY of smart grid and its key technologies*. in *2014 China International Conference on Electricity Distribution (CICED)*. 2014.
3. Haas, O. and E.J. Cairns, *Electrochemical energy storage.* Annual Reports on the Progress of Chemistry - Section C, 1999. **95**: p. 163-197.
4. Monti, D., et al., *Towards safer sodium-ion batteries via organic solvent/ionic liquid based hybrid electrolytes.* Journal of Power Sources, 2016. **324**: p. 712-721.
5. Kubota, K. and S. Komaba, *Review-practical issues and future perspective for Na-ion batteries.* Journal of the Electrochemical Society, 2015. **162**(14): p. A2538-A2550.
6. A. Ponrouch, D.M., A. Boschin, B. Steen, P. Johansson and M. R. Palacín, *Non-aqueous electrolytes for sodium-ion batteries.* J. Mater. Chem. A, 2015(1).
7. Luo, W., et al., *Na-Ion Battery Anodes: Materials and Electrochemistry.* Accounts of Chemical Research, 2016. **49**(2): p. 231-240.
8. Palomares, V., et al., *Na-ion batteries, recent advances and present challenges to become low cost energy storage systems.* Energy and Environmental Science, 2012. **5**(3): p. 5884-5901.
9. Michael D. Slater , D.K., Eungje Lee , and Christopher S. Johnson, *Sodium-Ion Batteries.* 2013. **23**(26, 3255,).
10. Kei Kubota, N.Y., Hiroaki Yoshida, Mouad Dahbi, *Layered oxides as positive electrode materials for Na-ion batteries.* 2014. **39**(5).
11. Braconnier, J.-J., et al., *Comportement electrochimique des phases NaxCoO2.*

Materials Research Bulletin, 1980. **15**(12): p. 1797-1804.

12. Sauvage, F., et al., *Study of the Insertion/Deinsertion Mechanism of Sodium into Na0.44MnO2.* Inorganic Chemistry, 2007. **46**(8): p. 3289-3294.
13. Didier, C., et al., *Electrochemical Na-Deintercalation from NaVO2.* Electrochemical and Solid-State Letters, 2011. **14**(5): p. A75-A78.
14. Sung-Wook Kim , D.-H.S., Xiaohua Ma , Gerbrand Ceder , * and Kisuk Kang * *Electrode Materials for Rechargeable Sodium-Ion Batteries:Potential Alternatives to Current Lithium-Ion Batteries.* 2012.
15. Ding, J.-J., et al., *Cycle performance improvement of NaCrO2 cathode by carbon coating for sodium ion batteries.* Electrochemistry Communications, 2012. **22**: p. 85-88.
16. Komaba, S., et al., *Electrochemical intercalation activity of layered NaCrO2 vs. LiCrO2.* Electrochemistry Communications, 2010. **12**(3): p. 355-358.
17. Makimura, Y. and T. Ohzuku, *Lithium insertion material of LiNi1/2Mn1/2O2 for advanced lithium-ion batteries.* Journal of Power Sources, 2003. **119**: p. 156-160.
18. Shinichi Komabaa, T.N., Atsushi Ogataa, Takaya Shimizua, Chikara Takeia, S Takadaa, A Hokuraa and I Nakaia, *Electrochemically Reversible Sodium Intercalation of Layered NaNi0.5Mn0.5O2 and NaCrO2.* The Electrochemical Society, 2009.
19. Kim, D., et al., *Enabling Sodium Batteries Using Lithium-Substituted Sodium Layered Transition Metal Oxide Cathodes.* Advanced Energy Materials, 2011. **1**(3): p. 333-336.
20. Delacourt, C., et al., *Toward Understanding of Electrical Limitations (Electronic, Ionic) in LiMPO4 (M = Fe , Mn) Electrode Materials.* Journal of The Electrochemical Society, 2005. **152**(5): p. A913-A921.
21. Teng, F., et al., *Hydrothermal synthesis of plate-like carbon-coated Li3V2(PO4)3 and its low temperature performance for high power lithium ion batteries.* Electrochimica Acta, 2013. **91**: p. 43-49.

22. Barker, J., M.Y. Saidi, and J.L. Swoyer, *A Sodium-Ion Cell Based on the Fluorophosphate Compound NaVPO4 F* Electrochemical and Solid-State Letters, 2003. **6**(1): p. A1-A4.

23. Jian, Z., et al., *Carbon coated Na3V2(PO4)3 as novel electrode material for sodium ion batteries.* Electrochemistry Communications, 2012. **14**(1): p. 86-89.

24. Kitajou, A., et al., *Novel synthesis and electrochemical properties of perovskite-type NaFeF3 for a sodium-ion battery.* Journal of Power Sources, 2012. **198**: p. 389-392.

25. Luo, W., et al., *Low-Surface-Area Hard Carbon Anode for Na-Ion Batteries via Graphene Oxide as a Dehydration Agent.* ACS Applied Materials & Interfaces, 2015. **7**(4): p. 2626-2631.

26. Sangster, J., *C-Na (Carbon-Sodium) System.* Journal of Phase Equilibria and Diffusion, 2007. **28**(6): p. 571-579.

27. Stevens, D.A. and J.R. Dahn, *The Mechanisms of Lithium and Sodium Insertion in Carbon Materials.* Journal of The Electrochemical Society, 2001. **148**(8): p. A803-A811.

28. Stevens, D.A. and J.R. Dahn, *High Capacity Anode Materials for Rechargeable Sodium‐Ion Batteries.* Journal of The Electrochemical Society, 2000. **147**(4): p. 1271-1273.

29. Wei Luo, a.J.S., b Clement Bommier,a Bao Wang,a Joshua Razink,c John Simonsen*b and Xiulei Ji*a *Carbon nanofibers derived from cellulose nanofibers as a long-life anode material for rechargeable sodium-ion batteries;*Journal of Materials Chemistry A, 2013(36).

30. Jiangfeng Qian, a.Y.C., a Lin Wu,a Yuliang Cao,a Xinping Aia and Hanxi Yang*a *High capacity Na-storage and superior cyclability of nanocomposite Sb/C anode for Na-ion batteries.* 2012(56).

31. Alcántara, R., et al., *NiCo2O4 Spinel: First Report on a Transition Metal Oxide for the Negative Electrode of Sodium-Ion Batteries.* Chemistry of Materials,

2002. **14**(7): p. 2847-2848.

32. Senguttuvan, P., et al., *Na2Ti3O7: Lowest Voltage Ever Reported Oxide Insertion Electrode for Sodium Ion Batteries.* Chemistry of Materials, 2011. **23**(18): p. 4109-4111.

33. Ponrouch, A., et al., *In search of an optimized electrolyte for Na-ion batteries.* Energy and Environmental Science, 2012. **5**(9): p. 8572-8583.

34. Xu, K., *Nonaqueous liquid electrolytes for lithium-based rechargeable batteries.* Chemical Reviews, 2004. **104**(10): p. 4303-4417.

35. Ong, M.T., et al., *Lithium Ion Solvation and Diffusion in Bulk Organic Electrolytes from First-Principles and Classical Reactive Molecular Dynamics.* The Journal of Physical Chemistry B, 2015. **119**(4): p. 1535-1545.

36. Kim, S.-P.v.D., A. C. T.; Shenoy, V. B, *Effect of Electrolytes on the Structure and Evolution of the Solid Electrolyte Interphase (SEI) in Li-Ion Batteries: A Molecular Dynamics Study.* J. Power Sources, 2011. **196**: p. 8590–8597.

37. Shakourian-Fard, M., et al., *Trends in Na-Ion Solvation with Alkyl-Carbonate Electrolytes for Sodium-Ion Batteries: Insights from First-Principles Calculations.* The Journal of Physical Chemistry C, 2015. **119**(40): p. 22747-22759.

38. Komaba, S., et al., *Electrochemical Na insertion and solid electrolyte interphase for hard-carbon electrodes and application to Na-ion batteries.* Advanced Functional Materials, 2011. **21**(20): p. 3859-3867.

39. Ponrouch, A., et al., *Towards high energy density sodium ion batteries through electrolyte optimization.* Energy and Environmental Science, 2013. **6**(8): p. 2361-2369.

40. Kamath, G., et al., *In silico based rank-order determination and experiments on nonaqueous electrolytes for sodium ion battery applications.* Journal of Physical Chemistry C, 2014. **118**(25): p. 13406-13416.

41. Strauss, S.H., *The search for larger and more weakly coordinating anions.* Chemical Reviews, 1993. **93**(3): p. 927-942.

42. Hong, S.Y., et al., *Charge carriers in rechargeable batteries: Na ions vs. Li ions.* Energy and Environmental Science, 2013. **6**(7): p. 2067-2081.

43. Cresce, A.V., et al., *Solvation behavior of carbonate-based electrolytes in sodium ion batteries.* Physical Chemistry Chemical Physics, 2017. **19**(1): p. 574-586.

44. Hatchard, T.D. and M.N. Obrovac, *Evaluation of Electrolyte Salts and Solvents for Na-Ion Batteries in Symmetric Cells.* Journal of The Electrochemical Society, 2014. **161**(10): p. A1748-A1752.

45. Aguesse, F., et al., *Electrochemical Performance of Na3Ni1.5Zn0.5SbO6 in Different Electrolytes.* Meeting Abstracts, 2015. **MA2015-01**(2): p. 379.

46. Bhatt, M.D., M. Cho, and K. Cho, *Conduction of Li+ cations in ethylene carbonate (EC) and propylene carbonate (PC): comparative studies using density functional theory.* Journal of Solid State Electrochemistry, 2012. **16**(2): p. 435-441.

47. Bhatt, M.D., M. Cho, and K. Cho, *Density functional theory calculations and ab initio molecular dynamics simulations for diffusion of Li + within liquid ethylene carbonate.* Modelling and Simulation in Materials Science and Engineering, 2012. **20**(6).

48. Masia, M., M. Probst, and R. Rey, *Ethylene Carbonate−Li+: A Theoretical Study of Structural and Vibrational Properties in Gas and Liquid Phases.* The Journal of Physical Chemistry B, 2004. **108**(6): p. 2016-2027.

49. Bhide, A., et al., *Electrochemical stability of non-aqueous electrolytes for sodium-ion batteries and their compatibility with Na0.7CoO2.* Physical Chemistry Chemical Physics, 2014. **16**(5): p. 1987-1998.

50. Allen, J.L., et al., *Combined quantum chemical/Raman spectroscopic analyses of Li+ cation solvation: Cyclic carbonate solvents - Ethylene carbonate and propylene carbonate.* Journal of Power Sources, 2014. **267**: p. 821-830.

51. Skarmoutsos, I., et al., *Li+ Solvation in Pure, Binary, and Ternary Mixtures of Organic Carbonate Electrolytes.* The Journal of Physical Chemistry C, 2015.

119(9): p. 4502-4515.

52. Yang, X., *Development of Property Prediction Methods for Lithium-ion Battery Electrolytes.* 2015.
53. Kumar, H., et al., *Fundamental Mechanisms of Solvent Decomposition Involved in Solid-Electrolyte Interphase Formation in Sodium Ion Batteries.* Chemistry of Materials, 2016. **28**(24): p. 8930-8941.
54. Wang, Y., et al., *Theoretical Studies To Understand Surface Chemistry on Carbon Anodes for Lithium-Ion Batteries: Reduction Mechanisms of Ethylene Carbonate.* Journal of the American Chemical Society, 2001. **123**(47): p. 11708-11718.
55. von Wald Cresce, A., et al., *Anion Solvation in Carbonate-Based Electrolytes.* The Journal of Physical Chemistry C, 2015. **119**(49): p. 27255-27264.
56. Klassen, B., et al., *Raman Spectra and Transport Properties of Lithium Perchlorate in Ethylene Carbonate Based Binary Solvent Systems for Lithium Batteries.* The Journal of Physical Chemistry B, 1998. **102**(24): p. 4795-4801.
57. Emsley, J., *The Elements*. 3rd edition ed. 1998: Oxford: Clarendon Press.
58. Pfennig, B.W., *Principles of Inorganic Chemistry*. 2015.
59. von Wald Cresce, A., O. Borodin, and K. Xu, *Correlating Li+ Solvation Sheath Structure with Interphasial Chemistry on Graphite.* The Journal of Physical Chemistry C, 2012. **116**(50): p. 26111-26117.
60. Dreizler, R.M. and E.K. Gross, *Density Functional Theory: An Approach to the Quantum Many-Body Problem Springer*. 1990, Berlin.
61. Perdew, J.P., *Density-functional approximation for the correlation energy of the inhomogeneous electron gas.* Physical Review B, 1986. **33**(12): p. 8822.
62. Perdew, J.P., P. Ziesche, and H. Eschrig, *Electronic structure of solids' 91*. Vol. 11. 1991: Akademie Verlag, Berlin.
63. Perdew, J.P., et al., *Accurate density functional with correct formal properties: A step beyond the generalized gradient approximation.* Physical review letters, 1999. **82**(12): p. 2544.

64. Neumann, R. and N.C. Handy, *Higher-order gradient corrections for exchange-correlation functionals.* Chemical physics letters, 1997. **266**(1-2): p. 16-22.

65. Catlow, R., *Computational Materials Science*. 2003.

66. Tsuneda, T., *Density Functional Theory in Quantum Chemistry*. 2014.

67. Kim, K. and K.D. Jordan, *Comparison of Density Functional and MP2 Calculations on the Water Monomer and Dimer.* The Journal of Physical Chemistry, 1994. **98**(40): p. 10089-10094.

68. Juan Andrés Bort, J.B.R., *Theoretical and Computational Chemistry: Foundations, Methods and Techniques*. 2007.

69. Becke, A.D., *Density-functional exchange-energy approximation with correct asymptotic behavior.* Physical Review A, 1988. **38**(6): p. 3098-3100.

70. Lee, C., W. Yang, and R.G. Parr, *Development of the Colle-Salvetti correlation-energy formula into a functional of the electron density.* Physical Review B, 1988. **37**(2): p. 785-789.

71. Vosko, S.H., L. Wilk, and M. Nusair, *Accurate spin-dependent electron liquid correlation energies for local spin density calculations: a critical analysis.* Canadian Journal of Physics, 1980. **58**(8): p. 1200-1211.

72. Valiev, M., et al., *NWChem: A comprehensive and scalable open-source solution for large scale molecular simulations.* Computer Physics Communications, 2010. **181**(9): p. 1477-1489.

73. Tirado-Rives, J. and W.L. Jorgensen, *Performance of B3LYP Density Functional Methods for a Large Set of Organic Molecules.* Journal of Chemical Theory and Computation, 2008. **4**(2): p. 297-306.

74. Marcus D Hanwell, D.E.C., David C Lonie, Tim Vandermeersch, Eva Zurek and Geoffrey R Hutchison, *Avogadro: An advanced semantic chemical editor, visualization, and analysis platform.* Journal of Cheminformatics 2012, 4:17., 2012.

75. Nachbar, T.A.H.a.R.B., *Merck molecular force field. IV. conformational*

energies and geometries for MMFF94. Journal of Computational Chemistry, 1996. **17**(5-6): p. 587-615.

76. McQuarrie, D.A.R., P.A., *General chemistry; second edition.* Journal of Chemical Education, 1988. **62**.
77. M. Hesse, H.M., B. Zeeh, *Spectroscopic methods in organic chemistry*. 2008.
78. Sibilia, J.P., *A guide to materials characterization and chemical analysis second edition* 1996.
79. Coleman, P.B., *Practical Sampling Techniques for Infrared Analysis.* 1993.
80. Harris, R.K., et al., *NMR nomenclature. Nuclear spin properties and conventions for chemical shifts (IUPAC recommendations 2001).* Pure and Applied Chemistry, 2001. **73**(11): p. 1795-1818.
81. Wang, I., C.O. Britt, and J.E. Boggs, *The Planarity of the Ring Atoms in Ethylene Carbonate.* Journal of the American Chemical Society, 1965. **87**(21): p. 4950-4951.
82. Fortunato, B., P. Mirone, and G. Fini, *Infrared and Raman spectra and vibrational assignment of ethylene carbonate.* Spectrochimica Acta Part A: Molecular Spectroscopy, 1971. **27**(9): p. 1917-1927.
83. Matias, P.M., et al., *Single crystal neutron diffraction analysis (15 K) and ab initio molecular orbital calculations for ethylene carbonate.* Journal of Molecular Structure: THEOCHEM, 1989. **184**(3): p. 247-260.
84. Frisch, M.J., Trucks, G.W., Schlegel, H.B., et al. , *Gaussian 09 revision C.01, Gaussian Inc. Wallingford, CT.*
85. ZHAO, Y., et al.,, *^{13}C NMR Studies on the Preferential Solvation of Li^{+} in PC+DMF Mixed Solvent.* ACTA CHIMICA SINICA, 2006. **64**: p. 2145-2150.
86. Brooksby, P.A. and W.R. Fawcett, *Infrared (attenuated total reflection) study of propylene carbonate solutions containing lithium and sodium perchlorate.* Spectrochimica Acta Part A: Molecular and Biomolecular Spectroscopy, 2006. **64**(2): p. 372-382